NORTHWESTERN UNIVERSITY

ISGF3-Mediated Chromatin Dynamics and Regulation of Type I Interferon-Stimulated Genes

A DISSERTATION

SUBMITTED TO THE GRADUATE SCHOOL
IN PARTIAL FULFILLMENT OF THE REQUIREMENTS

for the degree

DOCTOR OF PHILOSOPHY

Field of Interdisciplinary Biological Sciences

By

Nancy Au-Yeung (Weng Si Au Yeung)

EVANSTON, ILLINOIS

December 2018

ABSTRACT

ISGF3-Mediated Chromatin Dynamics and Regulation of Type I Interferon-Stimulated Genes

Nancy Au-Yeung
歐陽詠詩

Type I interferon (IFN) is the primary antiviral cytokine establishing a broad and potent antiviral response to protect mammalian cells from virus infection. The functional repertoire of IFN extends to innate and adaptive immunity, neoplastic transformation, resistance and cancer immunotherapy. IFN functions are primarily mediated through the Janus kinase (JAK) and signal transducers and activators of transcription (STAT) signaling pathway. Stimulation of the IFN-JAK-STAT signaling cascade drives the expression of hundreds of diverse IFN-stimulated gene (ISG) effectors underlying IFN functions.

Similar to other mammalian genes, ISGs are encoded within a chromatin structure in the human genome. ISG expression is activated primarily by the trimeric transcription factor complex, ISG factor 3 (ISGF3), consisting of STAT1, STAT2, and IRF9 proteins. ISGF3 engages target gene promoters and recruits coactivators, Mediator, and RNA polymerase II machinery. To access the native gene template and induce transcription, ISGF3 must engage with chromatinized ISG promoters. ISGF3-associated coactivators with chromatin modifying functions support the notion of a dynamic chromatin regulation in ISG activation; thus, necessitating recruitment of specialized factors to modulate gene accessibility during the IFN response. However, our characterization of the dynamic ISG chromatin environment is insufficient to understand the interplay between ISGF3 and ISG

chromatin. In particular, the chromatin architecture at ISG promoters and dynamic alterations following IFN stimulation remain relatively unexplored.

To advance our understanding of the dynamic ISG chromatin architecture in relation to ISGF3, I generated genome-wide maps of ISGF3 occupancy to accompany high-resolution nucleosome maps for 20 representative ISGs during steady state and following IFN stimulation. Characterization of the relationship between ISGF3 and ISG promoter nucleosomes led to uncovering a previously unknown role for the histone variant, H2A.Z, in ISG transcription. H2A.Z is present at ISG promoters, but rapidly removed following IFN. H2A.Z eviction from ISG promoter nucleosomes was inversely correlated with ISGF3 recruitment and was found to require the activity of the histone acetyltransferase, GCN5, and the bromodomain protein, BRD2. Reduction of H2A.Z led to enhanced ISGF3 recruitment, increased ISG expression and potentiated antiviral protection, implicating a suppressive role for H2A.Z nucleosomes in the IFN response. Proper gene accessibility is essential to the homeostasis of the IFN response in establishing a protective environment during infection, while preventing adverse effects of a prolonged IFN response. Coordinately controlled H2A.Z removal and incorporation at ISG promoter nucleosomes is an essential component for the activation and repression of ISG effectors for cellular protection and homeostatic integrity.

ACKNOWLEGDMENTS

No amount of words can express my eternal gratitude to the people who have supported me in my PhD journey and in my life. Thank you.

This dissertation, both the research findings and written document, would not be possible without my amazing mentor and cheerleader, Dr. Curt M. Horvath. I am not the first nor will I be the last to say, I am a better scientist and technical communicator because of Curt. Yet, this only covers the tip of the iceberg. Curt, thank you for everything you have taught me and for your support throughout my PhD journey.

To my thesis committee, Drs. Jason Brickner, Josh Leonard, and Ishwar Radhakrishnan, thank you for the intellectual discussions and guidance over the years, especially those final pieces of advice at my defense exam. These science and career-related conversations mean a lot to me and will continue to benefit me in the long run.

To P (aka Patrick Parisien), thank you for being there for me in and outside of lab, for always reminding me to keep “chipping away” to see the “light.” You have been my guiding light throughout the PhD process and I would not have made it past those dark times without you. To a lifelong friendship.

To Annie Bruns, for being my partner in crime in the first half of my PhD and for continuing to be my lifelong best friend. You taught me a lot about love and the expression of love to those I care about, a concept I am still learning to practice.

To Roli Mandhana Kasat, my labmate and partner in crime in the second half of the PhD. Thank you for being my sounding board and editorial consultant. I will reminisce those afternoon tea breaks and sharing our obstacles and triumphs.

To Jess (aka Jessica Lenoir), for your cheerful spirit and being there in the moments that matter. I am grateful for your time spent proofreading my thesis and the sweet treats for my sad and happy moments. These random acts of kindness mean the world to me.

And to all the Horvath lab members I have had the pleasure to work with, thank you for your friendship and scientific inspiration. May our paths cross again one day.

To my former mentors, Drs. Igor Brown, Svetlana Sarkisova, Amy Palmer, Schuyler VanEngelenburg, Hailong Zhang, Walt Voetgli, Wen-I Wu, Pinal Patel, Jonathan Freaney, and all the people who I got to work with and learn from at Northwestern University, NASA, Amy's lab at CU Boulder, and Array BioPharma, without your guidance I would not have become a scientist, and especially not the scientist I have grown to be today. Thank you.

To my best friends outside of lab, Di (aka Dr. Diana Oo), from childhood to adulthood we have been through thick and thin. Thank you for having my back, baking me delicious sweets, reading my thesis, and always believing in me; Louise, for being the best roommate turned best friend one could only wish for. Thank you for the conversations that transcend the philosophical to ones where we share our love of science, for the personalized cards, birthday bouquet, care package, reading my thesis, and checking in on me. Best friends forever.

To my friends Mai, Bruce, Linda, Seraphina, Nhien, Linh, Anna, Nhia, Choua, Liang, Houqing, Suchie, Vicky, Sandy, and many more friends whom I have not included here, thank you for your friendship and the fond memories that continue to make a difference in my life. I especially want to thank Mai for her friendship, cards, and care packages.

To my family, Grandma “Poh-poh” and my late grandparents, thank you for raising me, cooking delicious food for me, and always reminding me how loved I am. To Alan, Theresa, and the kids, thank you for always being there for me and for our memories from every annual Christmas reunion that remind me of the love at home.

To my siblings, Erica, Lily, and Ray, you mean the world to me. During some of the hardest times it was your love that warmed my heart and pulled me out of the dark. I love you all. Thank you for always being there for me and loving me unconditionally.

To my fiancé, Saeng Sivixay, thank you for putting up with me, loving me as I am, proofreading my thesis, and encouraging me throughout my life and through the PhD. You keep me grounded to reality and help me remember what life really is about, especially when I get too absorbed into my research and career.

Last, but not least to my parents. I owe both of you everything, literally. You sacrificed so much for me (and my siblings), working too many hours and days to count, all to provide me with an education and the freedom to choose my future. Mom and Dad, all that I have accomplished and experienced in life, in school, and in my career are the fruits of your love and labor, and I am forever indebted. Therefore, this thesis is dedicated to you both for your sacrifice, and most importantly, for your love.

最后，和最重要的. 多谢我妈咪爹地. 我欠你门一切. 你门为我（和弟弟妹妹）牺牲了很多. 辛辛苦苦工作, 工作时间和数日都太多了. 为我门提供了教育和有选择未来的自由和权利. 妈咪爹地，无论是我生活或学业和事业的成就, 都是你门的爱和努力的成果. 我拥有的一切都是你门给我的. 我永远感激不尽. 因此，本博士论文是献给你们的. 妈咪爹地, 多谢你门的牺牲和爱.

LIST OF ABBREVIATIONS

AAF	IFN-alpha activation factor	**ISGF3**	Interferon-stimulated gene factor 3
Ac	acetylated	**JAK**	Janus kinase
AIM2	Absent in melanoma 2	**MACS**	Model-based analysis for ChIP-Seq
ANP32a	Acidic nuclear phosphoprotein 32 member A	**Me**	methylated
ATF2	Activating transcription factor 2	**MED**	Mediator
BAF	BRG1- or HBRM-associated factor	**MX**	Myxovirus resistance protein
bp	Base pair(s)	**NES**	Nuclear export signal
BRD	Bromodomain extratermini domain	**NFκB**	Nuclear factor kappa-light-chain-enhancer of activated B cells
BRG1	Brahma-related gene 1	**NLS**	Nuclear localization signal
CBP	CREB-binding protein	**OAS**	2'-5'-oligoadenylate synthase
CD4	Cluster of differentiation 4	**P300**	E1A binding protein p300
CDK	Cyclin-dependent kinase	**PBAF**	Polybromo-associated BAF
cGAS	Cyclic GMP-AMP synthase	**Pol II**	RNA polymerase II
ChIP-chip	Microarray chromatin immunoprecipitation	**pp32**	Acidic nuclear phosphoprotein 32 member A
ChIP-Seq	Chromatin immunoprecipitation sequencing	**PRC**	Polycomb repressive complex
cJun	AP-1 transcription factor	**PRD**	Positive regulatory domain
DNA	Deoxyribonucleic acid	**pTEFb**	Positive transcription elongation factor
DRIP	Vitamin D receptor interacting protein	**RLR**	RIG-I-like receptor
GCN5	General control non-depressible 5	**RT-qPCR**	Reverse transcriptase-quantitative polymerase chain reaction
GTF	General transcription factors	**RVB**	RuvB-like
H3K4	Histone H3 lysine 4	**SH2**	Src homology 2
HAT	histone acetyltransferase	**SMARCA4**	SWI/SNF related, matrix associated, actin dependent regulator of chromatin, subfamily A
HDAC	Histone deacetylase	**SRCAP**	Snf2 related CREBBP activator protein
HOMER	Hypergeometric optimization of motif enrichment	**STAT**	Signal transducer and activator of transcription
IFI16	Interferon gamma inducible protein 16	**STING**	cGAS-stimulator of interferon genes
IFIT	Interferon-induced protein with tetratricopeptide repeats	**TBP**	TATA-binding protein
IFITM	Interferon-induced transmembrane	**TFIID**	Transcription factor D
IFN	Type I interferon	**TIP60**	Tat interacting protein, 60kDa
IFNAR	Interferon alpha receptor	**TLR**	Toll-like receptor
INO80	Inositol requiring	**TSS**	Transcription start site
IRF	Interferon regulatory factor	**TYK**	Tyrosine kinase
ISRE	Interferon-stimulated response element	**UCSC**	University of California Santa Cruz
ISG	Interferon-stimulated gene	**Y**	Tyrosine

TABLE OF CONTENTS

LIST OF FIGURES

LIST OF TABLES

CHAPTER 1.

INTRODUCTION

OVERVIEW

Within hours of a viral infection, host mammalian cells mount a broad and powerful antiviral response to protect cells from virus infection. The mysterious factor orchestrating this potent response was discovered in 1957. Virus-infected cells released an unknown substance into the media that conferred antiviral protection to uninfected cells, eventually identified as the host-secreted type I interferon (IFN) cytokine (Isaacs and Lindenmann, 1957). IFN is the primary antiviral cytokine, capable of signaling to virtually all cell types (Borden et al., 2007). This ubiquitous signaling ability also enables IFN to modulate the professional immune system. IFN-driven responses have broad cellular impacts that extend beyond its recognized antiviral properties, to neoplastic transformation, autoimmune diseases and immunotherapy (Gonzalez-Navajas et al., 2012; Parker et al., 2016; Zitvogel et al., 2015). Thus, investigation of the mechanisms underlying the IFN response are important to understanding human health and antiviral biology.

The IFN response is mediated by a Janus kinase (JAK) and signal transducers and activators of transcription (STAT) signaling pathway that generates an antiviral transcription factor, IFN-stimulated gene factor 3 (ISGF3) (Stark and Darnell, 2012). While much is known about the IFN-induced formation of ISGF3, less is known about how this factor engages native chromatin, recruits and activates RNA polymerase II (Pol II), giving rise to antiviral ISGs. In addition to being a key factor for immune regulation, ISGF3 transcriptional regulation of IFN-stimulated genes (ISGs) is an outstanding model for studying inducible transcription in eukaryotes. The contemporary view of transcription has evolved to the point that supports a functional and dynamic role of chromatin,

motivating the broad question of how a transcription factor engages chromatin. Specifically, this thesis aims to understand how ISGF3 engages ISG chromatin and mediates chromatin dynamics to activate ISG transcription during the IFN antiviral response.

Here in Chapter 1, the major discoveries that have established the IFN production and the activation of ISGF3 in the IFN-stimulated JAK-STAT pathway will be highlighted along with the established knowledge on ISG chromatin regulation prior to this thesis project. Complementing these prior studies is the featured thesis project in Chapters 2 and 3 to advance our understanding of ISGF3-mediated chromatin dynamics and chromatin regulation of type I IFN-stimulated genes (ISGs). Relative to the detailed understanding of the IFN-JAK-STAT signaling events, much less is known about the ISGF3 target chromatin and interplay of ISGF3 with chromatin or nucleosomes. This thesis project provides an in-depth analysis on the native ISG promoter nucleosome environment and ISGF3-mediated chromatin dynamics before and after IFN stimulation.

TYPE I INTERFERON-JAK-STAT SIGNAL TRANSDUCTION

Type I Interferon

Since its initial discovery as a soluble antiviral factor secreted from virus-infected cells (Isaacs and Lindenmann, 1957), type I interferon (IFN) is now known to govern a multitude of biological processes related to innate and adaptive immunity, neoplastic transformation (Parker et al., 2016), efficacy of cancer therapies (Zitvogel et al., 2015), and immuno-modulatory processes (Gonzalez-Navajas et al., 2012). IFN refers to a family of cytokine proteins that share a common transmembrane receptor, IFN alpha receptor 1 and 2 (IFNAR1/2), ubiquitously expressed on the cellular surface of virtually all cell types. This family of cytokines includes 13 IFNα subtypes (α1, α2, α4, α5, α6, α7, α8, α10, α13, α14, α16, α17 and α21), IFNβ, IFNε, IFNκ, and IFNω1 (Hoffmann et al., 2015). Their expression levels differ between cell types with IFNβ ubiquitously produced and IFNα subtypes expressed most highly in leukocytes.

IFN is the primary antiviral cytokine produced in response to a virus infection and has co-evolved with viruses in what is often called an arms race, where mutual antagonism between the two in their natural host achieves a balance over time (Hoffmann et al., 2015). Among IFN, IFNβ and certain IFNα subtypes (i.e. IFNα6, 8) have undergone strong purifying selection, wherein little to no difference in the nucleotide sequence can be seen within the human population. The nucleotide sequence constraints of IFNβ and these IFNα subtypes in the human population support their essential roles in the antiviral response as non-redundant proteins (Manry et al., 2011). In fact, viruses employ many

strategies to antagonize the host mammalian system to prevent IFN production and signaling (Garcia-Sastre, 2017).

IFN not only activates a robust antiviral program, it is known to mediate adaptive immune responses and is implicated in many human diseases (Gonzalez-Navajas et al., 2012; Parker et al., 2016; Rodero and Crow, 2016; Zitvogel et al., 2015). Its ability to signal to virtually all cell types in an autocrine and paracrine manner is the conduit ensuring cell-to-cell communication that protects cells from infection. It was also among the earliest anticancer therapy regimens and continues to be used in cancer immunotherapy and treatment of disease types such as multiple sclerosis (Reder and Feng, 2014; Sudhakar, 2009; Zitvogel et al., 2015). The underlying mechanism behind its anticancer and antiviral prowess began to be uncovered in the 1980s with the discovery of the IFN-induced JAK-STAT signaling cascade (Aaronson and Horvath, 2002; Stark and Darnell, 2012). However, in addition to the positive contributions of IFN signaling, the adverse effects of prolonged IFN exposure underlie several autoimmune and autoinflammatory diseases - some known as interferonopathies (Rodero and Crow, 2016; Trinchieri, 2010). Thus, the inactivation and activation of IFN signaling are equally important. Since all the actions of IFN are predominantly mediated by the transcription factor complex, ISGF3, it is essential to investigate how ISGF3 operates to understand complex human diseases and improve therapeutic applications related to IFN signaling.

IFN production: A model for inducible transcription regulation

In response to a virus infection, cytoplasmic pattern recognition receptors from the RIG-I-like receptor (RLR) family detect and bind to pathogen-associated molecular pattern (PAMP) substrates, such as double-stranded RNA (Bruns and Horvath, 2012). This initial PAMP recognition induces a series of signaling events that converge in the activation and nuclear translocation of transcription factors, NFκB and phosporylated IRF3 dimers, to activate transcription of IFN (Freaney et al., 2013) (Figure 1.1). Within the IFN family, IFNβ is the best characterized gene and serves as a general model for gene transcription activation and regulation. The IFNβ gene promoter contains a +1 and -1 nucleosome that flank a nucleosome-free enhancer region specifically recognized by NFκB and IRF3 (Agalioti et al., 2000; Lomvardas and Thanos, 2002). Similar to IFNβ, the promoters of the IFNα subtypes also feature a +1 and -1 nucleosome architecture (Freaney et al., 2014). The position of the +1 nucleosome obscures the TATA box and transcription start site (TSS), preventing Pol II recruitment to activate IFNβ transcription.

During virus infection, nuclear-translocated NFκB and IRF3, along with transcription factor ATF2/cJun and architectural protein HMG I(Y), bind to their respective positive regulatory domain (PRD) element in the enhancer region; together, they form the enhanceosome complex required for IFNβ transcription activation (Thanos and Maniatis, 1995). The enhanceosome recruits specialized coactivators including histone acetyltransferases GCN5 and CBP/p300 and SWI/SNF chromatin remodeler BRG1 to modify and evict the +1 nucleosome (Agalioti et al., 2000; Freaney et al., 2014). Recruitment of specialized remodeling machinery by the enhanceosome alleviates the +1

nucleosome barrier, enabling Pol II access to the TSS and IFNβ gene transcription. Once IFN is expressed and secreted from the cell, it signals in an autocrine and paracrine manner through the JAK-STAT signaling cascade to activate the transcription factor ISGF3 and ISG transcription (Stark and Darnell, 2012).

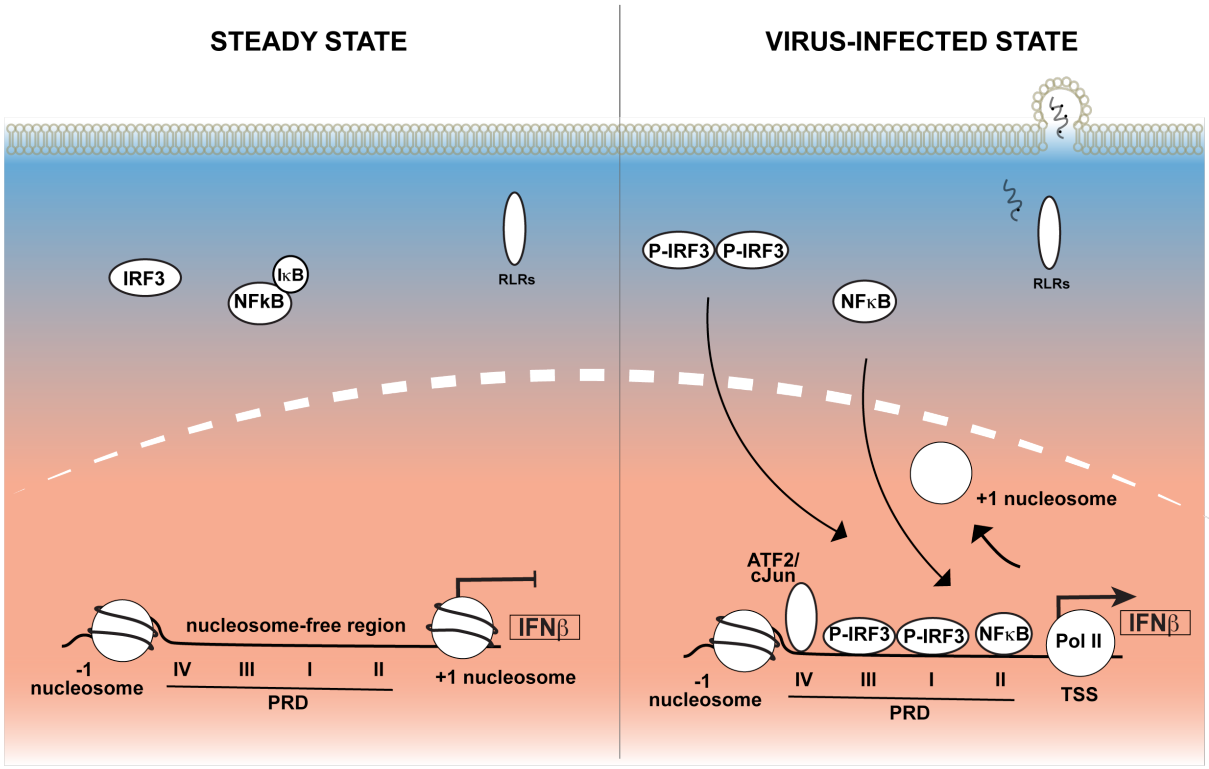

Figure 1.1: RIG-I-like receptor signaling pathway for IFN production
Illustration of the cell during steady state (uninfected) and following virus infection. (Left) During steady state, RIG-I-like receptors (RLRs) are present in the cytoplasm, along with transcription factors IRF3 and NFκB (bound to its inhibitor IκB). Inside the nucleus, the IFNβ promoter region is depicted with a -1 and +1 nucleosome flanking a nucleosome-free region. (Right) Following virus infection, viral substrates are recognized and bound by RLR family members and lead to IRF3 and NFκB activation and translocation into the nucleus. In the nucleus, IRF3 homodimer and NFκB bind to their respective positive regulatory domain (PRD), along with ATF2/cJun, to form the IFNβ enhanceosome. Enhanceosome recruitment of chromatin-modifying factors lead to the eviction of the +1 nucleosome, exposing the transcription start site (TSS) and enabling Pol II recruitment and IFNβ transcription.

ISGF3 transcription factor complex (STAT1, STAT2, IRF9)

ISGF3 is the predominant transcription factor complex that regulates ISG transcriptional activation in the IFN-induced JAK-STAT signaling pathway (Borden et al., 2007; Fu et al., 1990; Levy et al., 1989). It is formed through a heterotrimeric association of STAT1, STAT2 and IRF9 (IFN-regulatory factor 9) proteins. STAT1 and STAT2 are prototypes of the STAT family of transcription factors (Figure 1.2). Seven proteins (STAT1, 2, 3, 4, 5a, 5b, 6) constitute the STAT family, sharing structurally and functionally similar domains that allow them to function as both signal transducers and transcription activators; these domains include the N-terminal domain, coiled-coil domain, DNA-binding domain, linker domain, Src homology 2 (SH2) domain and transactivation domain (TAD) (Lim and Cao, 2006). STAT2 is also the only STAT factor pre-associated with an IRF transcription factor, IRF9 (Figure 1.2). Thus, ISGF3 is unique among STAT complexes because of the association with IRF9 and contributions from the STAT1 and STAT2 C-terminal transactivation domains (CTDs) that provide specific coactivator interactions.

Basal levels of the ISGF3 components, STAT1, STAT2, and IRF9, are present in the cytoplasm during steady state (Cimica and Reich, 2013; Reich, 2013). Monomeric STAT1 and STAT2 contain a nuclear export signal (NES) that retains them in the cytoplasm. IRF9 contains a bipartite nuclear localization signal (NLS) that allows IRF9 and pre-associated STAT2-IRF9 to transiently translocate into the nucleus (Lau et al., 2000). The nuclear residence for IRF9 associated with STAT2 is transient due to the

strong STAT2 NES. However, following IFN stimulation of the JAK-STAT signaling cascade, STAT1 and STAT2 are activated and can stably translocate into the nucleus.

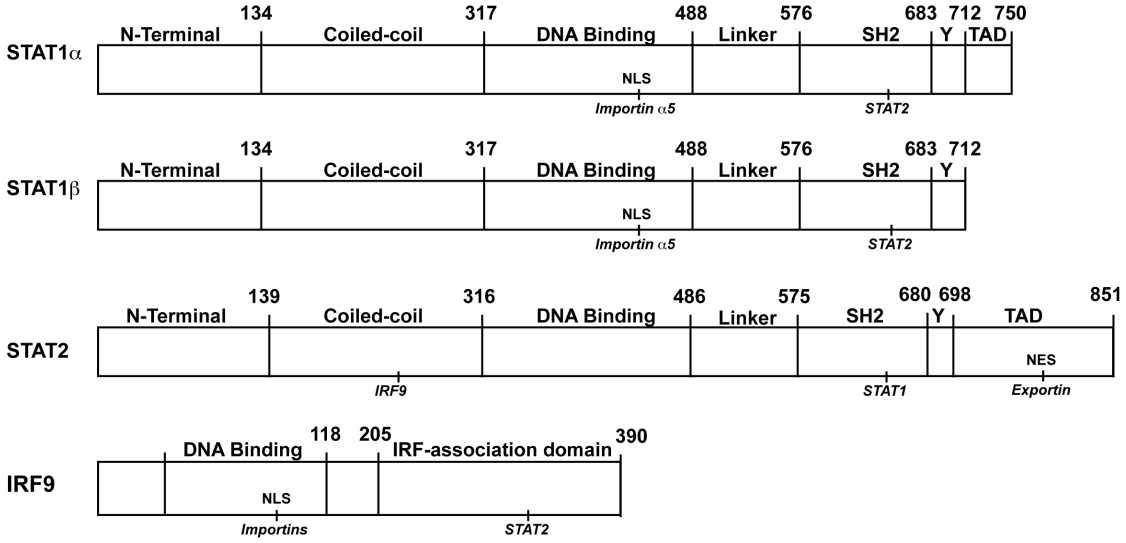

Figure 1.2: STAT1, STAT2, and IRF9 protein structure domains

In each diagram, the protein structure and functional domains of human STAT1α, STAT1β, STAT2, and IRF9 are depicted. Alternative mRNA splicing generates the longer STAT1α and shorter STAT1β isoforms. Above each diagram the functional domains are listed including the N-Terminal, Coiled-coil, DNA Binding, Linker, Src homology 2 (SH2), Phosphotyrosyl tail segment (Y), and Transactivation Domain (TAD). The numbers indicate the amino acid residue boundary of the domains. Below each diagram, the notable areas of functional interaction are highlighted. For STAT1 and STAT2, the nuclear localization signal (NLS) and interaction site with Importins and with one another are shown. For STAT2, the nuclear export signal (NES) and its binding site to Exportin are also depicted. For IRF9, the NLS and the binding site with Importins and STAT2 are indicated.

ISGF3 formation and activation through the IFN-stimulated JAK-STAT pathway

The JAK-STAT signaling cascade is a paradigm for transmission of extracellular information from specific ligands (i.e. IFN) to intracellular gene products (Stark and Darnell, 2012). Through both ligand-specific transmembrane receptors and the family of JAK and STAT proteins, target gene products are expressed and function in diverse biological processes (i.e. antiviral response). The mammalian JAK-STAT signaling model is formed on the basis of the seven STAT factors and four JAK kinases (JAK1, 2, 3 and Tyk2). Unique JAK and STAT proteins are activated in a ligand-dependent manner. When ligands bind to their cognate receptor and induce oligomerization, receptor-associated JAK kinases phosphorylate receptor tyrosine residues; this in turn creates a phosphotyrosine-SH2 recruitment site to activate latent STATs. Phosphorylation of STAT proteins induces a SH2-domain-mediated homodimerization for all STATs except STAT2, which typically heterodimerizes, resulting in active STAT transcription factors (Lim and Cao, 2006). Activated STAT dimers translocate into the nucleus to induce the expression of target genes such as ISGs.

IFN is a prototype cytokine that activates JAK-STAT signaling and ISGF3 assembly to induce ISG transcription (Ivashkiv and Donlin, 2014). In the canonical pathway, IFN binds to ubiquitously-expressed extracellular receptor chains IFN alpha receptor 1 and 2 (IFNAR1/2) and induces the oligomerization of the receptor chains (Borden et al., 2007). Receptor oligomerization brings the cytoplasmic receptor-associated JAK kinases JAK1 and TYK2 into close proximity, where they undergo reciprocal phosphorylation and phosphorylate the intracellular receptor tyrosines (Figure

1.3). Receptor phospho-tyrosine serve as SH2 domain docking sites that recruit transcription factors STAT1 and STAT2 for phosphorylation. Tyrosine phosphorylation of STAT1 Tyr701 and STAT2 Tyr690 enable reciprocal SH2-domain-mediated protein docking and heterodimerization of STAT1 and STAT2. Along with the STAT2-associated IRF9 transcription factor, the predominant transcription factor complex ISGF3 is assembled in the cytoplasm. STAT1 and STAT2 heterodimers acquire a non-typical NLS, enabling ISGF3 to bind to the importin-α5:importin-β1 nuclear transporter and translocate into the nucleus (Melen et al., 2003; Reich, 2013). In fact, the newly formed NLS from STAT1-STAT2 heterodimers coupled with the IRF9 NLS could increase the nuclear translocation efficiency of ISGF3 (Luo et al., 2004).

ISGF3 transcriptional activation of ISGs

Once ISGF3 is translocated into the nucleus, ISGF3 is directed to ISGs through a specific interaction with a consensus DNA sequence encoded at ISG promoters, 5'-AGTTTCNNTTTCNC/T-3', termed IFN-stimulated response element (ISRE) (Table 1.1, Figure 1.3) (Au-Yeung et al., 2013). The ISRE motif is a feature shared amongst primary target ISGs and is typically found at the gene promoter region. This sequence was discovered in the late 1980s from studying classical ISGs such as *IFIT2/ISG54* and *ISG15* (Levy et al., 1988; Reich et al., 1987). Verification of an ISRE at every known ISGs has not been explicitly documented, but numerous independent studies have confirmed the presence of one or more ISRE DNA motifs flanking ISG promoters (Table 1.1). IRF9 recognizes the core sequence of the ISRE, 5'-TTCNNTTT-3', while STAT1 interacts with

the 3' TTT motif, and STAT2 associates generally with GC nucleotides (Qureshi et al., 1995). Related to the ISRE motif is the IRF-E sequence, 5'-AANNGAAA-3'; it is recognized by IRF transcription factors, including IRF9 and is also the core sequence, 5'-TTTCNNTT-3', of the ISRE (Tamura et al., 2008). Although these binding sites were generally known, a recent structural analysis strengthens much of what was previously known (Horvath et al., 1996; Qureshi et al., 1995; Rengachari et al., 2018). The combined biochemical and structural information deepens our molecular view on the specificity of the ISGF3-ISRE interaction once ISGF3 is recruited to the ISG promoter and docks with specific DNA residues within the ISRE. However, since the ISG promoter does not exist as naked DNA in the cell, it is necessary to investigate the native chromatin structure ISGF3 interacts with at ISG promoters to understand the physiological interaction during the IFN-JAK-STAT signaling cascade.

In addition to binding to the ISRE, ISGF3 also recruits coactivators to ISGs as a part of its transcriptional regulation of ISGs (Au-Yeung et al., 2013; Ivashkiv and Donlin, 2014). A variety of co-regulators that function to alter chromatin and mediate Pol II assembly are known to be recruited by ISGF3 including histone acetyltransferases, chromatin remodeling factors and Mediator (Figure 1.3). Coactivator interactions with ISGF3 are primarily mediated through the STAT2 CTD. However, the STAT1α isoform can also associate with coactivators with its analogous CTD (Figure 1.2). (Jamieson et al., 2012; Lim and Cao, 2006). Since ISGF3-recruited co-activators are primarily associated through STAT2 and ISGF3 is the major STAT complex during the IFN response, it is not critical whether the ISGF3 complex contains the STAT1α or STAT1β

isoform, which lacks the transactivation domain (Bluyssen and Levy, 1997). This is in contrast to the minor STAT1 homodimer, IFNα- activated factor (AAF), formed in response to IFN (Decker et al., 1991). AAF relies on having at least one copy of STAT1α to provide the transactivation domain for co-activator recruitment. Thus, ISGF3 functions as the predominant transcription factor complex to activate ISG transcription by associating with both transcription coactivators and the ISRE at ISG promoters. The gene products of ISGs consists of diverse antiviral effectors and are essential to establishing an antiviral state that protects the cell from virus infection (Table 1.2).

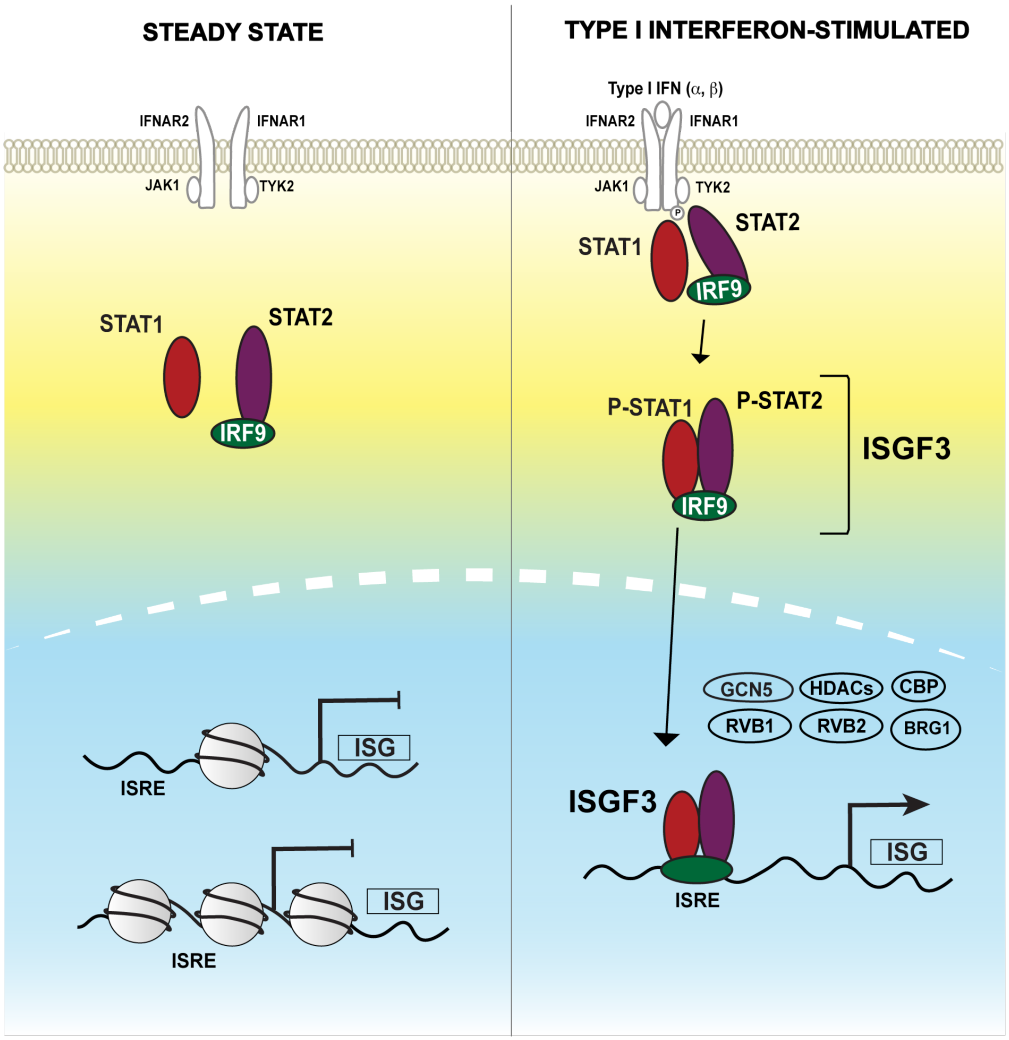

Figure 1.3 JAK-STAT signaling pathway
Illustration of the steady state (unstimulated) and type I interferon-stimulated cellular environment. (Left) During steady state, transmembrane-associated IFNAR1/2 receptor chains are associated with TYK2 and JAK1 kinases, respectively. Latent transcription factors STAT1 and STAT2 pre-associated with IRF9 are present in the cytoplasm and transiently translocate in and out of the nucleus, where transcriptionally silent ISGs are encoded in the chromatin template. (Right) IFN binding to the IFNAR1/2 receptor induces oligomerization and phosphorylation of the receptor chains by the associated TYK2 and JAK1 kinases. The phospho-IFNAR1/2 receptors provide a docking site to phosphorylate STAT2 Y690 and STAT1 Y701. Phosphorylated STAT1 and STAT2 undergo SH2-mediated dimerization forming the canonical ISGF3 complex, along with IRF9. ISGF3 translocates into the nucleus, where it recruits coactivators (GCN5, HDACs, CBP, RVB1, RVB2, BRG1) and binds to the ISRE DNA at ISG promoters.

Table 1.1: ISGs and their associated ISRE sequence(s)

Gene	ISRE sequence	Relevant source(s)
ISG15	CGGGAAAGGGAAACCGAAA	(Levy et al., 1988; Reich et al., 1987)
IFIT1/ISG56	TAGTTTCACTTTCCC	(Grandvaux et al., 2002)
IFIT2/ISG54	TAGTTTCACTTTCCC	(Levy et al., 1988)
6-16	GAGTTTCATTTTCCC	(Levy et al., 1988)
MX1	A/GAGTTTCATTTCTT(G)C	(Ronni et al., 1998)
IFITM1/9-27	AAGTTTCTATTTCCT	(Reid et al., 1989)
IFITM3/1-8U	C/TAGTTTCCTTTTCCT, TAGTTTCGGTTTCTC	(Lewin et al., 1991)
OAS1	TGGTTTCGTTTCCTC	(Rutherford et al., 1988)
CXCL10/IP10	AGGTTTCACTTTCCA	(Levy et al., 1988)
G1P2	CAGTTTCGGTTTCCC	(Levy et al., 1988)
G1P3	GAGTTTCATTTTCCC, CAGTTTCATTTTCCC	(Porter et al., 1988)
ADAR1	CGCTTTCGTTTCCTC	(George and Samuel, 1999)
PRKR/PKR	CAGTTTCGTTTTCCC	
INDO	TGGTTTCAGTTTTCC, TGGTTTCATTTTCTA	(Konan and Taylor, 1996)
BF	CAGTTTCTGTTTCCT	(Huang et al., 2001)
ISG20	CTGTTTCAGTTTCTA	(Gongora et al., 2000)

Table 1.2 ISG cellular and antiviral functions

IFN-stimulated gene effector(s)	Function(s)	References
IFITM proteins	Inhibits endocytic-fusion	(Schneider et al., 2014; Schoggins and Rice, 2011)
MX1	Blocks endocytic traffic of incoming virus and ribonucleocapsid uncoating	
IFIT proteins	Inhibits protein translation and viral RNA degradation	
ISG15	Inhibits viral translation, trafficking, and replication	
OAS proteins	Detects foreign RNA and generates 2'-5' adenylic acid to activate RNaseL	
AIM2/IFI16	Detects viral DNA	
MX2	Inhibits nuclear entry of reverse-transcribed genome; exhibits antiretroviral properties	
PKR	Degrades viral RNA	
TRIM22	Inhibits viral replication and viral protein trafficking	
CH25H	Affects viral protein maturation	
ADAR	Modifies viral and cellular RNA	

FUNDAMENTALS OF MAMMALIAN GENE REGULATION IN THE IFN SYSTEM

Many of the central principles of eukaryotic transcription regulation govern inducible mammalian gene regulation (Venters and Pugh, 2009). Eukaryotic genes are packaged within a chromatin structure, featuring a unique DNA activator element and initiator or TATA-box DNA element in its promoter. These elements direct the recruitment of specific transcription factors and transcription machinery, respectively. The specific transcription factors recruit coactivators to remodel and/or modifiy the chromatin as well as Mediator to engage Pol II for gene transcription activation.

IFN-stimulated genes (ISGs) are a group of hundreds of transcriptionally silent genes during steady state, distributed on all 23 chromosomes in a human cell, and simultaneously induced by IFN for transcription (Schneider et al., 2014). Here, steady state refers to wild-type cells that are not stimulated with IFN. Similar to other mammalian gene counterparts, ISGs exist within a chromatin structure that is configured in arrays of nucleosome particles where each nucleosome consists of a DNA-histone octamer (Luger et al., 2012). Nucleosomes can regulate gene accessibility as a physical unit occluding DNA access or chemically through nuanced histone interactions. To transcriptionally activate ISGs, the predominant IFN-activated STAT transcription factor complex, ISGF3, must interact with the chromatinized ISG core promoter and recruit coactivators, Mediator and Pol II machinery. ISGF3, primarily through STAT2, facilitates the assembly of histone-modifying and chromatin-remodeling coactivators to alter the local chromatin landscape in favor of Pol II transcriptional machinery binding and transcriptional activation.

The current understanding of several co-activator classes in the IFN system is reviewed here.

ISGF3 recruitment of coactivators to activate ISG transcription

ISGF3 association with histone modifying factors

Histone acetyltransferases (HATs) and histone deacetylases (HDACs) catalyze acetylation and deacetylation activities, respectively (Verdin and Ott, 2015). Traditional models of transcription regulation associate histone acetylation with transcription activation, and histone deacetylation with transcription repression. Since HATs were found to be cofactors for transcription activators and HDACs were found in several repressor complex, this notion was logical and generally accepted. However, for ISG transcription activation both histone acetylation and deacetylation activity are required (Chang et al., 2004; Nusinzon and Horvath, 2003; Paulson et al., 2002; Sakamoto et al., 2004).

The ISG transcription requirement for histone acetylation activity is consistent with the traditional model, where histone acetylation promotes transcription activation. HAT factors, CBP/p300 and GCN5, have been implicated for ISG activation and are recruited to ISGs through STAT2 association (Paulson et al., 2002). Yet, GCN5 activity was found to be required for STAT2 function, but not CBP/p300, suggesting specificity in histone acetyltransferase usage (Paulson et al., 2002). Both HATs have been shown to acetylate various histone residues. Consistent with HAT acetylation activity, total histone H3 and H4 acetylation have been shown to increase during the IFN response (Patel et al., 2013;

Paulson et al., 2002). Collectively, the association with HATs and increase in acetylation demonstrate the need for HAT activity during the IFN response

In contrast, it was surprising that ISG transcription also required the opposing histone deacetylation activity, as HDACs are associated with transcription repressor complexes, and this phenomenon contradicted with the traditional model (Chang et al., 2004; Kelly and Cowley, 2013; Nusinzon and Horvath, 2003). This original model was also supported by the notion that histone acetylation would destabilize the histone-DNA contact, which then enables access to the DNA for transcription. Instead, for ISGs inhibition of HDAC activity abrogated ISG expression and prevented both STAT2 and Pol II recruitment to ISGs (Sakamoto et al., 2004). Specifically, HDAC1 was shown to associate with STAT2 and negatively regulates ISG expression. These data indicated that histone deacetylation was required for ISG transcription. In agreement with the requirement for HDAC activity, histone H3 and H4 acetylation levels decreased after 1 hr IFN treatment (Nusinzon and Horvath, 2003) Another factor, pp32, has also been shown to associate with STAT2 and affects the maximal levels of ISG expression (Kadota and Nagata, 2011). It associates with HDACs both *in vitro* and *in vivo*, binds to unacetylated or hypoacetylated histones, and is a subunit of the Inhibitor of Acetyltransferase, INHAT, complex, but little is known about pp32 (Zeng and Zhou, 2002). Continued investigation is necessary to elucidate the intricacies of acetylation and deacetylation activities, but these studies to date have already uncovered the requirement of both HATs and HDACs in ISG regulation. Furthermore, the requirement of HDAC activity for positive ISG

transcription has contributed to the reconciliation of the role of HDACs beyond transcription repression.

Chromatin remodelers in the IFN response

IFN-activated ISGF3 is also known to engage proteins involved in chromatin remodeling (Figure 1.3). Remodeling subunits from the SWI/SNF or mammalian BAF/pBAF complex including BRG1, BAF200, and BAF47 are required for ISG transcription (Chi, 2004; Cui et al., 2004; Huang et al., 2002; Yan et al., 2005). Specifically, the ATPase subunit BRG1 interacts with STAT2 and is required for the transcription of a subset of ISGs indicating differential ISG regulation. Bromodomain-containing proteins such as BRG1 can bind to acetylated histone substrates, and consequently, their recruitment can be influenced by the acetylated status of the histone environment (Zeng and Zhou, 2002). This interplay between chromatin remodelers and histone acetylation has already been observed in the IFNβ gene model, where acetylated templates *in vitro* increased BRG1 recruitment, likely due to binding of the BRG1 bromodomain to the acetylated substrate (Agalioti et al., 2002; Lomvardas and Thanos, 2002). At ISGs, association of the bromodomain protein BRD4 is essential for recruitment of the transcription elongation factor pTEFb to promote ISG transcription progression (Patel et al., 2013). On the other hand, chromatin remodelers can influence the histone acetylation status. At ISGs, knockdown of the BAF47 subunit led to a decrease in histone H4 acetylation (Cui et al., 2004), which could alternatively be interpreted as a consequence of replacing an acetylated H4 with a non-acetylated H4. These examples demonstrate

the cooperativity between the ATP-dependent chromatin remodelers and histone acetylation and deacetylation activities to regulate ISG transcription (Agalioti et al., 2000).

Chromatin remodelers RVB1 and RVB2 are subunits of several chromatin remodeling complexes, including SRCAP, TIP60, URI, and INO80 (Jha and Dutta, 2009). RVB1 and RVB2 are required for ISG expression and associate through STAT2 (Gnatovskiy et al., 2013). RVB1 was found to be necessary for the recruitment of Pol II, but not for STAT2. However, the chromatin remodeling complexes that are known to contain RVB1 and RVB2 subunits were not required for ISG transcription. Both RVB1 and RVB2 feature AAA+ ATPase and Dexh box helicase domains, suggesting ATPase and helicase functions may be necessary for their activity, though their role in ISG regulation and their associated chromatin remodeling complex remain confounded.

Recruitment of Mediator and Pol II to ISGs

Mediator is a multisubunit complex that physically bridges and relays site-specific transcription factor signals to Pol II machinery for gene activation (Malik and Roeder, 2005). Up to 30 subunits are known to comprise Mediator, constituting three modules with a head, middle, and tail; and a transient association with a CDK8 module (Soutourina, 2018). For ISG transcription activation, ISGF3 has been shown to interact with Mediator subunits, MED14 and MED17 (also called DRIP150 and DRIP77), through STAT2 association (Lau et al., 2003). Specifically, MED14 enhances ISG, *IFIT2/ISG54*, expression in an ISRE-driven transcription activity assay following IFN stimulation. Structural studies have now demonstrated MED14 connects the head, middle, and tail

modules of Mediator, supporting the importance of the ISGF3 association with Mediator complex through MED14 at ISG promoters to recruit the Pol II complex.

Physical interactions through general transcription factors (GTFs), such as TFIID, connect Mediator with the Pol II complex (Soutourina, 2018). TFIID contains the TATA binding protein (TBP) subunit, which binds to the TATA box in the promoter region in one of the first steps for Pol II assembly at gene promoters. Interestingly, TBP is not required for ISG transcription, despite the presence of a TATA box at the *IFIT2/ISG54* promoter (Paulson et al., 2002). An important consequence of this transcriptional nuance for ISGs is protection against poliovirus, which is known to target TBP (Paulson et al., 2002). Thus, recruitment of a TBP-free, Pol II transcription unit is unique for promoting ISG expression.

Evaluation of the Pol II recruitment to ISGs generally supports the presence of a *de novo* Pol II, in contrast to an inactive Pol II (or paused Pol II) present at the gene promoter prior to stimulation (Adelman and Lis, 2012; Freaney et al., 2013; Mostafavi et al., 2016). Following IFN stimulation, Pol II is recruited to ISGs and activated by phosphorylation of its C-terminal domain tail by positive transcription elongational factor pTEFb through bromodomain protein BRD4 association. (Adelman and Lis, 2012; Patel et al., 2013). This results in the release of the Pol II-associated repressors NELF and DSIF, which negatively regulates ISG transcription, and enables Pol II transcription elongation to transcribe ISGs (Patel et al., 2013). The gene products of ISGs function in diverse biological processes and create an antiviral cellular environment that protects the cell from virus infection.

MOTIVATION FOR THE THESIS PROJECT

Similar to ISGs, the IFNβ gene described earlier is transcriptionally silent during steady state and activated in response to specific stimuli. Expression of IFNβ and ISGs are critical to the cell-autonomous antiviral system and regulated at multiple levels to prevent promiscuous activation, while ensuring specific transcriptional initiation in response to cognate stimuli. For IFNβ, access to the gene promoter region is highly regulated by a positioned +1 nucleosome and specific transcription factors, IRF3 and NFκB. For ISGs, relatively little was known about its nucleosome and chromatin landscape, notably at the promoter region where the ISGF3 transcription factor complex binds in response to IFN stimulation to activate ISG transcription. Yet, the native ISG chromatin organization underlies how chromatin and nucleosomes regulate access to the ISRE and the ISG DNA for transcription activation.

The aim of this thesis was to examine both the ISGF3-mediated chromatin dynamics at ISG promoters and the ISG chromatin regulation during the IFN response compared to the steady state. At the outset of this thesis project, genome-wide nucleosome occupancy in human cells was just uncovered (Schones et al., 2008; Valouev et al., 2011) and little information was available on histone post-translational modifications during IFN stimulation. Furthermore, examples of differential nuclease sensitivity at two ISG promoters, *IFITM1/9-27* and *IFITM3/1-8U*, during steady state compared to an IFN-induced state indicated IFN-induced nucleosome alteration (Cui et al., 2004; Liu et al., 2002). These data provided glimpses of the potential chromatin landscape at ISGs primarily during steady state.

A series of publicly available genome-wide deep sequencing data (mainly chromatin immunoprecipitation sequencing (ChIP-Seq)) in human cells became available in the early 2010s (Consortium, 2012), owing to the advent of commercial deep sequencing technology. These data provided more information on the steady-state chromatin architecture through ChIP-Seq data of histone variant H2A.Z and common histone modifications (i.e. H3K4me, H3K9ac) from one or more human cell lines (i.e. HeLa). However, information on the chromatin architecture and dynamics transitioning from the steady state to an IFN-stimulated state remained relatively unexplored. Since the transcription factor complex ISGF3 must engage with the chromatinized template that its target genes are configured in, determining the chromatin landscape during the steady state and the IFN-stimulated state is essential to understand the interaction and regulation that enables transcriptional activation of ISGs. This lack of information on the steady-state and IFN-stimulated ISG nucleosome landscape motivated the research described in Chapter 2 on the dynamics of the primary transcription factor complex ISGF3 and ISG nucleosomes. Discoveries from Chapter 2 prompted an in-depth examination of the composition of ISG promoter nucleosomes and led to an investigation of an unknown role for histone variant H2A.Z in the IFN response, described in Chapter 3.

CHAPTER 2.

ISGF3 AND ISG NUCLEOSOME DYNAMICS

INTRODUCTION

Hundreds of transcriptionally silent genes are activated following IFN stimulation and are collectively called IFN-stimulated genes (ISGs; (Schneider et al., 2014; Schoggins and Rice, 2011). Their gene products perform diverse cellular functions that protect the cell from virus infection, including inhibiting viral replication, nuclear trafficking, nucleocapsid unraveling, etc. (Table 1.2; (Schneider et al., 2014). A common feature at ISG promoters is the consensus DNA motif, AGAAANNNAAATA, known as the IFN-stimulated response element (ISRE; (Levy et al., 1988; Reich et al., 1987). To activate ISGs, the transcription factor complex ISGF3 must translocate into the nucleus; bind to the promoter ISRE DNA element; and assemble coactivators, Mediator, and Pol II machinery. ISGF3 navigates the genome, amidst ~60,000 genes, to locate the ISRE regulatory element unique to at least a few hundred ISGs (GENCODE, 2017). The human genome is organized by an array of nucleosome particles, which are packaged into chromatin. While this efficient mode of packaging enables the 3 billion base pairs (bp) of DNA to fit into the confines of the nuclear compartment, the naked ISRE DNA is not readily accessible. In order for ISGF3 to bind to the ISRE, it must engage the chromatinized ISG promoter. This dynamic interaction between ISGF3 and the chromatin structure is essential to gaining access to the ISRE DNA to activate ISG transcription.

Little is known about how chromatin structure and nucleosome dynamics influence ISGF3 promoter engagement at ISGs during steady state and especially following IFN stimulation. Recruitment of chromatin remodeling and histone modifying factors by STAT2, with support from STAT1, suggests chromatin alteration is essential to the

transcriptional activation of ISGs (Gnatovskiy et al., 2013; Huang et al., 2002; Nusinzon and Horvath, 2003; Paulson et al., 2002). To investigate ISGF3-mediated chromatin dynamics, examination of the chromatin changes at sites corresponding to ISGF3 recruitment is necessary.

ISGF3 is distinguished from other STAT transcription factor complexes through the heterodimerization of STAT1 and STAT2 and the presence of IRF9 (Lim and Cao, 2006). Microarray chromatin immunoprecipitation (ChIP-chip) data examining STAT1 and STAT2 occupancy on chromosome 22 following IFNα stimulation was available at the beginning of this thesis project (Hartman et al., 2005). In addition to identifying sites occupied by both STAT1 and STAT2, the ChIP-chip analysis on chromosome 22 identified STAT1 sites independent of STAT2. Many of these STAT2-independent STAT1 sites contained a related gamma-interferon-associated site (GAS) motif specific to type II IFNγ target genes. GAS sites utilize STAT1 homodimers, which can also be formed during IFNα signaling as the minor species AAF (Decker et al., 1991). Despite the lack of STAT2, some of these STAT1-only or AAF targets had upregulated gene expression indicating some ISGs may not be ISGF3 targets. In fact, without the detection of IRF9, even sites co-occupied by STAT1 and STAT2 cannot be confirmed to be ISGF3 targets. Therefore, to unambiguously identify ISGF3 targets, presence of STAT1, STAT2 and IRF9 is necessary. However, no genome-wide data examining all three ISGF3 factors at ISGs had been performed at the time of this thesis project. This gap has now been filled with STAT1, STAT2, and IRF9 chromatin immunoprecipitation deep sequencing (ChIP-Seq) data presented in Chapter 2.

With the timely advent of next generation sequencing at the start of this project, genome-wide studies became feasible. At the time, ChIP-Seq of the related STAT1 homodimer complex in the type II IFNγ systems was a prototype for examining mammalian transcription factors (Robertson et al., 2007). Simultaneously, genome-wide methods for nucleosome occupation were being pioneered in lower eukaryotes with small genomes (Kaplan et al., 2009; Lee et al., 2007); the size of the yeast genome is approximately 12.1 Mbp, while the human genome is 3300 Mbp which is over 270 times larger. These methods were promising for the examination of ISGF3 genome-wide; however, they could not couple sites of ISGF3 recruitment with nucleosome occupancy changes during the IFN response to enable correlation of ISGF3 with IFN-mediated chromatin changes. The standard sequencing yield at the time was about 10-20 million unique sequencing reads per experiment and was sufficient depth for transcription factor coverage in the genome (Consortium, 2012; Kchou et al., 2017). On the other hand, nucleosomes occupy ~75-90% of the genome and to achieve a sequencing depth of 16-28 times the human genome required about 300-600 million reads (Richmond and Davey, 2003; Valouev et al., 2011). Although this level of 16-28 times the sequencing coverage was sufficient for determining steady state nucleosome occupancy, it may still not be sufficient for examining and quantifying subtle IFN-induced nucleosome changes in human cells.

A novel method developed by Erbay Yigit in Jonathan Widom's lab at the time was the state-of-the-art solution to overcome this challenge of sequencing coverage and depth (Yigit et al., 2013). This method utilized bacterial artificial chromosomes (BAC) to directly

select and enrich for specific genomic target regions and was named BAC-Enriched Mono-nucleosomal DNA sequencing (BEM-seq) (Appendix C). Through the direct selection method coupled with micrococcal nuclease (MNase) deep sequencing, individual ISG genomic regions could be enriched hundreds of fold higher, enabling more confident assignment to IFN-induced nucleosome dynamics. Furthermore, adaptation of this procedure to the IFN locus was ongoing in the lab (Freaney et al., 2014).

To investigate ISGF3-mediated interactions with the native chromatin, ISGF3 localization at ISGs and nucleosome organization was characterized using chromatin immunoprecipitation sequencing (ChIP-Seq) and targeted high-resolution nucleosome position analysis of 20 representative ISGs, respectively. ChIP-quantitative PCR (qPCR) assays of STAT1, STAT2, and IRF9 recruitment was performed to identify ISGF3 recruitment at a relevant snapshot of time during the IFN response. Parallel analyses of ISGF3 ChIP-Seq and nucleosome profiles at individual ISGs correlate ISGF3 activity to the corresponding nucleosome alterations during ISG transcriptional activation. Together, these experiments could identify genomic target sites that undergo IFN-induced, ISGF3-mediated chromatin remodeling to activate ISG transcription.

RESULTS

IFN-INDUCED ISGF3 RECRUITMENT GENOME-WIDE

Temporal analysis of ISGF3, Pol II, and ISG dynamics

The response to IFN signaling is rapid from the onset of IFN engaging its cellular surface receptor to the attenuation of the primary ISG transcriptional activity (Stark and Darnell, 2012). Examining chromatin dynamics mediated by ISGF3 during the IFN response from a snapshot in time requires determining the temporal recruitment of ISGF3 and ISG transcription initiation. A time course of IFN-induced STAT1, STAT2 and IRF9 recruitment to a representative ISG, *OAS3*, was performed to delineate the temporal dynamics of ISGF3 recruitment. Low levels of ISGF3 recruitment can be seen as early as 15 min to 1 hr (Figure 2.1A-C). These initial recruitment events likely represent the earliest assembled ISGF3 complexes bound to chromatin and corroborate with the timing of the preceding events identified from previous studies - assembly of ISGF3 and translocation into the nucleus happens within 30 min of IFN stimulation (Larner et al., 1984; Levy et al., 1989). The ChIP-qPCR time course experiments demonstrate maximal levels of ISGF3 recruitment to *OAS3* occur after 2 hr IFNα treatment, and continue at least until 4 hr IFNα treatment (Figure 2.1A-C). Attenuation is observed after 6 hr IFNα treatment for STAT1, STAT2, and IRF9 at *OAS3* (Figure 2.1A-C).

Interestingly, maximal levels of all three ISGF3 components to *OAS3* are achieved within a similar time frame of 2-6 hr, but their respective maxima differ. While the recruitment of STAT1 and STAT2 occurs maximally after 2 hr of IFN stimulation, the

maximum recruitment of IRF9 was not achieved until 4 hr post-IFN. Since IRF9 can readily translocate in and out of the nucleus due to an NLS (Lau et al., 2000), its retention time or nuclear presence may be extended and appear longer in the ChIP-qPCR time course assays. An attenuated STAT1 and STAT2 signal after 6 hr IFN corresponds to dephosphorylated STAT1 and STAT2 and the nuclear export of the dephosphorylated ISGF3 complex (Banninger and Reich, 2004; Lee et al., 1997).

Correspondingly, the temporal patterns of Pol II association at *OAS3* are in accordance with ISGF3 recruitment dynamics with increased Pol II occupancy from 1-4 hr IFNα treatment and attenuating by 6 hr (Figure 2.1D). This is further confirmed by gene expression patterns of three representative ISGs, *OAS3*, *IFIT1/ISG56,* and *IFITM1/9-27*, with an evident upregulation around 1-2 hr IFNα treatment and increasing until its peak expression generally around 6-8 hr IFNα stimulation (Figure 2.1E). Cumulatively, these data suggest ISGF3-mediated activation of ISG transcription operates within a time frame of ~30 min to 6 hr. Maximal levels of the key ISGF3 and Pol II recruitment occurs between 2-4 hrs. Thus, to examine maximal recruitment of ISGF3 genome-wide and associate ISGF3-mediated chromatin dynamics during the relevant transcription initiation processes, IFN-induced nucleosome dynamics should be observed at 2 hr based on the ChIP-qPCR time course assays. These results set the parameters for ISGF3 ChIP-Seq and ISG nucleosome analyses.

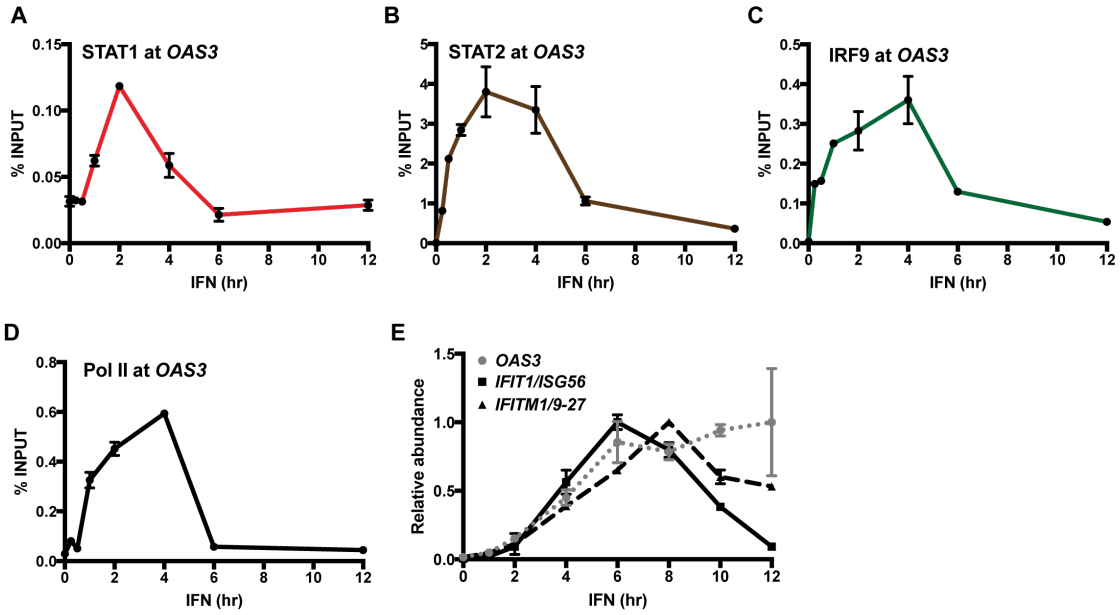

Figure 2.1 IFN-stimulated ISGF3 recruitment

ChIP analysis of IFNα-induced (A) STAT1, (B) STAT2, and (C) IRF9 at the *OAS3* promoter locus in HeLa cells after mock treatment (0 min) or IFNα stimulation for 15 min, 30 min, 1 hr, 2 hr, 4 hr, 6 hr and 12 hr. (D) ChIP analysis of IFNα-induced Pol II CTD recruitment as in (A-C). (E) Gene expression analysis of *OAS3*, *IFIT1*/*ISG56* and *IFITM1/9-27* after mock treatment (0 hr) or 1 hr, 2 hr, 4 hr, 6 hr, 8 hr, 10 hr, or 12 hr IFNα treatment. Relative gene expression abundance is normalized to *GAPDH*.

ChIP-Seq sample library generation

Utilizing the temporal information from the previously described ChIP-qPCR and mRNA analyses (Figure 2.1), a genome-wide analyses of ISGF3 was carried out using the mock- and 2 hr IFNα-treated STAT1, STAT2 and IRF9 ChIP-Seq libraries. Examination of ISGF3 recruitment after 2 hr of IFN treatment would yield maximal detection of ISGF3 at ISG targets compared to steady state (mock). Briefly, as depicted in Figure 2.2A, 5 x 10^7 – 1 x 10^8 HeLa cells were crosslinked with formaldehyde and chemically lysed to isolate the chromatin-containing nuclei (Appendix C). The chromatin was sonicated to ≤1000 bp, immunoprecipitated with STAT1, STAT2, and IRF9 antisera conjugated to magnetic beads, and then the ChIP DNA was eluted. The ChIP DNA was subjected to reverse crosslinking and purified (Figure 2.2A). Approximately 3% of the ChIP DNA was tested to verify and select the sample with the maximal immunoprecipitation of target loci, prior to generating a sequencing library with the remaining sample (Figure 2.1-2.2).

To generate the ChIP library for sequencing on the SOLiD 5500xl platform, ChIP DNA was prepared according to the ABI SOLiD 5500xl library preparation protocol. Generally, the ChIP DNA ends were digested (end-polished) to generate blunt-end fragments and size-selected to more accurately represent the regions bound by STAT1, STAT2, and IRF9. Too large of DNA fragments could inadvertently misconstrue the true binding site for these transcription factors. Though the size of DNA fragments could be further reduced by increasing the sonication time or power, the drawback is the potential disruption of STAT1, STAT2 or IRF9 bound to the chromatin. Following size selection, a

dA-tail is added to generate an overhang that enables ligation of a corresponding SOLiD 5500xl DNA adaptors, dT-tailed P1 and barcoded P2. Using a primer specific to the P1 adaptor, 11-13 cycles of PCR was performed to amplify the DNA sample. These samples were analyzed on the Bioanalyzer as a quality check for an appropriate range of DNA products (~250 bp) for deep sequencing.

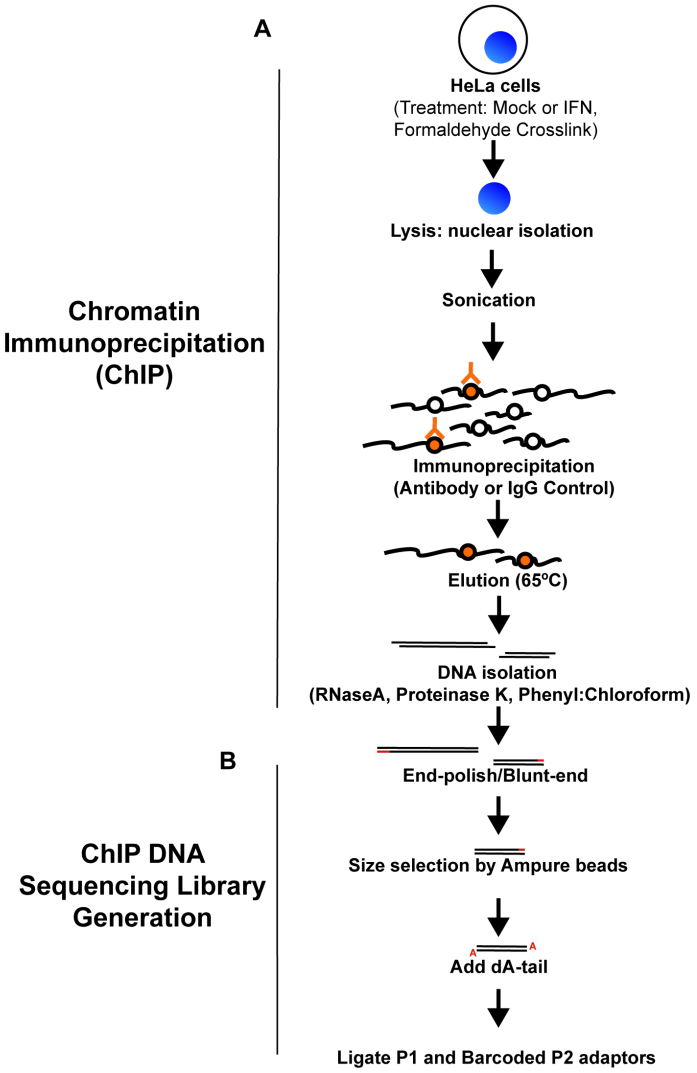

Figure 2.2: Chromatin immunoprecipitation and library generation procedure

Illustration of the procedure to generate a chromatin immunoprecipitation sequencing library. (A) HeLa cells are mock-treated or IFN-treated for 2 hrs and crosslinked with formaldehyde prior to cellular lysis and nuclear isolation. Disruption of the nuclei and shearing of the chromatin by sonication is followed by STAT1, STAT2 or IRF9 immunoprecipitation of the corresponding protein-bound chromatin fragments. Chromatin immunoprecipitated (ChIP) DNA was isolated following elution at 65ºC, digestion of RNA and proteins by RNase A and Proteinase K, respectively, phenyl:chloroform extraction and ethanol precipitation. (B) Following the ChIP procedure depicted in (A), ChIP DNA is digested to blunt ends, size selected, then ligated with a dA-tail followed by addition of SOLiD adaptors P1 and P2 to generate the library for SOLiD 5500xl deep sequencing.

ISGF3 genome-wide occupancy and characterization

ChIP DNA was subjected to next generation sequencing on the SOLiD 5500xl sequencer and reads were aligned to the human genome (hg19/GR37 build) using the Bioscope software (Figure 2.3, Appendix C). Only uniquely mapped reads were retained for further analysis. Peaks were identified using the MACS software (p-value ≤ 1 x 10^{-5} ; (Zhang et al., 2008). Further analysis of ChIP STAT1, STAT2, and IRF9 (ISGF3) target sites were performed with the HOMER software and visualized using Galaxy tools and the UCSC genome browser (Afgan et al., 2016; Heinz et al., 2010; Kent et al., 2002). Approximately 13-22 million sequencing reads were obtained among the three ISGF3 factors (Table 2.1).

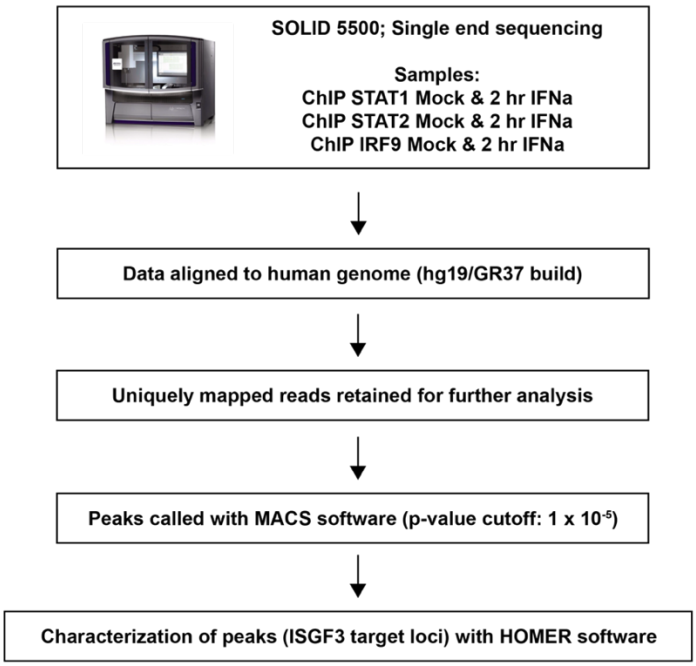

Figure 2.3: Bioinformatic analysis procedure for ISGF3 ChIP-Seq data analysis
Flowchart of bioinformatic data processing workflow following SOLiD 5500xl single-end DNA sequencing.

Table 2.1: ChIP-Seq results of STAT1, STAT2 and IRF9 reads

ChIP sequencing reads and peaks identified from MACS software analysis of ChIP

	STAT1		STAT2		IRF9		INPUT
	Mock	IFN	Mock	IFN	Mock	IFN	
Total Reads Mapped	13,586,577	22,440,449	17,324,511	15,590,548	16,242,700	13,510,886	17,927,477
Unique Reads	8,081,674	13,144,306	11,344,570	10,344,514	9,528,712	7,980,137	N/A
Peaks (4-fold over INPUT)	617	5714	2262	4158	1511	3212	N/A
Diff peak (2-fold over Mock)	2531		3209		2129		N/A

STAT1, STAT2, and IRF9 samples from mock- and 2 hr IFNα-treated HeLa cells.

Specific recruitment of ISGF3 was observed throughout the genome following IFN stimulation, with STAT1, STAT2 and IRF9 recruitment to 2531, 3209, 2129 target loci, respectively, based on a 2-fold increase over Mock samples (Table 2.1, Figure 2.4, Appendix C). A strong localization at the IFN-stimulated target peak center is apparent in IFN-stimulated samples compared to Mock samples (Figure 2.4A). During steady state, STAT1, STAT2, and IRF9 reside in the cytoplasm with only transient nuclear translocation (Lau et al., 2000; Lim and Cao, 2006), thus little to no signal at any specific genomic site would be expected. Sequence reads detected in mock samples represent a random population of DNA, where no specific DNA is enriched over another and serve as the background signal. In contrast, in IFN-treated samples STAT1, STAT2 and IRF9 have translocated into the nucleus and are bound at target chromatin. Higher sequencing reads observed at the IFN-treated over mock-treated samples for all three factors confirm efficient ChIP signal over background signal, providing confidence for further analysis and characterization of ISGF3 binding (Figure 2.4A, Table 2.1).

The most frequent *de novo* motif discovered for STAT1, STAT2, and IRF9 was the ISRE, further validating the specificity of ISGF3 to ISRE target sites (Figure 2.4B). The ISRE motif is referred interchangeably in literature as AGTTTCNNTTTCNC/T or its complementary TCAAAGNNAAAGNG/A. In addition to the ISRE motif, other significant motifs were discovered (Table 2.2). In particular, both STAT2 and IRF9 bound to a similar percent of targets with the TGANTCA motif. This motif was not detected for STAT1, but may reflect the higher efficiency of the STAT2 and IRF9 antibody during the immunoprecipitation. The TGANTCA motif is identified as a Fra1/bZIP motif. The bZIP

motif is structurally recognized by basic region leucine zipper (bZIP) proteins including the FRA1 transcription factor from the Fos family of proteins which includes AP-1, JunD, etc (Mechta-Grigoriou et al., 2001). The Fos family of proteins have implicated roles in the immune response and oncogenesis.

Similar to other human transcription factors, IFN-activated STAT1, STAT2 and IRF9 occupy a large number of loci annotated as intergenic and intronic regions (Fig 2.4C) (Freaney et al., 2013; Schmidt et al., 2010). Whether these intergenic and intronic sites bound by STAT1, STAT2 or IRF9 represent functional sites remain to be investigated. Notably, a greater proportion of STAT2 and IRF9 mapped to TSS loci compared with STAT1 and may reflect the unique and obligatory association of STAT2 and IRF9 in gene regulation (Banninger and Reich, 2004).

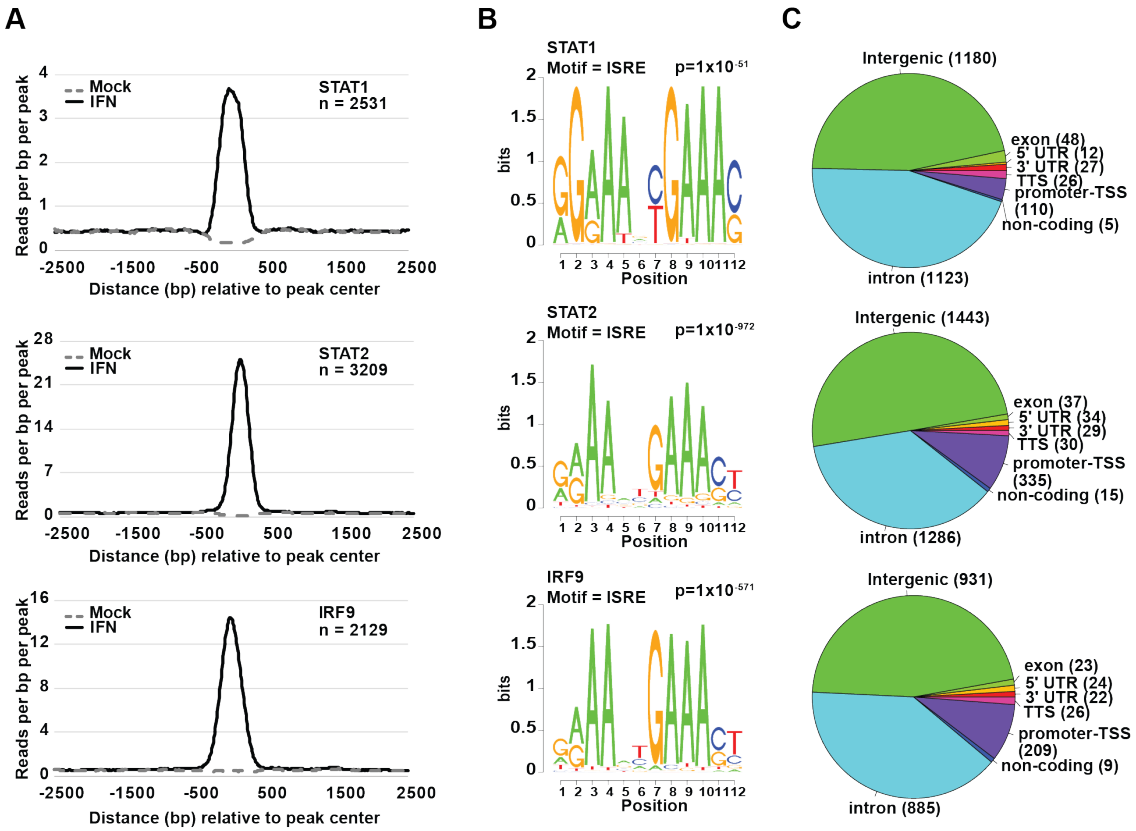

Figure 2.4: STAT1, STAT2 and IRF9 (ISGF3) ChIP-Seq characterization

(A) Normalized sequencing tag density of mock-treated (dashed line) and IFNα-stimulated (solid line) reads from STAT1 (top), STAT2 (middle) and IRF9 (bottom) binding at 2531, 3209 and 2129 genomic loci representing sites with a ≥ 2-fold increase in occupancy after IFNα treatment. Tag density is computed 2500 bp upstream and downstream of the peak center and is grouped into 10 bp bins. (B) DNA sequence logo of the most frequent *de novo* motif identified from 2531 STAT1 peaks (top), 3209 STAT2 peaks (middle) and 2129 IRF9 peaks (bottom) as described in Table 2.1. For each position, the sequence logo bit height corresponds to its relative frequency within the sequence. The associated motif name and p-value are identified above the logo. (C) Distribution of specific annotated DNA (intergenic, intron, promoter-TSS, exon, 5' UTR, 3' UTR, non-coding) and the corresponding number of peaks from 2531 STAT1 peaks (top), 3209 STAT2 peaks (middle), and 2129 IRF9 peaks (bottom).

Table 2.2: *De novo* motif analysis of STAT1, STAT2, and IRF9

De novo motifs identified from ChIP STAT1, STAT2, and IRF9 sequencing reads using the HOMER software.

Rank	STAT1 Motif	p-value	% of Targets	% of Background
1		1e-51	2.88%	0.24%
2		1e-20	10.15%	5.46%
3		1e-19	14.90%	9.18%
4		1e-17	44.25%	35.85%

The rank is based on the p-value of the most significant motifs bound. The corresponding p-value and percent (%) of the reads in the target and background for each motif is listed.

Rank	STAT2 Motif	p-value	% of Targets	% of Background
1		1e-972	30.91%	1.47%
2		1e-155	28.17%	11.02%
3		1e-144	15.61%	4.05%
4		1e-43	24.71%	15.28%

The rank is based on the p-value of the most significant motifs bound. The corresponding p-value and percent (%) of the reads in the target and background for each motif is listed.

Rank	IRF9 Motif	p-value	% of Targets	% of Background
1		1e-571	29.50%	1.65%
2		1e-94	17.61%	5.16%
3		1e-39	36.92%	24.03%
4		1e-32	11.60%	4.99%

The rank is based on the p-value of the most significant motifs bound. The corresponding p-value and percent (%) of the reads in the target and background for each motif is listed.

IFN-MEDIATED NUCLEOSOME DYNAMICS AT ISGS

ISGF3 access to the ISRE DNA element requires interaction with the chromatinized ISG promoter template. Several studies have implicated chromatin-remodeling factors and histone-modifying factors as ISGF3 coactivators. These coactivators are commonly recruited by the strong STAT2 transcriptional activation domain, often with support from STAT1 (Chang et al., 2004; Gnatovskiy et al., 2013; Huang et al., 2002; Nusinzon and Horvath, 2003; Paulson et al., 2002). Employment of these specialist factors suggests alteration of the chromatin landscape is required. However, little is known about the chromatin dynamics and regulation at ISGF3 target genes. To determine the nucleosome changes within the ISG chromatin environment and ensure sufficient signal enrichment is achieved, BAC-based direct selection micrococcal nuclease (MNase) sequencing (also referred as BEM-seq) was performed.

Direct selection MNase sequencing library generation and quality control

Ten BACs were used to enrich for the genomic loci of 20 representative ISGs (Appendix C). These ISGs were selected based on several criterion including well-characterized ISGs, differential requirement based on previous studies and/or clustered within a genomic region encoded by a single BAC (Table 2.3; Gnatovskiy et al., 2013; Huang et al., 2002; Tenoever et al., 2007). Mononucleosomes from mock and IFN-treated samples were isolated following MNase digestion, BAC hybridization, and adaptor ligation to generate barcoded genomic loci of 20 representative ISGs (Figure 2.5, Appendix C). To ensure the barcoded sample contains directly selected ISG regions,

approximately 1 μl of the barcoded sample was cloned into a TOPO vector, transformed into DH5α bacteria and ~50 bacterial colonies were sequenced to verify ISG direct selection efficacy for deep sequencing. Most of the colonies sequenced (~86-92%) contained a sequence that matched one of the ten BAC-encoded regions (Table 2.4).

Table 2.3: Direct selection nucleosome selection criteria and summary

Gene	Known ISGF3 Targets	Cluster		Locus	Gene Size (bp)	Total Nucleosomes	Nucleosomes per bp
IFIT1 (ISG56)	✓	✓		chr10:91,152,322-91,163,742	11,420	64	0.0056
IFIT2 (ISG54)	✓			chr10:91,061,706-91,069,032	7,326	35	0.0048
IFIT3 (ISG60)	✓			chr10:91,092,239-91,100,724	8,485	47	0.0055
IFIT5				chr10:91,174,325-91,180,758	6,433	21	0.0033
ISG15	✓			chr1:948,847-949,915	1,068	6	0.0056
IFITM1 (9-27)	✓	✓		chr11:313,991-315,271	1,280	6	0.0047
IFITM2				chr11:308,107-309,409	1,302	9	0.0069
IFITM3 (1-8U)	✓			chr11:319,673-320,914	1,241	10	0.0081
IFITM5				chr11:298,203-299,526	1,323	7	0.0053
OAS1	✓	✓		chr12:113,344,739-113,357,711	12,972	66	0.0051
OAS2	✓			chr12:113,416,274-113,449,527	33,253	172	0.0052
OAS3	✓			chr12:113,376,249-113,411,052	34,803	177	0.0051
MX1	✓	✓		chr21:42,797,978-42,831,140	33,162	165	0.0050
MX2	✓			chr21:42,733,950-42,780,869	46,919	227	0.0048
STAT1				chr2:191,833,762-191,878,976	45,214	222	0.0049
STAT2				chr12:56,735,384-56,753,909	18,525	85	0.0046
IFI6 (6-16)	✓			chr1:27,992,572-27,998,724	6,152	23	0.0037
AIM2		✓		chr1:159,032,275-159,046,647	14,372	61	0.0042
IFI16				chr1:158,979,682-159,024,943	45,261	204	0.0045
IFI27	✓			chr14:94,577,079-94,583,033	5,954	30	0.0050

Summary of the rationale in selecting 20 representative ISGs for nucleosome profiling and characterization of the ISG nucleosome composition (total nucleosomes, average nucleosome per bp).

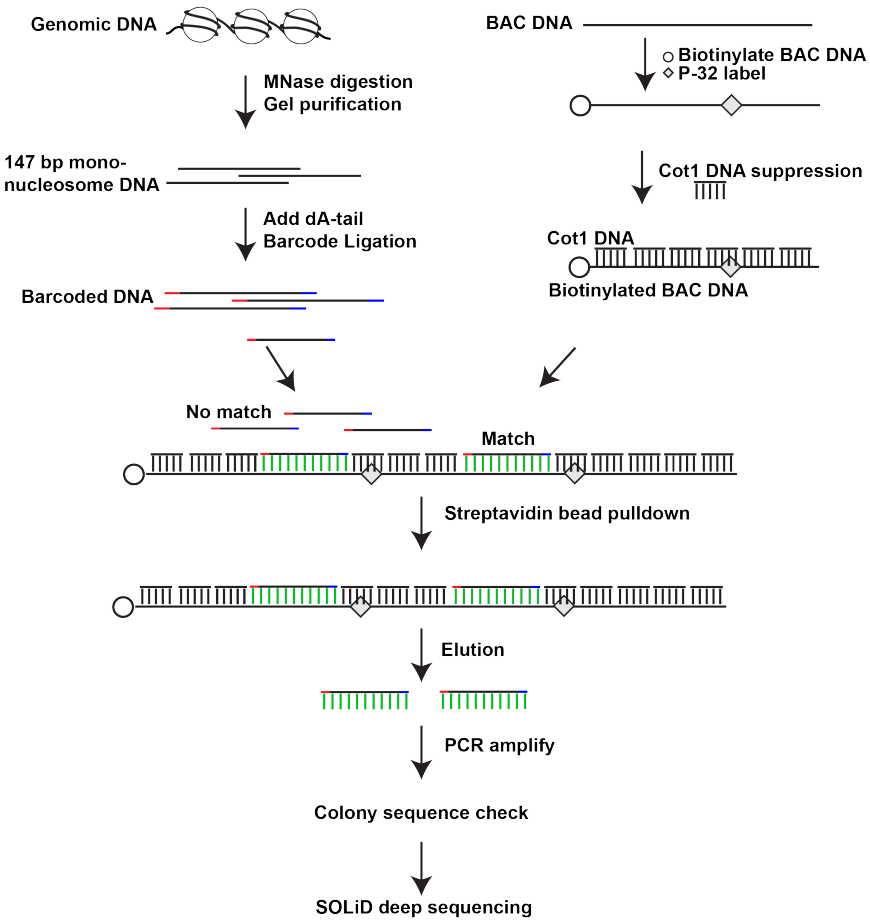

Figure 2.5: Direct selection micrococcal nuclease sequencing library generation workflow

Diagram of direct selection of mononucleosomal DNA and library generation for SOLiD 5500xl deep sequencing. (Top left) Isolated genomic DNA is digested with micrococcal nuclease (MNase) into nucleosomal fragments. Mononucleosome-sized (~147-167 bp) fragments were purified and subjected to a series of library preparatory steps including dA-tail addition and ligation of barcoded DNA adaptors. To directly select for genomic regions corresponding to 20 specific ISGs, the barcoded mononucleosome DNA was hybridized to (Top right) 10 corresponding bacterial artificial chromosomes (BACs) that were P32-label and biotinylated and suppressed with Cot-1 DNA for repetitive regions. (Bottom) Hybridized ISG matches were pulled down with the biotinylated BACs using streptavidin-conjugated magnetic beads. Hybridized or direct selection genomic ISG DNA were eluted from the streptavidin-biotin BAC and PCR amplified. A sample of the eluted DNA library was colony sequenced to ensure enrichment of the BAC regions corresponding to the 20 ISGs. The verified DNA library was subjected to SOLiD 5500xl deep sequencing.

Table 2.4: Number of positive colonies sequenced containing BAC region

	# positive colonies out total sequenced
Mock	43 out of 48
2 hr IFNα	44 out of 48
6 hr IFNα	51 out of 59
10 hr IFNα	37 out of 42

Direct selection MNase deep sequencing and bioinformatic analysis

Taking advantage of the BAC-based direct selection MNase sequencing method enabled direct selection and enrichment of gene regions of interest to achieve sufficient sequencing depth of mononucleosomal ISG DNA (Figure 2.5). Following alignment of the sequencing reads to the human reference genome hg19/GR37, uniquely mapped sequencing reads were retained for further analysis. Nucleosome maps were generated using the Dynamic Analysis of Nucleosome Positioning and Occupancy Software (DANPOS) software or center-weighted algorithm and visualized with the UCSC genome browser (Chen et al., 2013; Freaney et al., 2014; Kent et al., 2002). Changes in nucleosome occupancy from IFN treatment were quantified from the unique sequence reads using the DANPOS software (Figure 2.6). Enrichment of the genomic loci of 20 ISGs achieved over 400-fold read coverage (Table 2.5). High-resolution nucleosome maps of 20 representative ISGs during steady state and after IFN stimulation were generated (Figure 2.7-2.9). Nucleosome profiles following 2 hr, 6 hr and 10 hr of IFN stimulation were determined to correlate with the recruitment and attenuation kinetics of ISGF3 and ISG transcription. Selection of the IFN treatment timing was based on the temporal information of ISGF3 recruitment and transcription activity that guided the ISGF3 ChIP-Seq experiments (Figure 2.1, 2.4). Well-positioned nucleosomes were found at the 20 ISGs in HeLa cells at steady state and were similar to data from other cell lines (i.e. GM, K562) available on the UCSC genome database (Figure 2.7-2.9; Consortium, 2012).

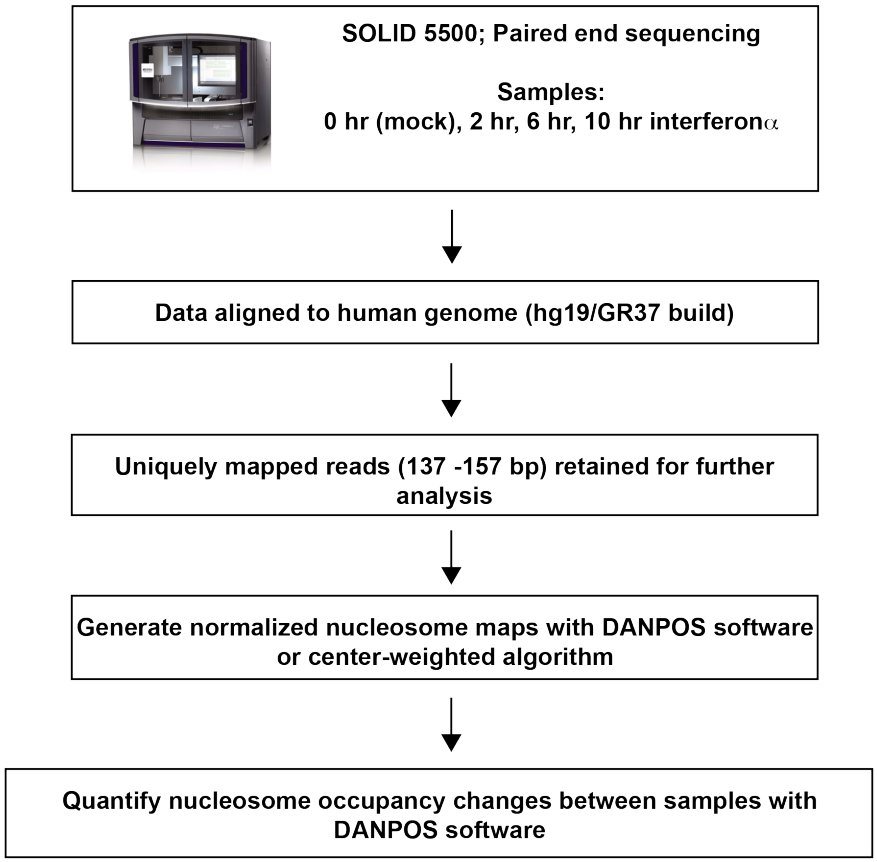

Figure 2.6: Bioinformatic pipeline of direct selection nucleosome sequencing data analysis

Flowchart of the bioinformatic data processing workflow following SOLiD 5500xl DNA sequencing. Sequencing reads were aligned to the human genome build hg19/GR37 using Bowtie software for paired-end sequencing reads. Uniquely mapped reads of approximately 137-157 bp were retained for further analysis. Nucleosome maps were generated via a center-weighted algorithm or the DANPOS software and loaded onto the UCSC genome browser directly or via the Galaxy online interface. Nucleosome occupancy changes were quantified using the DANPOS software.

Table 2.5: Direction selection nucleosome sequencing reads and fold coverage summary

Total and unique sequencing reads from each sample and the read coverage enrichment calculated from (number of reads x 147 bp)/(1758135 bp length of BACs).

	Total reads	Unique reads	137-157 bp reads	Read coverage (fold)
Mock	104,796,614	55,463,526	6,720,135	562
2 hr IFNα	106,756,227	56,949,366	4,302,688	360
6 hr IFNα	94,274,867	51,243,148	5,050,067	422
10 hr IFNα	103,862,266	55,437,595	7,280,912	608

Nucleosome profiles and ISGF3 occupancy of 20 representative ISGs

To correlate ISG nucleosome dynamics with sites of ISGF3 interaction, STAT1, STAT2, and IRF9 ChIP-Seq data (Figure 2.4) were used to accompany the ISG nucleosome profiles in genome browser maps (Figure 2.7-2.9). Comparing mock-treated and IFN-stimulated nucleosome samples over time allows observation of ISGF3 recruitment and corresponding changes to the nucleosome positions. Consistent with contemporary models of nucleosome positioning (Radman-Livaja and Rando, 2010), most of the 20 ISGs were found to have well-positioned nucleosomes in the ISRE region at steady state, with varying degrees of promoter demarcation by nucleosome-depleted regions (NDRs; Figure 2.7-2.9). Unlike textbook depictions of a +1 nucleosome located directly downstream the TSS and occupying approximately 150 bp, variations of the positioning of nucleosomes relative to the TSS are observed. These variations may reflect the differential packaging and compaction unique to each ISG.

Gene-specific variations include those with well positioned +1 and NDR nucleosomes (Figure 2.7A), +1 and -1 nucleosomes (Figure 2.7B), only -1 nucleosomes (Figure 2.8A), and genes with no apparent NDR (Figure 2.8B), or those with only +1 nucleosomes (Figure 2.8C). The -1 and +1 positions are defined here as approximately 150 bp (nucleosome size) upstream or downstream of the TSS. Additionally, some ISG promoters did not contain a common +1 or -1 nucleosome category and had relatively lower nucleosome signal compared to adjacent nucleosomes in the 5' intergenic region (Figure 2.9). Accumulating literature suggests genomic regions that are devoid of a nucleosome signal or feature a characteristic NDR might not truly lack nucleosomes, but

instead may represent fragile nucleosomes more susceptible to nuclease digestion (Kubik et al., 2015; Voong et al., 2016). In all cases, IFN stimulation resulted in decreased nucleosome positioning strength, with clear disruption over the course of IFN treatment followed by a return to steady state. In most cases this is evident from a loss of an ISRE-proximal nucleosome (arrows in Figure 2.7-2.9).

To quantify the nucleosome loss, the DANPOS software (Chen et al., 2013) was used to indicate changes to nucleosome positions with a p-value ≤ 1×10^{-5} following IFN stimulation. The normalized tag counts between mock-treated and IFN-treated samples confirmed statistically significant nucleosome loss at ISG promoters that propagated over time throughout the gene bodies (red bars in Figure 2.7-2.9). Similar to an analogous ATAC-seq dataset quantifying chromatin accessibility following IFNβ induction in B cells (Mostafavi et al., 2016), increased chromatin accessibility was observed at the TSS for IFN-induced ISGs. Specifically, within the 20 ISGs examined the most prominent chromatin alterations coincided with strong ISGF3 peaks and well-positioned nucleosomes (i.e. *OAS1*), but not strictly at the TSS (i.e. *ISG15*).

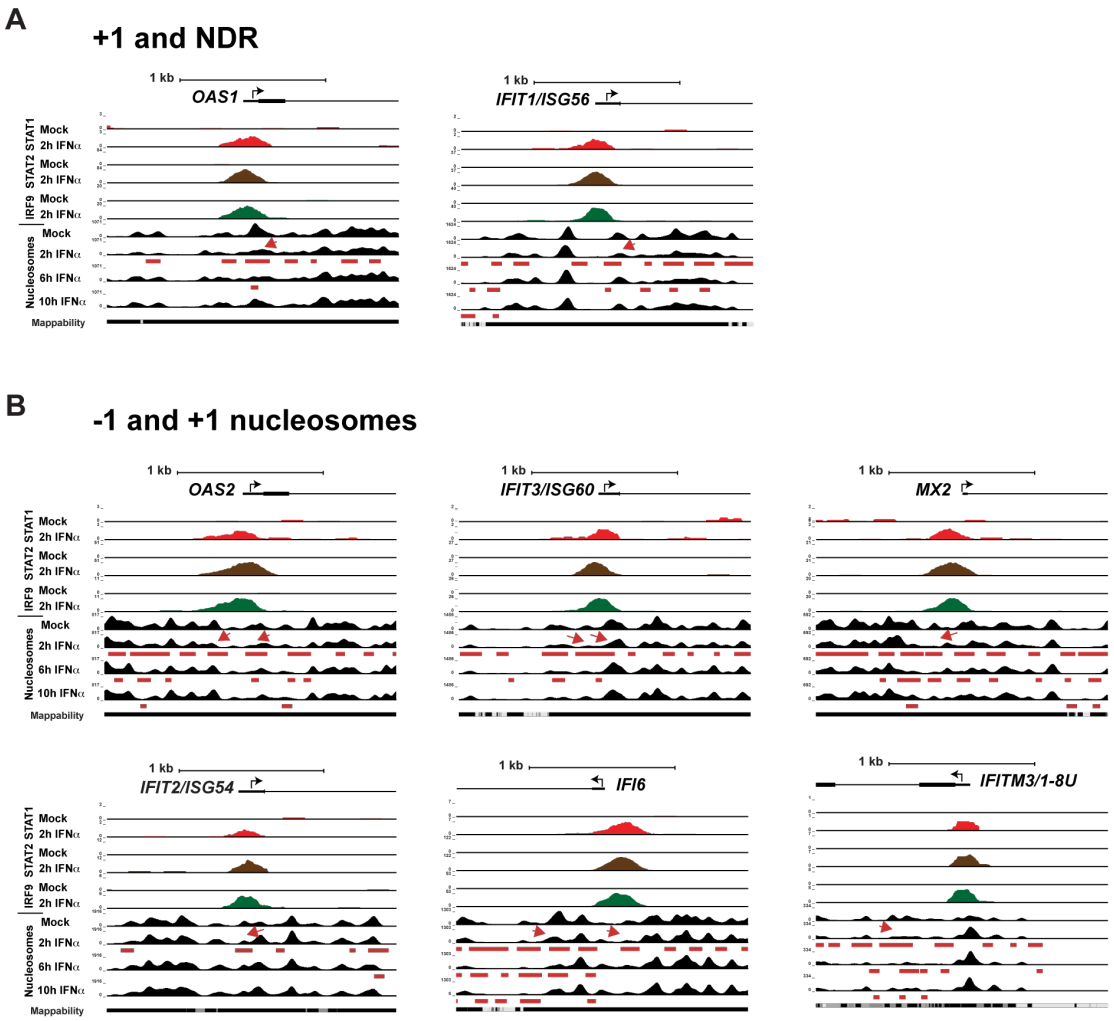

Figure 2.7: IFN-stimulated nucleosome reorganization at ISGs with +1 and NDR or -1 and +1 nucleosome configuration

Genome browser diagram of IFN-induced ISGF3 recruitment and nucleosome dynamics at select ISGs within 2000 bp +/- TSS. (A) ISGs, *OAS1* and *IFIT1/ISG56*, with a +1 and nucleosome depleted region (NDR). (B) ISGs, *OAS2*, *IFIT3/ISG60*, *MX2*, *IFIT2/ISG54*, *IFI6*, and *IFITM3/1-8U*, with -1 and +1 nucleosomes. (A-B) (Top) 5' end of gene depicted with the black arrow depicting the direction of transcription, the small and large black bars represent untranslated and exonic regions, respectively, and the line represents intronic regions. (Middle) ChIP-Seq density of STAT1, STAT2 and IRF9 occupancy after mock or 2 hr IFNα treatment in HeLa cells. (Bottom) Nucleosome occupancy after mock, 2 hr, 6 hr, or 10 hr IFNα treatment in HeLa cells. Red arrows highlight nucleosome loss at ISGF3-ISRE proximal regions. Red bars beneath nucleosome maps denote nucleosome loss due to 2 hr, 6 hr, or 10 hr IFNα treatment compared to Mock (p-value ≤ $1x10^{-5}$). All sequencing reads are normalized to 10 million reads.

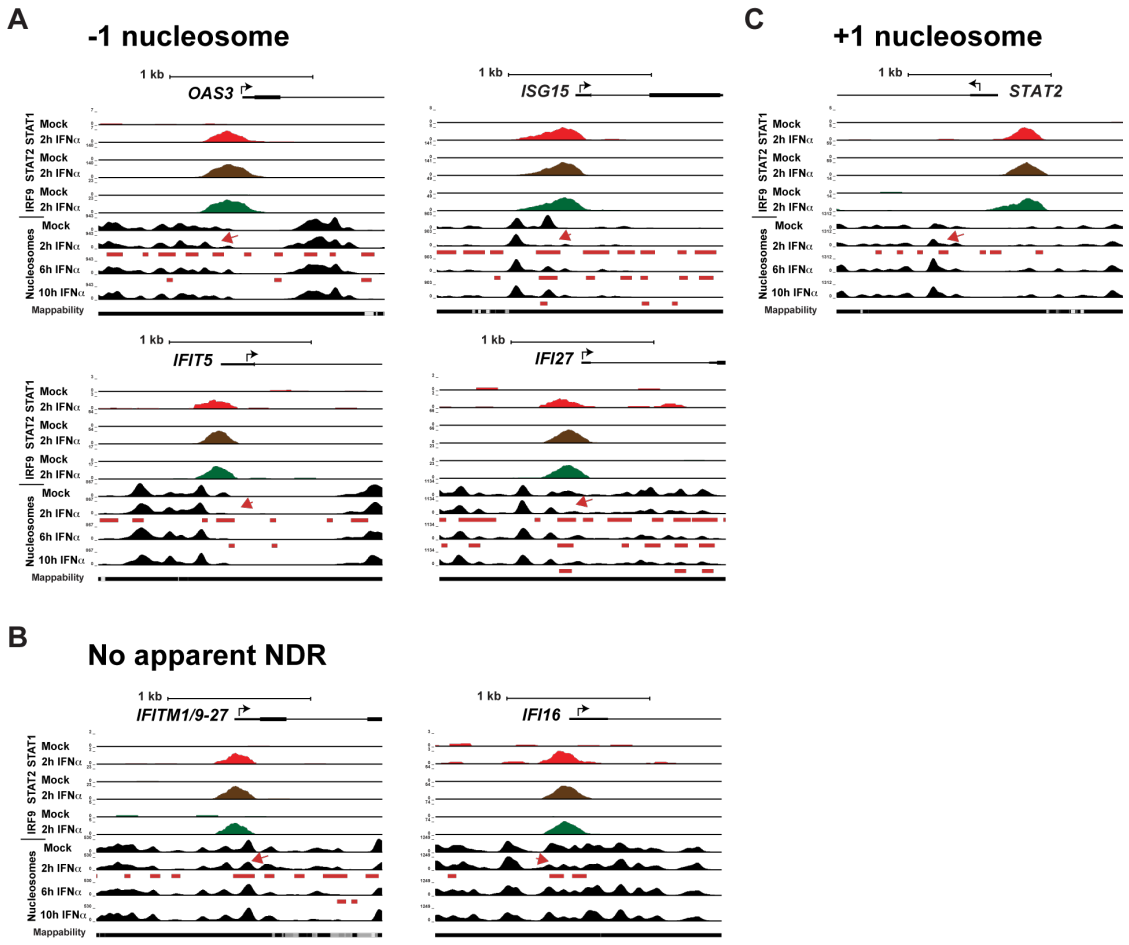

Figure 2.8: IFN-stimulated nucleosome reorganization at ISGs with -1, no NDR, or +1 nucleosome configuration

Genome browser diagram of IFN-induced ISGF3 recruitment and nucleosome dynamics at select ISGs within 2000 bp +/- TSS. (A) ISGs, *OAS3*, *ISG15*, *IFIT5*, and *IFI27*, with a -1 nucleosome. (B) ISGs, *IFITM1/9-27* and *IFI16*, with no apparent nucleosome depleted region (NDR). (C) ISG, *STAT2,* with a +1 nucleosome. (A-C) (Top) 5' end of gene depicted with the black arrow depicting the direction of transcription, the small and large black bars represent untranslated and exonic regions, respectively, and the line represents intronic regions. (Middle) ChIP-Seq density of STAT1, STAT2, and IRF9 occupancy after mock or 2 hr IFNα treatment in HeLa cells. (Bottom) Nucleosome occupancy after mock, 2 hr, 6 hr, or 10 hr IFNα treatment in HeLa cells. Red arrows highlight nucleosome loss at ISGF3-ISRE proximal regions. Red bars beneath nucleosome maps denote nucleosome loss due to 2 hr, 6 hr, or 10 hr IFNα treatment compared to Mock (p-value ≤ $1x10^{-5}$). All sequencing reads are normalized to 10 million reads.

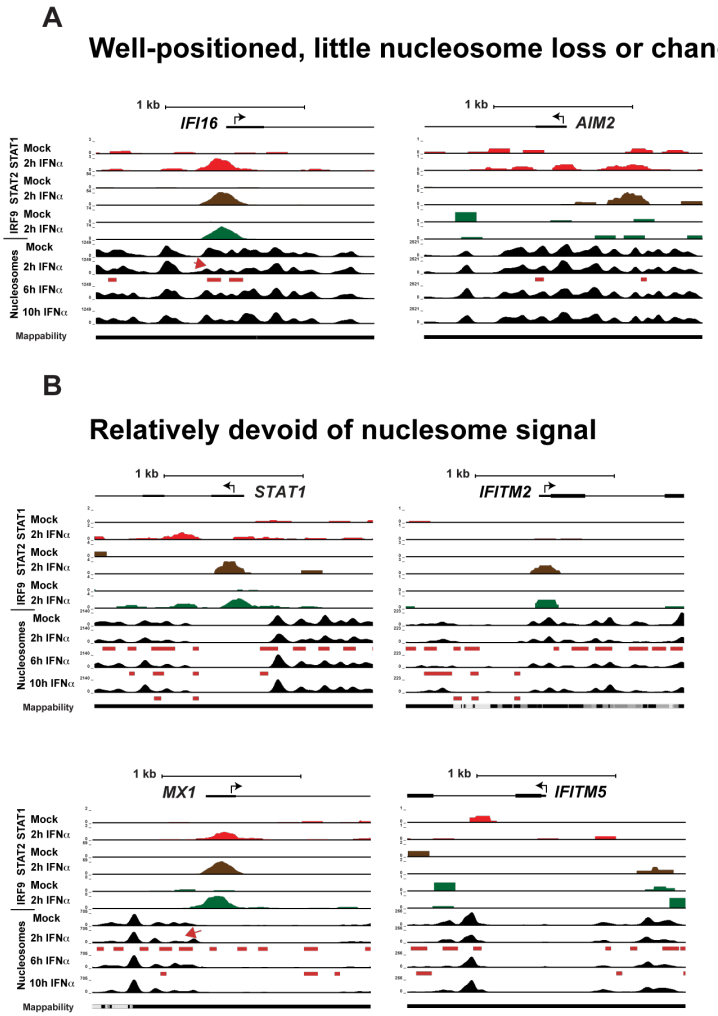

Figure 2.9: IFN-stimulated nucleosome reorganization at ISGs with little nucleosome change or low distribution of nucleosome signal

Genome browser diagram of IFN-induced ISGF3 recruitment and nucleosome dynamics at select ISGs within 2000 bp +/- TSS. (A) ISGs, *IFI16* and *AIM2,* with well-positioned nucleosomes and little nucleosome loss or change. (B) ISGs, *STAT1, IFITM2, MX1*, and *IFITM5*, are relatively devoid of nucleosome signal. (A-B) (Top) 5' end of gene depicted with the black arrow depicting the direction of transcription, the small and large black bars represent untranslated and exonic regions, respectively, and the line represents intronic regions. (Middle) ChIP-Seq density of STAT1, STAT2, and IRF9 occupancy after mock or 2 hr IFNα treatment in HeLa cells. (Bottom) Nucleosome occupancy after mock, 2 hr, 6 hr. or 10 hr IFNα treatment in HeLa cells. Red arrows highlight nucleosome loss at ISGF3-ISRE proximal regions. Red bars beneath nucleosome maps denote nucleosome loss due to 2 hr, 6 hr, or 10 hr IFNα treatment compared to Mock (p-value ≤ $1x10^{-5}$). All sequencing reads are normalized to 10 million reads.

IFN induction increases chromatin susceptibility and reorganization

The previous section demonstrates well-positioned nucleosomes at ISGs during steady state followed by IFN-induced nucleosome alterations. Unexpectedly, IFN stimulation not only induced nucleosome occupancy level changes at ISGs, but also at adjacent genes and intergenic regions that were within the BAC direct selection boundaries (Figure 2.10). These results suggest IFN induction leads to a widespread nucleosome reorganization. To test this hypothesis, mock and IFN-treated nuclei were subjected to a time course of DNase I digestion (Figure 2.11A). IFNα treatment for 2 hr and 10 hr led to increased sensitivity to DNase I digestion, evidenced by shorter DNA fragments. To examine whether this was unique to IFN treatment, cells that were treated with the type II IFNγ or heat-shocked at 42ºC were subjected to the same DNase I digestion conditions and compared to IFNα treatment (Figure 2.11B). Although 10 hrs of heat shock and type II IFNγ treatment resulted in some sensitivity to DNase I digestion, it was less extensive compared to IFN. This suggests IFN stimulation induces a comprehensive chromatin reorganization that renders genomic DNA to become more susceptible to nuclease cleavage.

IFN stimulation simultaneously activates the transcription of hundreds and possibly thousands of ISGs encoded in the genomic DNA. Simultaneous ISG transcription activation is achieved by ISRE-directed recruitment of ISGF3 to ISG target sites and ISGF3-mediated associations with coactivators and Pol II machinery. Since ISGs are encoded throughout the human genome, one hypothesis is that simultaneously occurring transcription and chromatin-modifying activities at ISG sites manifest to extensive regions

of exposed DNA for digestion (Figure 2.12). However, further investigation is needed to determine the underlying mechanism.

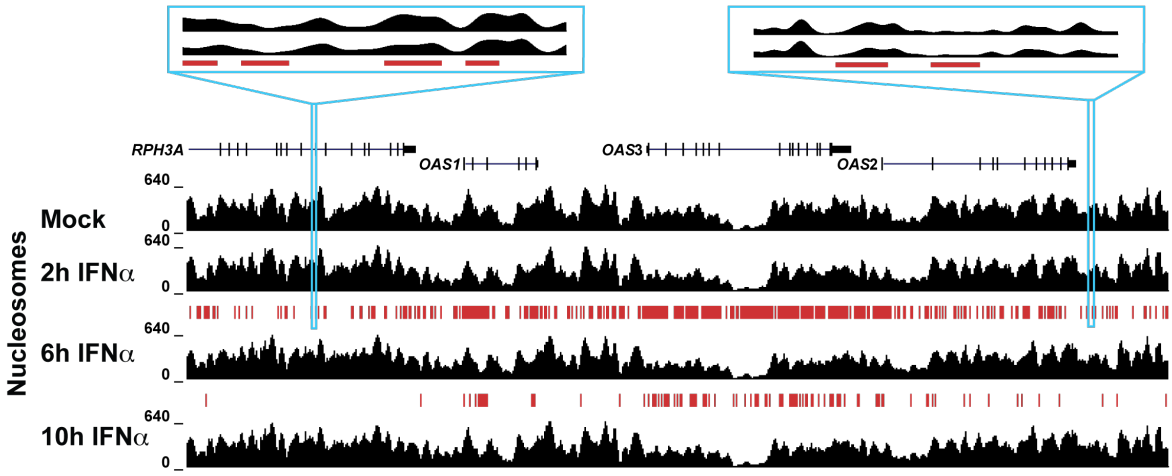

Figure 2.10: IFN-stimulated nucleosome loss extends beyond ISG boundaries
Genome browser map of the IFN-stimulated nucleosome loss at the *RPH3A* gene, adjacent to the *OAS* genes, and at intergenic regions. Nucleosome occupancy after mock, 2 hr, 6 hr, or 10 hr IFNα treatment in HeLa cells. Red bars beneath nucleosome maps denote nucleosome loss due to 2 hr, 6 hr, or 10 hr IFNα treatment compared to Mock (p-value ≤ $1x10^{-5}$). All sequencing reads are normalized to 10 million reads. (Left inset) Zoomed in view of RPH3A gene region of ~800 bp. (Right inset) Zoomed in view of intergenic region of ~1100 bp at chr12:113452133-113453242

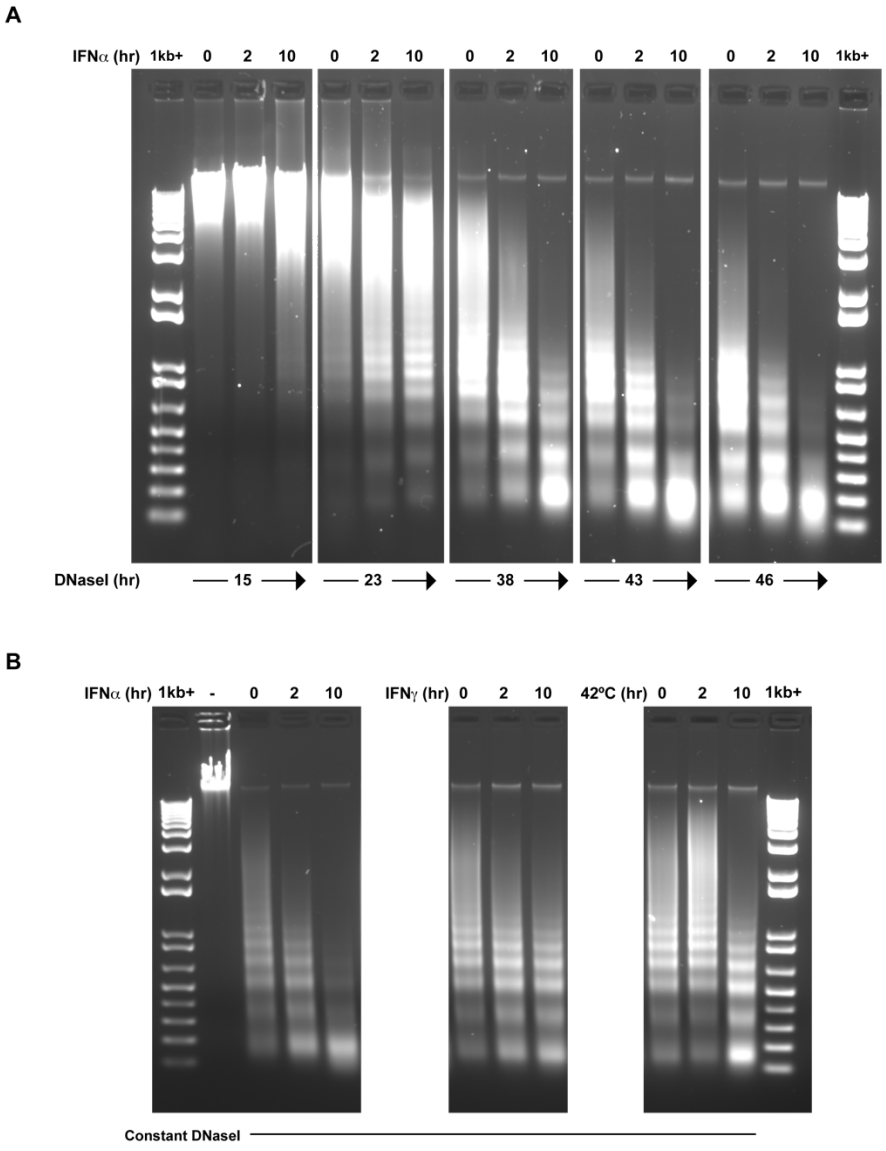

Figure 2.11: IFN-stimulated comprehensive chromatin reorganization
Genomic DNA from HeLa nuclei were digested with DNase I, purified and visualized by ethidium bromide agarose gel electrophoresis. (A) Lane 1, 17: 1kb+ ladder, lane 2-16: nuclei/chromatin from mock-treated and 2 hr or 10 hr IFNα-treated HeLa cells were digested with DNase I for 15 hr, 23 hr, 38 hr, 43 hr and 46 hr. (B) Lane 1 and 12: 1kb+ ladder; lane 2: untreated and undigested mock DNA; lane 3-11: nuclei-chromatin DNA following 0 hr, 2 hr or 10 hr IFNα (lane 3-5), IFNγ (lane 6-8), or 42°C heat-shock (lanes 6-8) treatment digested with 50 units of DNase I per 5 x 10^7 cells for 43 hr.

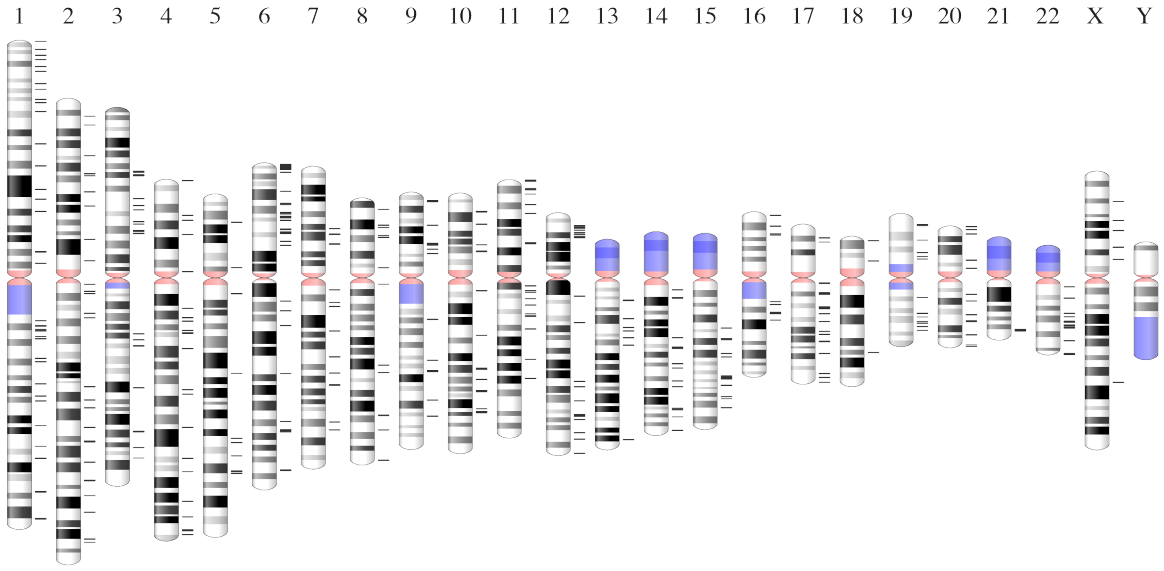

Figure 2.12: ISGs are distributed throughout the human genome
Distribution of 300+ ISGs encoded in the human genome are mapped onto the cytogenetic ideogram representation of human chromosomes.

DISCUSSION

Transcriptional initiation of ISGs is regulated at the chromatin level by the transcription factor complex ISGF3 and its interaction with chromatinized ISG targets during the IFN response. While many classic ISGs (i.e. *IFIT2/ISG54)* are known to be transcriptionally activated by ISGF3 following IFN stimulation, most ISGs are presumed to be targets of ISGF3. Through ChIP-Seq analysis of the ISGF3 components (STAT1, STAT2, and IRF9), thousands of genomic loci including classic ISGs were identified to be ISGF3 targets following IFN stimulation. These data not only demonstrate ISGF3 recruitment to specific target loci, it also enables correlation of the ISGF3-mediated interactions to ISG loci.

During ISG transcription initiation, ISGF3 recruits coactivators that can remodel chromatin or modify histones, suggesting a role for chromatin in regulating ISGs. To better understand the contribution of chromatin and nucleosome dynamics to mammalian antiviral transcription regulation, the chromatin architecture and nucleosome organization of ISG loci were characterized to correlate IFN-mediated changes with the activation of ISGF3 components, STAT1, STAT2, and IRF9. Overall, stable steady-state nucleosome positions at ISG loci were rearranged by IFN stimulation, giving rise to a transient alteration in chromatin structure during the response. These alterations were particularly evident at ISGF3-ISRE promoter regions, supporting the notion that ISGF3-mediated recruitment of chromatin-modifying enzymes serves to remodel chromatin.

Parallel visualization of the IFN-induced ISGF3 occupancy and nucleosome profiles at ISG promoters reveals diversity in the nucleosome configuration of 20

representative ISGs, which are simultaneously activated during the IFN response. Generally, we observe well-positioned nucleosomes and IFN-induced nucleosome loss that correlates with the activities of ISGF3. Many of the classical ISGs were confirmed to strongly recruit ISGF3, but anomalies such as the *IFI16*/*AIM2* family of ISGs suggest some ISGs may be targeted by ISGF3 or an alternate STAT complex. Since *IFI16* and *AIM2* are recognized antiviral ISG effectors in viral DNA sensing, their activation may also be redundantly mediated by other immune regulators in the TLR or cGAS/STING pathway. In contrast, in the case of the *STAT1* promoter, a strong recruitment of ISGF3 is found approximately 6000 bp upstream, suggesting regulation of STAT1 may occur at a distal enhancer or through chromatin looping.

In addition to the IFN-induced nucleosome loss observed at ISG promoter and gene body regions, the nucleosome loss extended beyond ISGs to neighboring genes and intergenic regions. Independent experiments demonstrated IFN-induced nuclei subjected to DNase I digestion were more susceptible to nuclease digestion, corroborating with widespread nucleosome loss observed from the IFN-stimulated high-resolution nucleosome data. Though the mechanism driving this phenotype genome-wide remains to be elucidated, two hypotheses are proposed. Since ISGs are encoded throughout the genome (Figure 2.12), one possibility is the widespread nucleosome loss and increased nuclease sensitivity reflect a high level of transcriptional and remodeling activity induced by IFN stimulation. Another postulation is the potential prevalence of “fragile nucleosomes,” which are more susceptible to nuclease digestions, among ISG nucleosomes. Given the thousands of IFN-induced ISGF3 targets, simultaneous

transcription could increase the abundance of highly nuclease-sensitive nucleosomes and yield increased regions of cleaved DNA observed in the DNase I assays. The prevalence of IFN-stimulated ISGF3 recruitment genome-wide, notably at the ISRE and ISG promoter region, correlates with the dynamic activity observed at IFN-induced ISG promoter nucleosomes and supports its predominant role in IFN-induced transcription activation.

RESEARCH CONTRIBUTIONS AND PUBLICATION

Dr. Curt M. Horvath and I designed and interpreted the experiments. I conducted all of the experiments and bioinformatic analyses. The major findings are published in the following manuscript:

Au-Yeung, N., and Horvath, C.M. (2018). Histone H2A.Z Suppression of Interferon-Stimulated Transcription and Antiviral Immunity is Modulated by GCN5 and BRD2. iScience *6*, 68-82.

CHAPTER 3.

HISTONE H2A.Z REGULATION IN THE IFN RESPONSE

INTRODUCTION

In Chapter 2, we observed nucleosome occupancy levels at ISGs decreased following IFN stimulation and recovered at later IFN treatment times. The most prominent nucleosome reorganization occurred at the promoter region, coinciding with or near sites bound by ISGF3. Although it is well known that ISGF3 binds to the promoter DNA element to activate ISG transcription, how ISGF3 engages the chromatin to access the ISRE remains largely unknown. Little is known about how chromatin structure and nucleosome dynamics influence ISGF3 promoter engagement, transcriptional activity, and innate immunity, but several studies have implicated chromatin-remodeling, histone-modifying, and polymerase-activating factors as ISGF3 co-activators (Gnatovskiy et al., 2013; Huang et al., 2002; Kadota and Nagata, 2014; Nusinzon and Horvath, 2003; Patel et al., 2013; Paulson et al., 2002).

ISGF3 has been linked to many transcription co-activators that are commonly recruited by the strong STAT2 transcriptional activation domain, often with support from STAT1. Notably, ISGF3 has an absolute requirement for histone deacetylase (HDAC) activity for transcriptional stimulation, and STAT2 interacts with HDAC1 (Chang et al., 2004; Nusinzon and Horvath, 2003; Sakamoto et al., 2004). Conversely, ISGF3 also engages histone acetyltransferase (HAT) activities from CBP/p300 and GCN5 for ISG transcription via STAT2 (Bhattacharya et al., 1996; Gnatovskiy et al., 2013; Paulson et al., 2002). Through STAT2, ISGF3 has been linked to the SWI/SNF (human BAF/pBAF) and INO80 chromatin remodeling complexes via specific interaction partners, including BRG1, RVB1, and RVB2 (Bhattacharya et al., 1996; Cui et al., 2004; Gnatovskiy et al.,

2013; Huang et al., 2002; Liu et al., 2002; Patel et al., 2013; Paulson et al., 2002). HDAC and HAT activity are linked to recruitment of the bromodomain protein BRD4 to control Pol II elongation through association with positive elongation factor pTEFb and release of elongation repressors, NELF and DSIF (Patel et al., 2013). STAT2 association with Mediator subunits and general transcription factors (GTFs) directly connect ISGF3 to Pol II initiation and elongation machinery (Lau et al., 2003; Paulson et al., 2002). Together, the patterns of co-activator and remodeler recruitment are consistent with a highly regulated general and gene-specific ISGF3-mediated transcriptional activation process for ISGs, and suggest a role for chromatin in IFN-stimulated antiviral gene regulation.

Nucleosome positioning and reorganization regulate gene activation by controlling DNA accessibility (Bell et al., 2011). Current evidence indicates that most eukaryotic promoters feature positioned nucleosomes flanking regions that contain regulatory elements for the assembly of transcription regulators, Pol II, and essential or gene specific co-activators (Huminiecki and Horbanczuk, 2017; Venters and Pugh, 2009). In addition to nucleosomes composed of an octamer of the core histones H2A, H2B, H3, and H4 wrapped with ~147bp of DNA, less abundant nucleosomes contain histone variants that are associated with specific regulatory phenomena. Histone variants are thought to allow for greater control of DNA replication, repair, or transcription, and contribute to the efficiency of Pol II elongation, termination, and processivity (Buschbeck and Hake, 2017).

Histone variant, H2A.Z

Histone H2A.Z is a variant of H2A that is enriched at eukaryotic gene promoters and can also be found at heterochromatin boundaries, sites of DNA damage repair, and

in segregating chromosomes (Buschbeck and Hake, 2017). H2A.Z is conserved across many species, but its role remains contextual: having both positive and negative functions in transcription and association with active, repressed, and silent chromatin (Zlatanova and Thakar, 2008). For example, depletion of H2A.Z can result in increased expression of the *p21* gene and decreased expression of estrogen receptor target genes in human cells (Gevry et al., 2007; Gevry et al., 2009; Marques et al., 2010). In *Mus musculus* (mouse), *Tetrahymena thermophile* (ciliate), *Drosophila melanogaster* (fly), *Xenopus leavis* (frog), H2A.Z deficiency was found to be embryonic lethal, while yeast lacking H2A.Z survived but had growth defects (Clarkson et al., 1999; Faast et al., 2001; Iouzalen et al., 1996; Jackson and Gorovsky, 2000; Liu et al., 1996; Ridgway et al., 2004; van Daal and Elgin, 1992). Even though H2A.Z is conserved across species, there are differences between species that need to be considered while evaluating its role. Fly H2A.Z (called H2AvD) resembles both H2A.Z and another histone H2A variant, H2A.X (Redon et al., 2002; van Daal and Elgin, 1992). Mice and human encode two non-allelic H2A.Z genes, H2A.Z.1 and H2A.Z.2, compared with one H2A.Z gene in other organisms (i.e. yeast, fly). H2A.Z.1 (*h2afz*) knockout mice are embryonic lethal and the presence of the H2A.Z.2 gene (*h2afv*) did not rescue the lethality, suggesting non-redundant or unique roles for the H2A.Z products of these two non-allelic genes (Faast et al., 2001; Matsuda et al., 2010). Here, H2A.Z generally refers to the H2A.Z.1 encoded by the *h2afz* gene, as it is the essential H2A.Z in the viability of embryonic mice and the principal component of H2A.Z enriched at mammalian gene promoters (Consortium, 2012; Faast et al., 2001; Subramanian et al., 2013).

The extended acidic patch of H2A.Z compared to histones H2A and H2A.B

H2A.Z differs from H2A by approximately 40% at the sequence level, but is structurally similar except for an extended acidic patch. At the nucleosome surface, histone H2A contributes most of the negatively charged residues via its acidic patch (Luger et al., 1997; Millar, 2013). H2A.Z has an extended acidic patch and this extension results in increased nucleosome array compaction (Bonisch and Hake, 2012). Conversely, the H2A variant, H2A.B, has a truncated acidic region and presence of H2A.B reduces the nucleosome array compaction compared to H2A (Fan et al., 2004). This suggests that even a minor structural difference in the acidic patch that distinguishes H2A.Z from H2A can alter the nucleosome packaging density. Despite the structural similarity between H2A and H2A.Z, contrasting information from *in vitro* and *in vivo* suggests H2A.Z can stabilize or destabilize the nucleosome compared to H2A (Bonisch and Hake, 2012).

H2A.Z nucleosome positioning and gene regulation

Although H2A.Z is commonly found at active gene promoters, it was originally associated with silent heterochromatin and colocalization with HP1α, a heterochromatin associated protein (Dhillon and Kamakaka, 2000; Guillemette et al., 2005; Raisner et al., 2005). This seemingly inconsistent association with heterochromatin is attributed to H2A.Z presence at heterochromatin boundaries, where it might function to prevent heterochromatin spread (Meneghini et al., 2003). H2A.Z is also found at silent (repressed) or inducible eukaryotic genes and in yeast is found at genes sensitized by prior exposure

to carbon sources, further confounding the function of H2A.Z in gene regulation (Brickner et al., 2007; Surface et al., 2016; Zanton and Pugh, 2006). Dissection of the properties of nucleosome positioning and histone modifications related to H2A.Z and H2A.Z-containing nucleosomes have begun formulating hypotheses that in time may reconcile its seemingly contradictory roles in eukaryotic gene regulation.

Evaluation of the nucleosome position H2A.Z occupies has continuously been used to correlate with its positive or negative impact on gene activation. H2A.Z is commonly found at the +1, -1, or +1 and -1 nucleosome positions relative to the TSS (Guillemette and Gaudreau, 2006). The +1 H2A.Z-containing nucleosome in flies is thought to lower the barrier for Pol II elongation and H2A.Z has been associated with destabilizing the +1 nucleosome (Guillemette et al., 2005; Jin and Felsenfeld, 2007; Meneghini et al., 2003). In contrast to fly and *Schizosaccharomyces pombe* (fission yeast), the -1 nucleosome is relatively enriched in *Saccharomyces cerevisiae* (budding yeast) and human (Millar, 2013). Recent studies on the repressed mesenchymal genes and active epithelial genes in MDCK cells demonstrated the presence of H2A.Z at the +1 position correlates with gene repression (Dai et al., 2017; Domaschenz et al., 2017). A similar correlation was observed in plants where the +1 H2A.Z nucleosome correlated with high gene accessibility and the -1 nucleosome with low gene accessibility (Dai et al., 2017). These and other developments are beginning to reconcile the differential regulation H2A.Z imparts by incorporating multiple components of the H2A.Z-containing nucleosome to modulate the transcriptional outcome (Subramanian et al., 2015).

H2A.Z regulation by histone post-translational modifications

Acetylated H2A.Z is commonly associated with active gene promoters and ubiquitylated H2A.Z with repressed genes (Ku et al., 2012; Sevilla and Binda, 2014). In addition to acetylation and ubiquitylation modifications, H2A.Z can be methylated and sumoylated (Sevilla and Binda, 2014). Post-translational modifications (PTMs) of H2A.Z and its nucleosomal histone partners influence protein interactions at H2A.Z-containing nucleosomes. For example, monoubiquitylated H2A.Z has been shown to influence the binding of the polycomb repressor complex (PRC) in mouse embryonic stem cells, while inhibiting binding of the bromodomain protein BRD2 (Surface et al., 2016). Bromodomain proteins, including BRD2, bind to acetylated substrates and BRD2 has been shown to preferentially associate with H2A.Z rather than H2A nucleosomes (Cheung et al., 2017; Draker et al., 2012). In another example, monoubiquitination of H2B prevents H2A.Z from being evicted at enhancers (Segala et al., 2016). These examples implicate both the PTM status of H2A.Z and its intranucleosomal histones in regulating H2A.Z nucleosome dynamics and interactions with cofactors.

H2A.Z deposition and removal

The precise machinery required for deposition of H2A.Z was identified in yeast to be the chromatin remodeling complex, SWR1, and was described by three independent groups (Billon and Cote, 2013; Kobor et al., 2004; Krogan et al., 2003; Mizuguchi et al., 2004; Papamichos-Chronakis et al., 2011). Conversely, removal of H2A.Z in yeast was attributed to the chromatin remodeling complex, INO80, but later studies show INO80

does not account for most H2A.Z loss (Alatwi and Downs, 2015; Jeronimo et al., 2015; Tramantano et al., 2016). In mice, the ANP32E factor was implicated as a H2A.Z histone chaperone, but closer examination reveals that similar to INO80, ANP32E does not account for all of the H2A.Z loss (Obri et al., 2014). H2A.Z-specific remodelers continue to be investigated in more complex organisms. Thus, while the H2A.Z histone variant has been investigated in diverse systems and organisms, its precise function(s) and the cellular machinery used to deposit or remove H2A.Z is difficult to generalize between organisms and within specific contexts in an individual organism.

The accumulating data on H2A.Z regulation and transcriptional outcome continues to be context-dependent, yet patterns are emerging. For the first time, the role and dynamics of H2A.Z was evaluated in the IFN response system. Evidence is presented here indicating that ISG promoters are decorated with the variant histone H2A.Z. In particular, the role and mechanism of H2A.Z regulation at ISGs was examined in detail, focusing on its impact on ISG transcription and dynamics during the IFN antiviral response.

RESULTS

IFN-induced histone dynamics at ISG promoters

In Chapter 2, IFN stimulation led to a reduction and reorganization of ISG promoter nucleosomes. To investigate potential mechanisms underlying nucleosome dynamics at ISGs observed in Chapter 2, the presence of core histones was examined using ChIP-qPCR and primers specific to either the ISRE region of the promoter or distal regions of the gene bodies of *OAS3*, *IFIT1/ISG56*, and *IFITM1/9-27* (Figure 3.1, Appendix Figure 1). In the gene bodies, all four core histones (H2A, H2B, H3, and H4) were present at steady state (mock-treated) and remained relatively constant following a 2 hr IFN treatment (Figure 3.1A-C, Appendix Figure 1A-C and G-I). In contrast, while the core histones H2B, H3, and H4 were readily detected at ISG promoters, H2A was notably underrepresented. Instead, the histone variant H2A.Z was detected at the ISG promoters (Figure 3.1D-F, Appendix Figure 1D-E and J-L). Stimulation with IFN decreased promoter-associated histones, observed most dramatically for H2A.Z, consistent with the observed nucleosome reorganization identified at ISG promoters. H2A.Z is well known for its association with the promoter-TSS region and colocalization with specific histone modification marks (i.e. H3K4me3) in a variety of biological systems, including genes that respond to environmental stimuli (Barski et al., 2007; Hu et al., 2013; Ku et al., 2012). As such, the presence of H2A.Z at ISG promoters provides a tractable system for investigating H2A.Z dynamics and biological impact in mammalian cells.

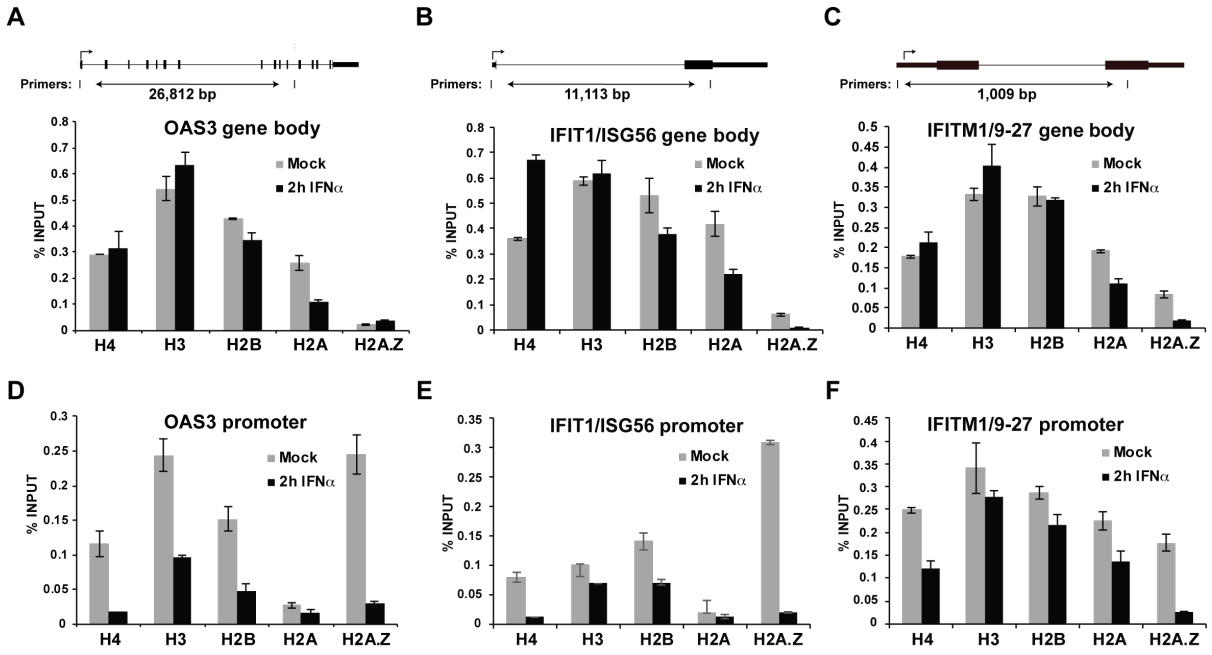

Figure 3.1: IFN-stimulated loss of histones H2A.Z, H2B, H3 and H4 at ISG promoters

(A-F) ChIP analysis of histones H4, H3, H2B, H2A and H2A.Z occupancy at the gene body (A-C) or gene promoter (D-F) of *OAS3*, *IFIT1/ISG56*, *IFITM1/9-27* during steady state (Mock) and after 2 hr IFNα stimulation. The position of the gene body and promoter specific primers and their relative distance are indicated in the upper panel of (A-C). Error bars denote standard deviation of technical replicates. Histone occupancy is computed based on the percent input method. See Appendix Figure 1.

H2A.Z is inversely correlated with ISGF3 recruitment

The previously unrecognized association of H2A.Z with ISG promoters suggested this histone variant might be a more general feature of ISGF3 target genes. To test this idea, a HeLa cell H2A.Z ChIP-Seq dataset (Consortium, 2012; Rosenbloom et al., 2013) was compared to the top 250 IFN-induced STAT2 targets (Figure 3.2A). During steady state STAT2/ISGF3 is absent and only recruited to these loci after IFN stimulation. These same genomic regions are packaged in H2A.Z-containing nucleosomes during the steady state. A clear correlation was found between the IFN-activated target genes and H2A.Z occupancy at steady state (R^2=0.83), and examination of target promoter regions indicates that peaks of H2A.Z deposition closely overlap with STAT2-binding ISRE sites (Figure 3.2B). Strictly speaking, the presence of H2A.Z inversely correlates with IFN stimulation, and this relationship is further verified by IFN stimulation and recovery experiments. H2A.Z is lost from ISG promoters while ISGF3 is active, but recovers by 8 hr post-stimulation when ISGF3 is inactivated (Figure 3.2C). H2A.Z has been shown to colocalize at active genes with H3K4me3 and at bivalent promoters containing both H3K4me3 and H3K27me3 marks (Ku et al., 2012). Consistent with this observation, the top STAT2 targets also bear the active mark H3K4me3 (Figure 3.2A), which is coordinately lost from ISGs *OAS3* and *IFIT1/ISG56* following IFN stimulation (Figure 3.2D).

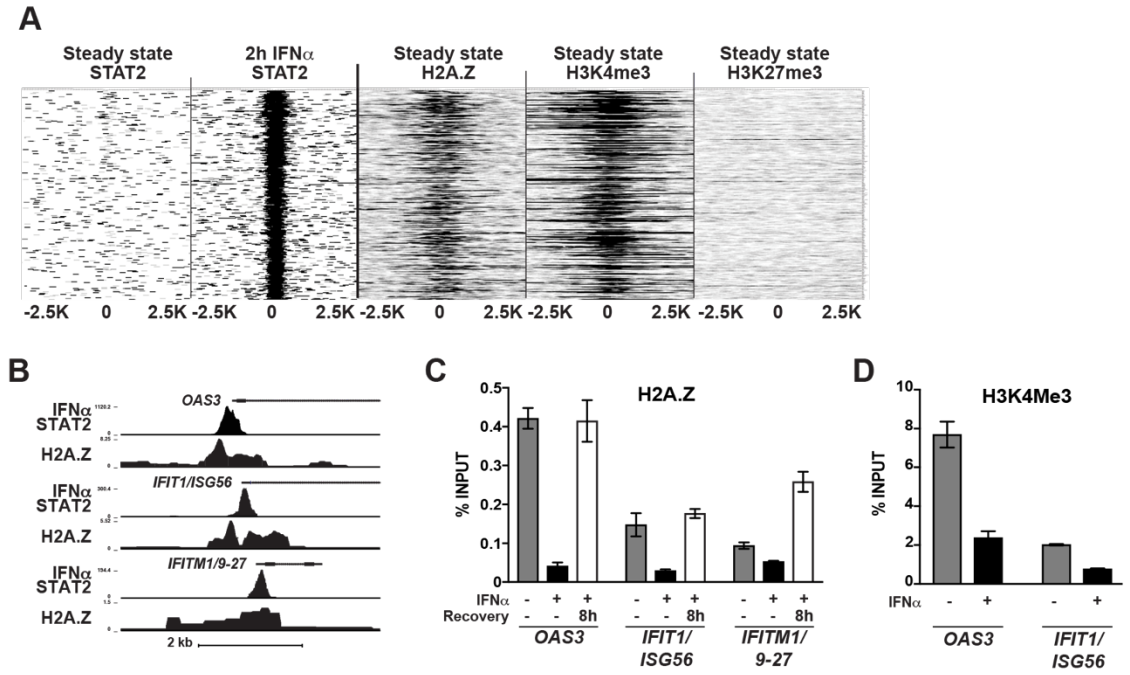

Figure 3.2: Histone variant, H2A.Z., is a dynamic component of ISG promoters

(A) Heatmap depicting steady state and IFNα-recruited STAT2 occupancy (in-house ChIP-Seq) compared with steady state H2A.Z, H3K4me3 and H3K27me3 occupancy (ENCODE ChIP-Seq) at the top 250 enriched STAT2 target loci spanning +/- 2500 bp from the STAT2 peak center. H2A.Z and STAT2 occupancy at these loci had a Pearson correlation coefficient of R^2 = 0.83. (B) Genome browser view of H2A.Z occupancy at steady state and STAT2 occupancy after 2 hr IFNα stimulation at three ISGs, *OAS3*, *IFIT1/ISG56* and *IFITM1/9-27*. (C) ChIP analysis of H2A.Z removal and recovery after 3 hr IFNα followed by recovery without IFNα for 0 hr or 8 hr at the *OAS3*, *IFIT1/ISG56*, and *IFITM1/9-27* promoters. Error bars denote standard deviation of technical replicates. Histone occupancy is computed based on the percent input method. (D) ChIP analysis of steady state and IFN-stimulated H3K4me3 at *OAS3* and *IFIT1/ISG56* promoters.

Coupling IFN pre-treatment-siRNA demonstrates H2A.Z negatively regulates ISGs

The uniform decoration of ISG promoters with H2A.Z, and its IFN-induced loss and recovery, suggested a potential role for H2A.Z in ISG regulation and biological activity. To examine the impact of H2A.Z in ISG transcription, knockdown experiments were conducted in cells harboring siRNA against H2A.Z or a non-targeting control sequence. H2A.Z-siRNA reduced the H2A.Z gene expression in both mock- and IFN-treated samples (Figure 3.3A). ISG expression analysis of ISGs *OAS3* and *IFI6* with reverse transcriptase-quantitative PCR (RT-qPCR) demonstrated little to no difference in their transcript abundance between H2A.Z-siRNA cells and control siRNA (Figure 3.3B-C). Although this data suggests disrupting H2A.Z expression does not produce an effect on ISG transcription, this result does not consider that the knockdown with siRNA may not have affected the insoluble H2A.Z population deposited within the chromatin. A lack of H2A.Z disruption at the chromatin level in H2A.Z-siRNA cells would therefore be similar to the chromatin status of H2A.Z in control siRNA or wild-type cells. In that case, we expect to observe little difference on ISG transcription between H2A.Z-siRNA and siRNA control cells, as they both contain intact H2A.Z nucleosomes at ISG chromatin.

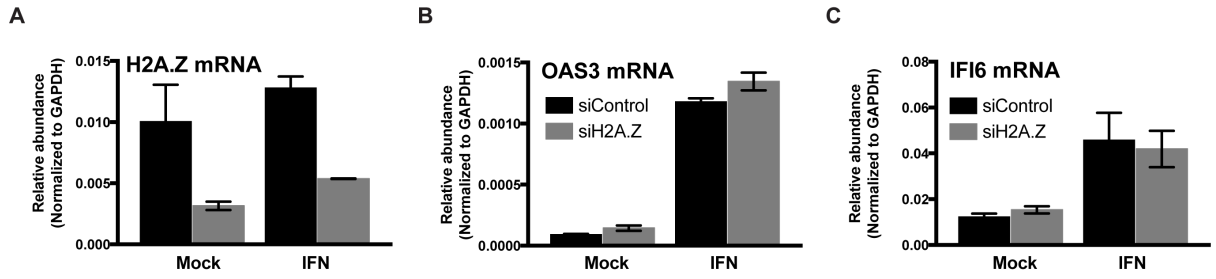

Figure 3.3: Targeting H2A.Z via siRNA is insufficient to observe the effects of chromatinized H2A.Z on ISG expression
Gene expression analysis of the relative abundance of (A) *H2A.Z*, (B) *OAS3,* and (C) *IFI6* from HeLa cells transfected with siRNA against H2A.Z for 48 hr followed by either 3 hr mock or IFN treatment. Error bars denote standard deviation of technical replicates. Relative abundance was normalized to GAPDH.

With two populations of H2A.Z to consider in the cell, the newly synthesized soluble H2A.Z and the insoluble H2A.Z deposited into chromatin, employing a method that can target both populations is essential to observe the effect of H2A.Z nucleosomes on ISG transcription. However, knockout cell lines were not available to ensure total H2A.Z was eliminated, as the lack of H2A.Z is embryonic lethal in mammalian cells (Faast et al., 2001). Since IFN treatment can result in removal of the chromatin H2A.Z from ISG promoters, an alternative method using IFN coupled with H2A.Z-siRNA was devised to reduce both the chromatin-based H2A.Z protein and the newly synthesized H2A.Z (Figure 3.4). As depicted in Figure 3.4, cells were subjected to an IFN pretreatment to remove H2A.Z nucleosome(s), followed by RNA interference with siRNA to knockdown H2A.Z mRNA and prevent newly synthesized H2A.Z from being deposited into the chromatin. The modified experimental setup with IFN pre-treatment led to a reduction of H2A.Z at the chromatin in mock and IFN cells compared to cells with no pre-treatment (Figure 3.5).

H2A.Z mRNA levels were reduced following IFN pre-treatment coupled with H2A.Z-siRNA knockdown in both mock- and IFN-treated cells (Figure 3.6). IFN pre-treatment coupled with siRNA did not disrupt ISGF3-dependent transcription, but instead resulted in higher ISG mRNA levels (Figure 3.6). These findings for the first time link H2A.Z to IFN and ISG responses, and are consistent with a repression function for H2A.Z in IFN-stimulated gene expression. However, the use of IFN stimulation as a prerequisite to investigate ISG regulation called for a complementary strategy to test this preliminary conclusion.

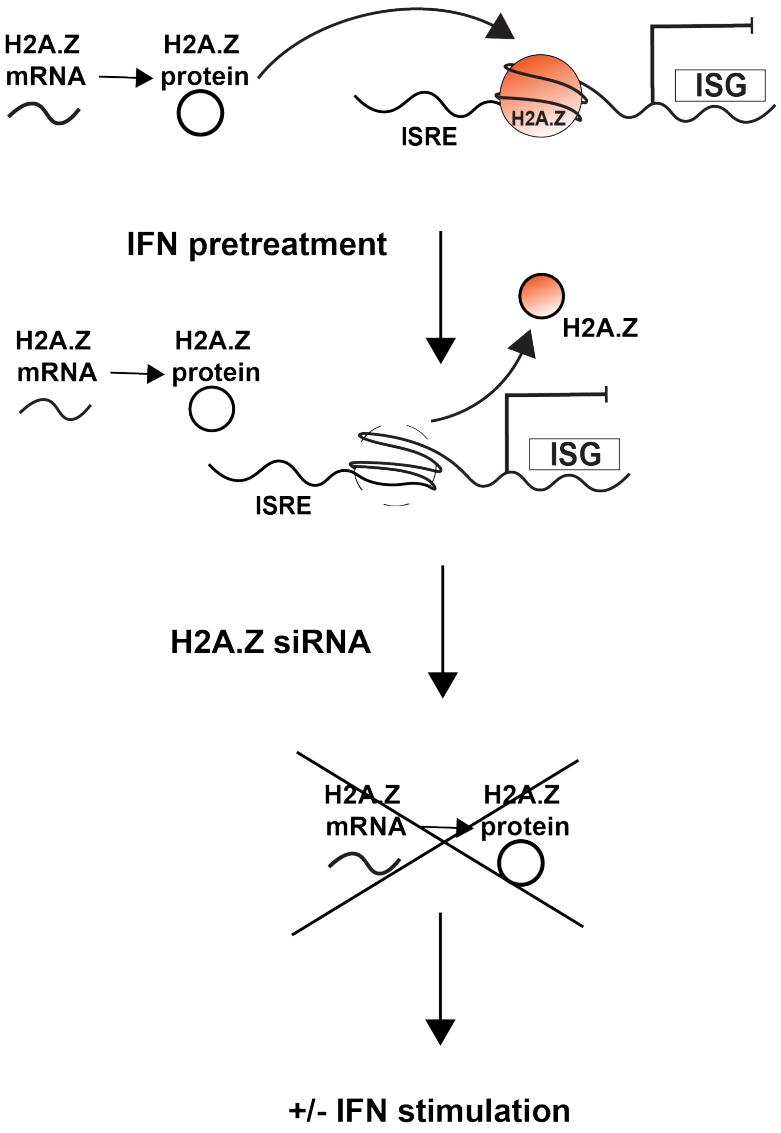

Figure 3.4: Schematic of the IFN pre-treatment coupled with siRNA procedure for H2A.Z depletion

In the first phase, HeLa cells are pretreated with IFN for 3 hr to remove the chromatin-incorporated H2A.Z. During the second phase following IFN pre-treatment, a smartpool of four siRNA targeting H2A.Z are transfected into HeLa cells for 48 hr to knockdown H2A.Z expression and prevent newly synthesized H2A.Z protein. Cells that have undergone the dual-phase H2A.Z depletion procedure are treated with 2-6 hr IFN for further analysis.

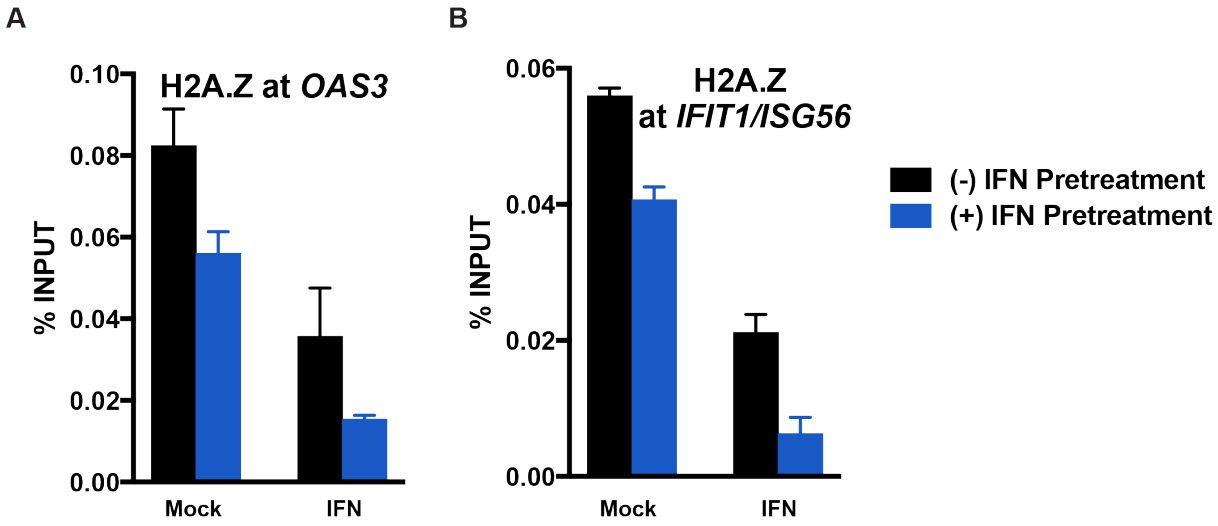

Figure 3.5: IFN pre-treatment reduces H2A.Z occupancy
HeLa cells subjected to mock (-) or IFN (+) pre-treatment are subsequently assayed using ChIP-qPCR for H2A.Z occupancy levels at the promoters of A) *OAS3* or B) *IFIT1/ISG56* during mock (steady state) or following IFN stimulation. Error bars denote standard deviation of technical replicates. H2A.Z occupancy is computed based on the percent input method.

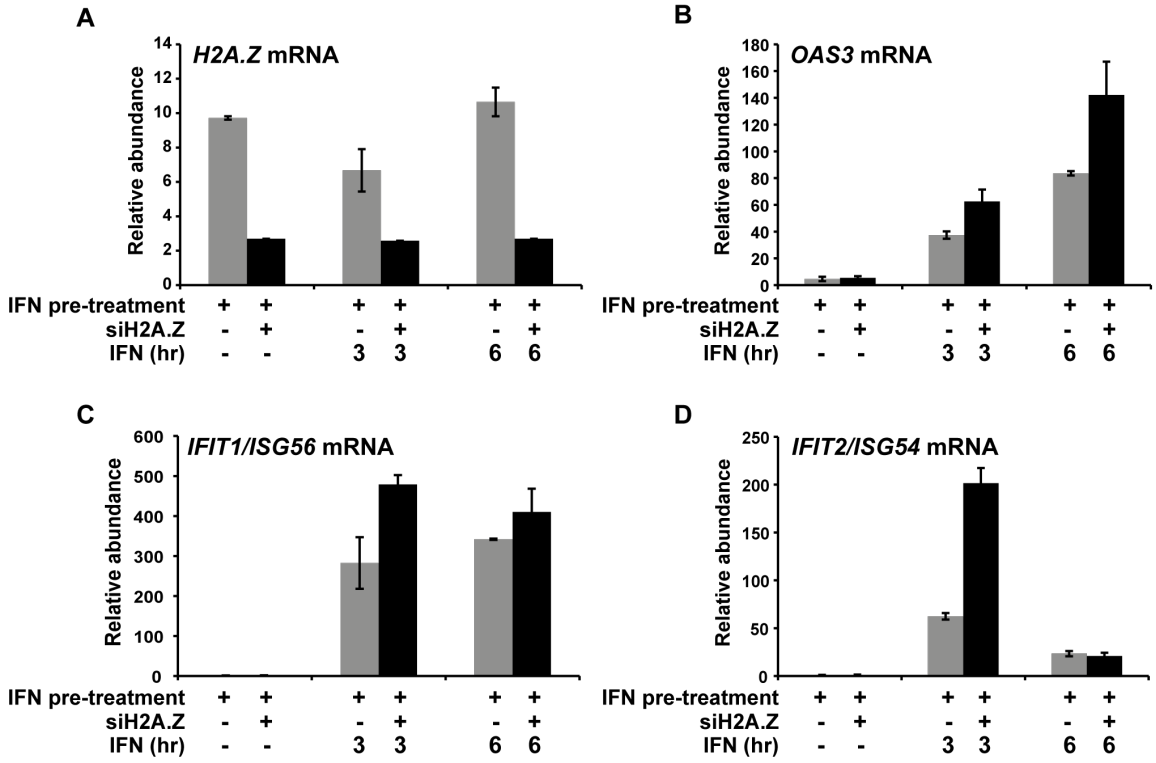

Figure 3.6: IFN pre-treatment coupled with siH2A.Z demonstrates H2A.Z negatively regulates ISG expression

(A-D) Using the same procedure outlined in Figure 3.4, HeLa cells that were IFN pretreated and transfected with either siRNA against control or H2A.Z for 48 hr were analyzed for mRNA expression of A) *H2A.Z*, B) *OAS3*, C) *IFIT1/ISG56,* or D) *IFIT2/ISG54* in HeLa cells mock- or IFN-treated for 3 or 6 hr. Error bars denote standard deviation of technical replicates. Relative gene expression was normalized to *GAPDH*.

Lentivirus-mediated shRNA targeting H2A.Z enhances ISG response

Loss of H2A.Z increases ISG mRNA induction

Previously, the use of an IFN pre-treatment coupled with H2A.Z-siRNA knockdown scheme achieved disruption of H2A.Z at the chromatin and led to an upregulation of ISG expression during the IFN response compared to control cells, indicating H2A.Z negatively regulates ISG transcription. However, being able to demonstrate this phenomenon in the absence of IFN pre-treatment would eliminate the dual IFN treatments. In contrast to the transient knockdown siRNA (Bartlett and Davis, 2006), lentivirus-packaged shRNA is incorporated into the genome providing a more stable and robust knockdown system. Therefore, as an alternative method to investigate the impact of H2A.Z in the IFN response and ISG transcription, knockdown experiments were conducted in HeLa cells harboring lentivirus-mediated shRNA targeting H2A.Z or a non-silencing control sequence (Figure 3.7). H2A.Z mRNA levels did not change due to IFN stimulation and shRNA expression resulted in a significant decrease in H2A.Z mRNA (70-78%) (Figure 3.8A, Appendix Figure 2A, 2C, and 2E). Cells harboring lentivirus-H2A.Z-shRNA reduced H2A.Z protein levels by 64-67% (Figure 3.8B). ISG mRNA levels were measured by RT-qPCR in H2A.Z-shRNA and control cells (Figure 3.8C, Appendix Figure 2B, 2D, and 2F). For all loci tested, increased ISG mRNA levels (2-6 fold) were observed in H2A.Z-shRNA cells compared to control cells. This data indicates H2A.Z negatively regulates ISG transcription and supports the initial conclusion derived from the IFN pre-treatment coupled with H2A.Z-siRNA experiment (Figure 3.6).

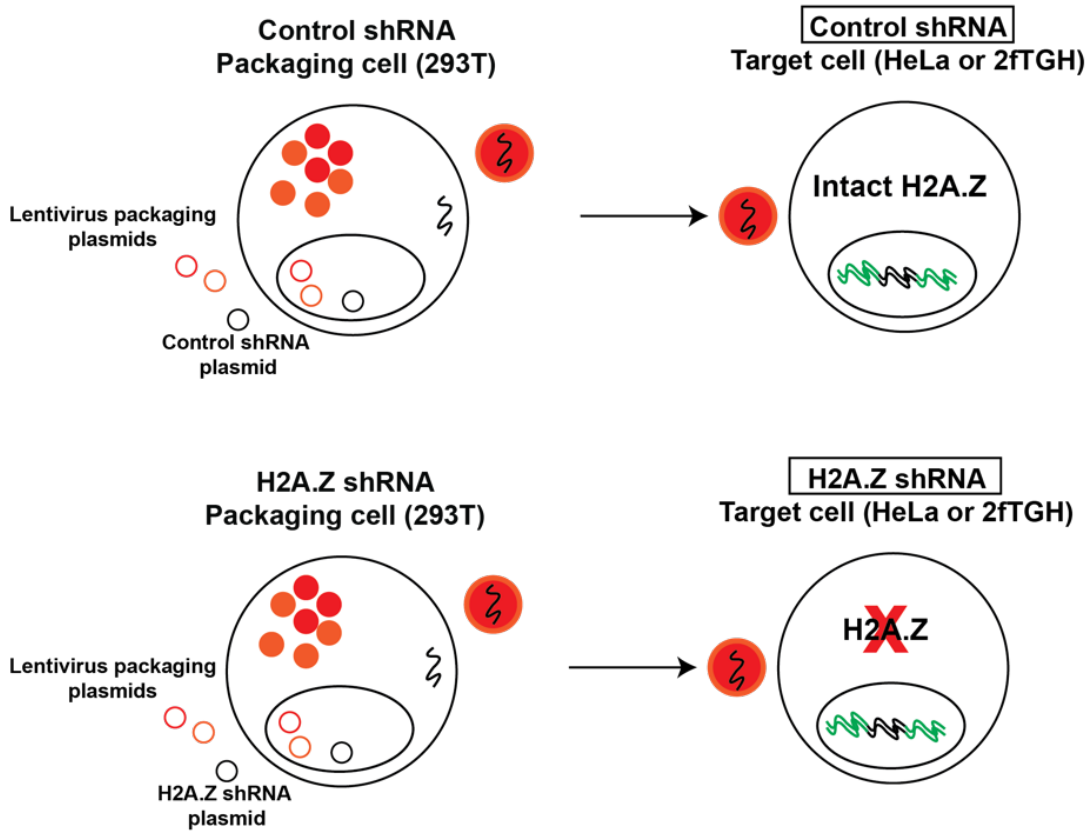

Figure 3.7: Schematic of control and H2A.Z knockdown using lentivirus-mediated shRNA interference

Lentivirus packaging plasmids, pUC-MDC and pΔ8.91, and either shRNA plasmid against control (top) or H2A.Z (bottom) were transfected into 293T cells. Lentivirus containing control or H2A.Z shRNA from 293T cells were harvested after 24 hr and used to transduce target HeLa or 2fTGH cells for 24 hr. HeLa or 2fTGH cells were transduced with fresh lentivirus after 20-24 hrs for up to 3-4 times. H2A.Z or control knockdown cells, containing either a reduced or intact abundance of H2A.Z, respectively, were harvested after 3-4 times of transduction for further analysis.

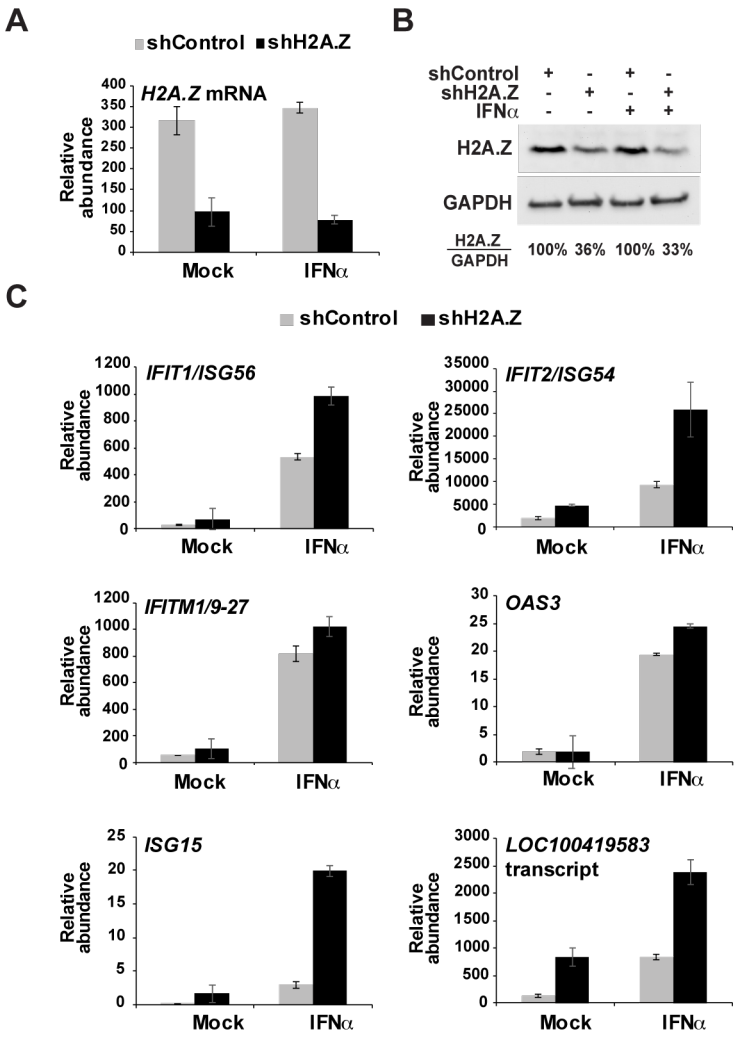

Figure 3.8: H2A.Z suppresses ISG mRNA expression

HeLa cells were transduced with an shRNA vector targeting H2A.Z or a non-targeting control. (A) H2A.Z mRNA levels were quantified by RT-qPCR in unstimulated and 10 hr IFNα-stimulated H2A.Z knockdown or control cells. (B) Immunoblot of protein expression in control or H2A.Z knockdown HeLa cells with or without 1 hr IFNα treatment. Error bars denote standard deviation of technical replicates. H2A.Z expression level normalized to *GAPDH* indicated at % of control. (C) Levels of ISG mRNAs, *IFIT1/ISG56*, *IFIT2/ISG54*, *IFITM1/9-27*, *OAS3*, *ISG15*, and *LOC100419583* were measured as in A. See Appendix Figure 2.

Loss of H2A.Z enables greater ISGF3 recruitment

The predominant transcription factor that activates ISG transcription is ISGF3 (STAT1, STAT2, IRF9). The increased ISG expression observed in H2A.Z-shRNA cells suggested the possibility of altered ISGF3 occupancy. In H2A.Z shRNA-incorporated cells, ChIP assays of STAT2 occupancy demonstrated that depletion of H2A.Z results in increased levels of STAT2 occupancy at ISG promoters after IFN stimulation, compared to control cells (Figure 3.9A, Appendix Figure 3), resulting in a 51-98% increase in ChIP signals at individual ISG loci. This observation was not only observed at classic ISG promoters (i.e. *IFIT1/ISG56*), but also at sites with a strong recruitment of ISGF3 including *LOC100419583* (Figure 2.4, Figure 3.9A, Appendix Figure 3). Similar levels of total and tyrosine-phosphorylated STAT1 and STAT2 were found in control and knockdown cells, confirming that H2A.Z knockdown did not alter IFN-JAK-STAT signaling (Figure 3.9B). These results indicate H2A.Z-containing nucleosomes restrict maximal IFN-induced ISGF3 occupancy at ISG promoters. The increase in ISGF3 occupancy due to H2A.Z deficiency results in increased ISG mRNA expression (Figure 3.8C).

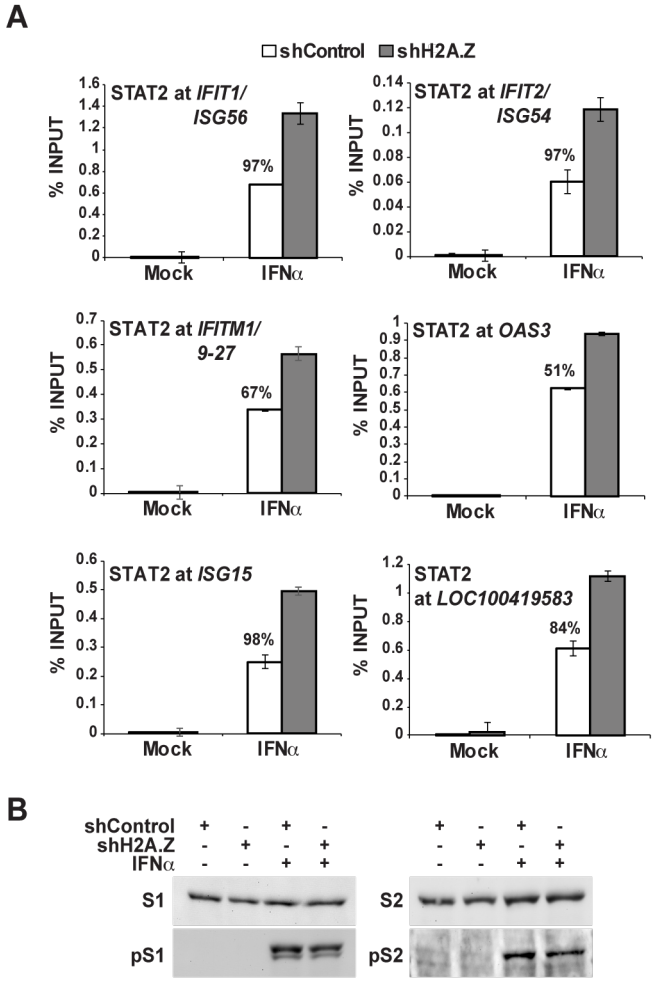

Figure 3.9: H2A.Z suppresses ISGF3 occupancy

HeLa cells were transduced with an shRNA vector targeting H2A.Z or a non-targeting control. (A) ChIP analysis of STAT2 occupancy in H2A.Z knockdown or control HeLa cells with or without 1 hr IFNα stimulation at promoters of *IFIT1/ISG56*, *IFIT2/ISG54*, *IFITM1/9-27*, *OAS3*, *ISG15*, and *LOC100419583*. % indicates the increased percentage of STAT2 occupation in shH2A.Z cells compared to non-targeting control cells. Error bars denote standard deviation of technical replicates. STAT2 occupancy is computed based on the percent input method. (B) Immunoblot of STAT1, phospho-tyrosine 701 STAT1, STAT2, and phospho-tyrosine 690 STAT2 protein expression in control or H2A.Z knockdown HeLa cells with or without 1 hr IFNα treatment. See Appendix Figure 3.

Loss of H2A.Z enhances the IFN-stimulated antiviral response

The IFN-stimulated transcriptional response is the primary cell-autonomous innate antiviral response that inhibits virus replication (Stark and Darnell, 2012). To test the overall phenotypic impact of H2A.Z deficiency in the IFN response, a biological response assay was used to assess a role for H2A.Z in IFN-induced antiviral protection. H2A.Z-shRNA and control shRNA cells were stimulated with IFN for 9 hr to establish an antiviral state, then challenged with vesicular stomatitis virus (VSV) infection, overlayed with agarose, and quantified the viral plaques. Virus replication was virtually identical in H2A.Z-shRNA or control shRNA cells in the absence of IFN stimulation, irrespective of H2A.Z depletion (Figure 3.10A). In contrast, IFN-mediated virus interference was clearly increased in the H2A.Z-shRNA cells compared to control cells, resulting in 2-5x fewer plaques in the absence of H2A.Z in 2fTGH (Figure 3.10B-C) and HeLa cells (Figure 3.10D). This increased antiviral protection observed under reduced H2A.Z conditions is consistent with increased ISGF3 recruitment and ISG transcription, and supports the conclusion that H2A.Z acts as a negative regulator of antiviral responses in human cells.

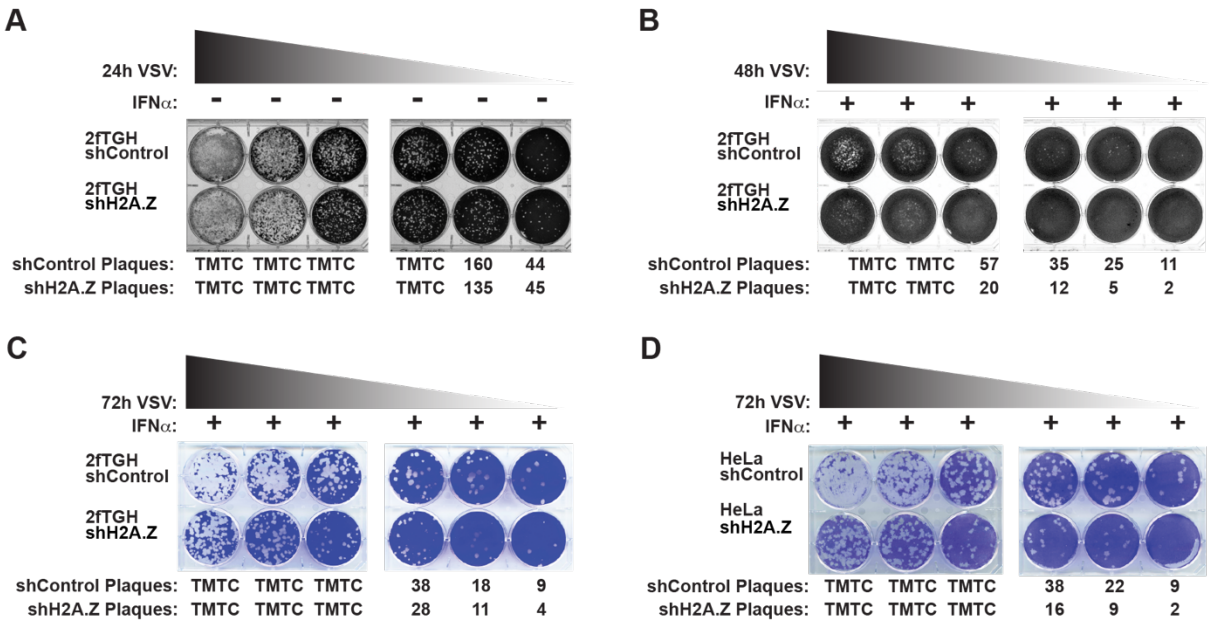

Figure 3.10: H2A.Z suppresses IFN-mediated antiviral protection

(A) Plaque assay in 2fTGH cells harboring a non-targeting control shRNA or H2A.Z shRNA. Cells were inoculated with a VSV titration for 1.5 hr with no IFN stimulation and overlaid with 2% DMEM-agar at 37ºC for 24 hr before staining with crystal violet. (B) Plaque assay of 2fTGH cells harboring shRNA non-targeting control or H2A.Z shRNA. Cells were treated for 9 hr with IFNα before inoculation with VSV, then incubated for 48 hr before staining with crystal violet. (C) Plaque assay in 2fTGH cells harboring control shRNA or H2A.Z shRNA. Cells were treated for 9 hr with IFNα, followed by 1.5 hr inoculation with a titration of vesicular stomatitis virus (VSV), then overlaid with DMEM-agar at 37ºC for 72 hr before staining with crystal violet. (D) Same as C, but in control or H2A.Z-deficient HeLa cells.

IFN-stimulated H2A.Z eviction requires ISGF3

The findings from the previous section, where reduction of H2A.Z expression results in the enhancement of IFN-stimulated antiviral protection, ISGF3 occupancy, and ISG expression, implicate a negative role for H2A.Z in IFN signaling. To complement these functional studies, I sought to characterize the cellular machinery required for H2A.Z remodeling by IFN. During the IFN response, ISGF3 mediates the recruitment of coactivators that function to modify histones and remodel chromatin. Furthermore, IFN-induced H2A.Z removal coincides temporally with ISGF3 recruitment (Figure 3.2), suggesting that ISGF3 may recruit cofactors that remodel H2A.Z nucleosomes following IFN stimulation. To determine whether IFN-induced H2A.Z dynamics requires ISGF3 activity, H2A.Z loss was examined in a series of cell lines with single gene defects in ISGF3 components STAT1, STAT2, or IRF9 (John et al., 1991; Leung et al., 1995; McKendry et al., 1991). In the IFN-responsive parent 2fTGH cells, H2A.Z localized at ISG promoters and was lost following IFN stimulation (Figure 3.11A). In contrast, in the daughter cell lines U3A, U6A, and U2A, with defects in either STAT1, STAT2, or IRF9, H2A.Z remained at ISG promoters following IFN stimulation, indicating that ISGF3 is required for efficient H2A.Z removal (Figure 3.11B-D).

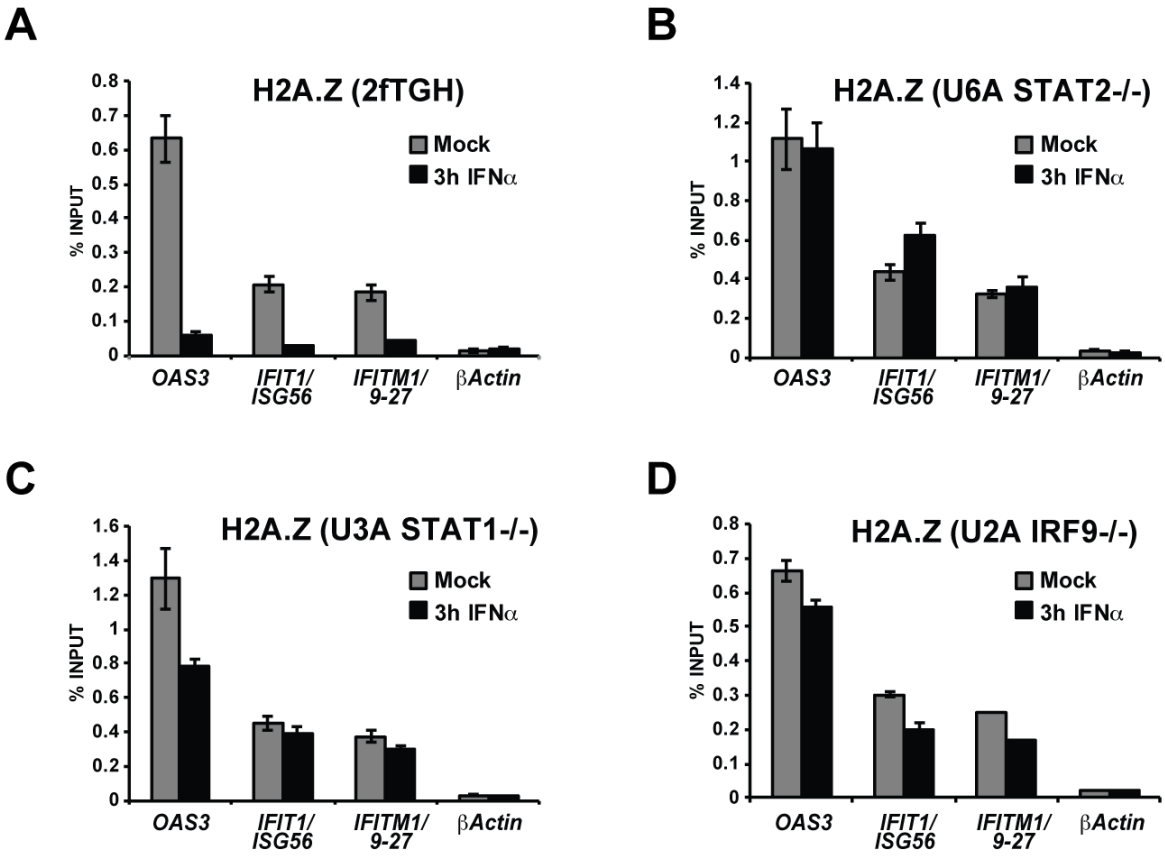

Figure 3.11: H2A.Z removal requires ISGF3
(A) ChIP analysis of H2A.Z in 2fTGH cells with intact ISGF3 at the promoter region of *OAS3*, *IFIT1/ISG56* and *IFITM1/9-27* with mock or 3 hr IFNα treatment. Error bars denote standard deviation of technical replicates. (B) Same as A but with STAT2-deficient U6A cells. (C) Same as A but with STAT1-deficient U3A cells. (D) Same as A but with IRF9-deficient U2A cells.

Investigating Candidate Factors Facilitating the IFN-induced H2A.Z Eviction

Several histone and chromatin modifying activities have been linked to transcriptional activation by IFN signaling and ISGF3, including HATs, HDACs, and the remodeling machines related to BAF/pBAF (termed SWI/SNF in yeast) and INO80 (Bhattacharya et al., 1996; Chang et al., 2004; Cui et al., 2004; Gnatovskiy et al., 2013; Huang et al., 2002; Liu et al., 2002; Nusinzon and Horvath, 2003; Patel et al., 2013; Paulson et al., 2002; Sakamoto et al., 2004). In lower eukaryotes homologous machinery has been implicated in H2A.Z deposition and removal; the yeast chromatin remodeling complexes SWR1 (human SRCAP) and INO80 have been implicated in H2A.Z deposition and removal, respectively, (Kobor et al., 2004; Mizuguchi et al., 2004; Yen et al., 2013). In mouse, the ANP32E factor is recognized as a histone H2A.Z chaperone at some genomic loci (Obri et al., 2014). These factors are associated with the IFN response, H2A.Z regulation, or both and are potential candidates to evaluate for facilitating the IFN-induced eviction of H2A.Z.

RVB1 and RVB2 do not alter IFN-induced H2A.Z eviction in siRNA experiments

In mammals, the RVB1 (RUVBL1) and RVB2 (RUVBL2) proteins that are subunits of chromatin remodeling complexes, BAF, INO80, SWR1 (SRCAP), and TIP60 (Huen et al., 2010), were found to cooperate with STAT2 and regulate ISGF3 transcriptional activity, but through an unknown mechanism (Gnatovskiy et al., 2013). Furthermore, SWI/SNF (BAF) can remodel the chromatin structure of the ISGs *IFITM1/9-27* and *IFITM3/1-8U* (Cui et al., 2004; Liu et al., 2002) and the ATPase subunit BRG1 (SMARCA4) is required

for a subset of ISG transcription (Huang et al., 2002). While SWR1 (SRCAP) and INO80 machinery are implicated in the deposition and removal of H2A.Z (Mizuguchi et al., 2004; Papamichos-Chronakis et al., 2011).

To determine whether RVB1 and/or RVB2 regulates H2A.Z at ISG promoters during the IFN response, RNA interference was performed with siRNA against RVB1 and RVB2 compared with a non-targeting control siRNA. RVB1- and RVB2-siRNA knockdown reduced RVB1 and RVB2 gene expression in mock and IFN-treated cells (Figure 3.12A-B). In cells with reduced RVB1 and/or RVB2 under mock conditions, an increase in H2A.Z occupancy was observed at ISG promoters of *OAS3*, *IFIT1/ISG56,* and *IFITM1/9-27* compared to control cells (Figure 3.12C-E). In RVB1- and RVB2-siRNA knockdown and control cells, IFN induced the loss of H2A.Z (Figure 3.12C-E). These results suggest RVB1 and RVB2 are not required for IFN-induced H2A.Z removal, though they may alter steady state H2A.Z occupancy.

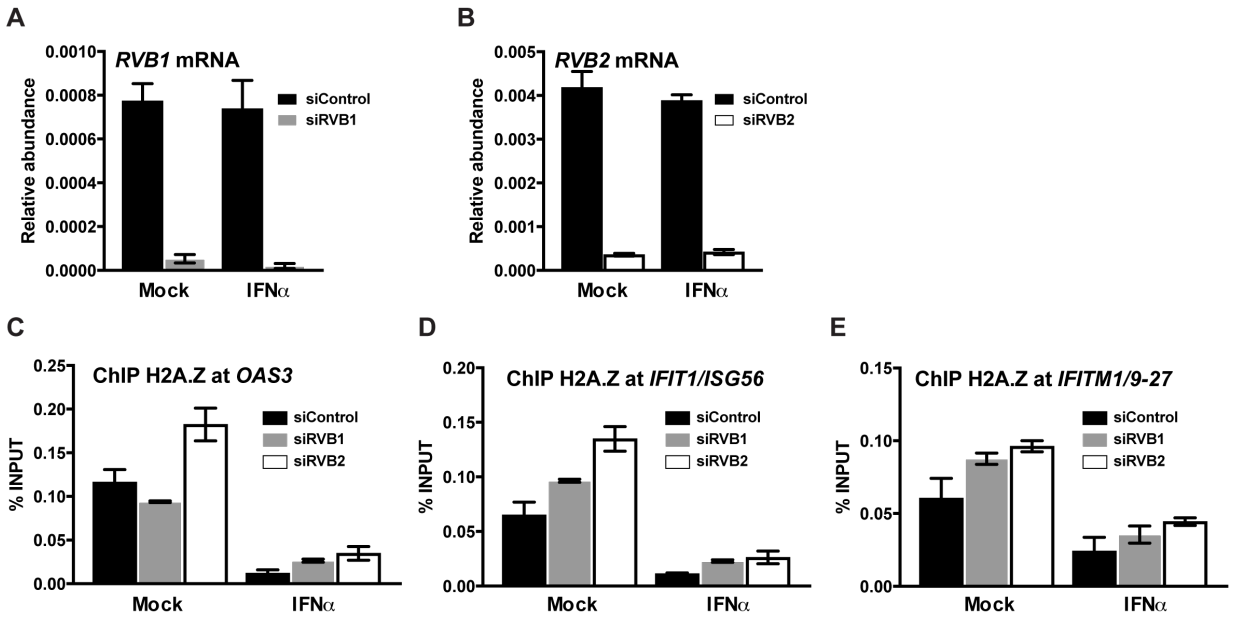

Figure 3.12: siRNA targeting RVB1 and RVB2 did not inhibit IFN-induced H2A.Z loss
HeLa cells were transfected with siRNA against control, RVB1, or RVB2 for 48 hr then mock- or IFN-treated for 2 hr. (A-B) The mRNA abundance of A) *RVB1* and *B) RVB2* in siControl, siRVB1, or siRVB2 knockdown cells. Relative abundance was normalized to *GAPDH.* (C-E) ChIP assays of H2A.Z occupancy in siControl, siRVB1, or siRVB2 knockdown cells at the ISG promoters of A) *OAS3*, B) *IFIT1/ISG56,* or C) *IFITM1/9-27*. Error bars denote standard deviation of technical replicates. ChIP H2A.Z occupancy was measured as a percent of the input DNA.

INO80 and its RVB associates do not alter IFN-induced H2A.Z eviction

Due to the connection RVB1 and RVB2 had with both the IFN system and H2A.Z regulation, an alternative experiment was performed to verify the previous siRNA-based result and examine the associated INO80 complex, which is implicated in H2A.Z removal (Papamichos-Chronakis et al., 2011). To target the INO80 complex, shRNA was used to knockdown the INO80 ATPase subunit and its associates, RVB1 and RVB2 (Figure 3.13). A reduction in INO80, RVB1 and RVB2 expression was demonstrated in shRNA knockdown cells (Figure 3.13A). INO80, RVB1 and RVB2 were not upregulated following IFN treatment indicating they are not ISGs (Figure 3.13A). INO80 and RVB2 interference had little effect on IFN-induced mRNA expression, whereas RVB1 interference effectively prevented ISG transcription (Figure 3.13B). Examination of H2A.Z occupancy revealed that none of these INO80 complex proteins were required for H2A.Z removal following IFN stimulation, although it is interesting to note that RVB1 shRNA led to greater H2A.Z ChIP signals at steady state (Figure 3.13C). Together, this shRNA experiment and the previous siRNA experiment rule out RVB1, RVB2, and INO80 in the process of IFN-mediated H2A.Z removal.

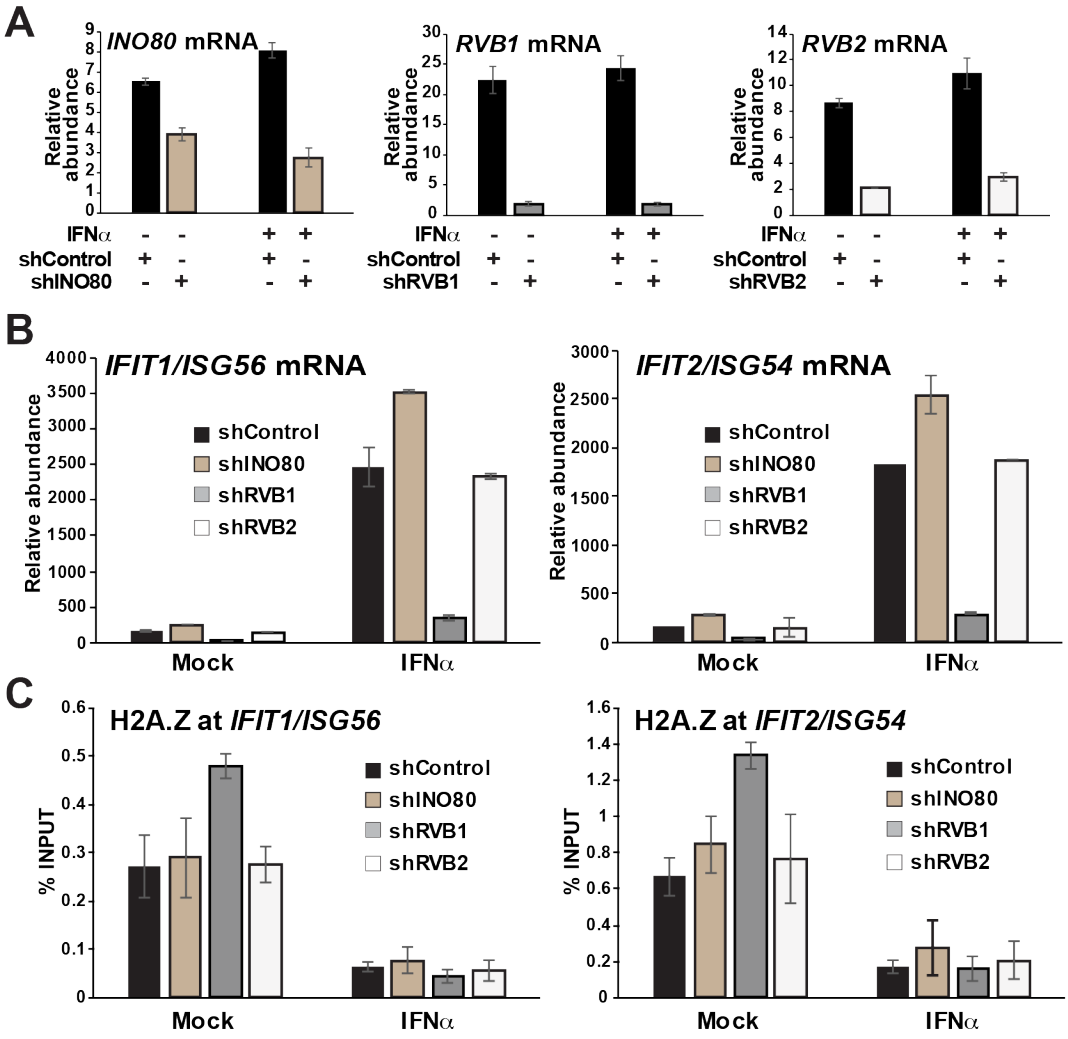

Figure 3.13: shRNA targeting INO80, RVB1 and RVB2 do not mediate H2A.Z eviction (A-C) HeLa cells were transduced with shRNA vectors targeting INO80, RVB1, RVB2 or control. (A) Expression of shRNA targets in mock and 3 hr IFNα-treated cells was measured by RT-qPCR. (B) *IFIT1/ISG54* and *IFIT2/ISG56* mRNA expression in mock and 3 hr IFNα-treated cells harboring the indicated shRNA was measured by RT-qPCR. (C) ChIP assay of H2A.Z occupancy at *IFIT1/ISG56* and *IFIT2/ISG54* promoters in mock and 2 hr IFNα-treated cells containing the indicated shRNA target. Error bars denote standard deviation of biological replicates. ChIP occupancy was computed as a percent of the input DNA.

SRCAP and ANP32E do not regulate IFN-induced H2A.Z eviction

Two additional factors implicated in H2A.Z regulation are the chromatin remodeling complex SWR1 and the mammalian histone chaperone ANP32E. The SWR1 remodeling complex contains RVB1, RVB2, and the ATPase subunit SWR1 (SRCAP), among other subunits. SWR1 (SRCAP) catalyzes the exchange of H2A.Z for H2A in yeast (Mizuguchi et al., 2004; Obri et al., 2014). It is not known whether SWR1 (SRCAP) can also participate in the reverse exchange of H2A for H2A.Z though. The second candidate, ANP32E, is recognized as a mammalian histone H2A.Z chaperone for removing H2A.Z at genomic loci in mice (Obri et al., 2014).

Neither the SRCAP nor ANP32E factor have been implicated in the IFN system, but their role in regulating H2A.Z dynamics in other systems supports examining whether they facilitate IFN-induced H2A.Z removal. To determine whether SRCAP and/or ANP32E mediates H2A.Z removal during the IFN response, disruption with siRNA against SRCAP or ANP32E was performed (Figure 3.14A-B). In cells containing siRNA against SRCAP, mRNA expression of SRCAP was reduced (Figure 3.14A). Both SRCAP knockdown and control cells exhibited IFN-induced H2A.Z removal, indicating SRCAP is not required for IFN-induced H2A.Z removal (Figure 3.14C-D). On the other hand, knockdown of SRCAP resulted in an unexpected increase in steady-state H2A.Z occupancy at ISG promoters (Figure 3.14C-D). Since SRCAP (SWR1) had a role in depositing H2A.Z into chromatin (Kobor et al., 2004; Krogan et al., 2003; Mizuguchi et al., 2004), the initial expectation was that under reduced SRCAP conditions, less H2A.Z deposition would be observed. Instead, reducing SRCAP resulted in increased levels of

steady state H2A.Z occupancy at ISGs, which may have resulted in the higher residual H2A.Z occupancy even after IFN-induced removal (Figure 3.14C-D). This data indicates SRCAP does not catalyze the loss of H2A.Z during the IFN response, but does regulate steady state H2A.Z occupancy levels in mammalian cells and may not be limited to its previously recognized H2A.Z deposition role during steady state.

The mammalian H2A.Z chaperone ANP32E (Figure 3.14B) is implicated in the removal of H2A.Z from many genomic loci in mice and can interact with H2A.Z based on a structural analysis (Obri et al., 2014). In both ANP32E knockdown and control cells (Figure 3.14B) similar levels of steady-state H2A.Z were observed at ISG, *OAS3* and *IFIT1/ISG56*, promoters (Figure 3.14C-D). IFN stimulation resulted in H2A.Z loss from ISG promoters in ANP32E knockdown and control cells (Figure 3.14C-D). Similar to SRCAP knockdown cells but to a lesser extent, the IFN-stimulated ANP32E knockdown cells also exhibited higher H2A.Z occupancy levels than control cells, notably at the *IFIT1/ISG56* promoter (Figure 3.14C-D). This data suggests ANP32E is not required for facilitating IFN-induced H2A.Z eviction at ISGs, but does not completely rule out a supportive role for ANP32E in a gene-specific manner.

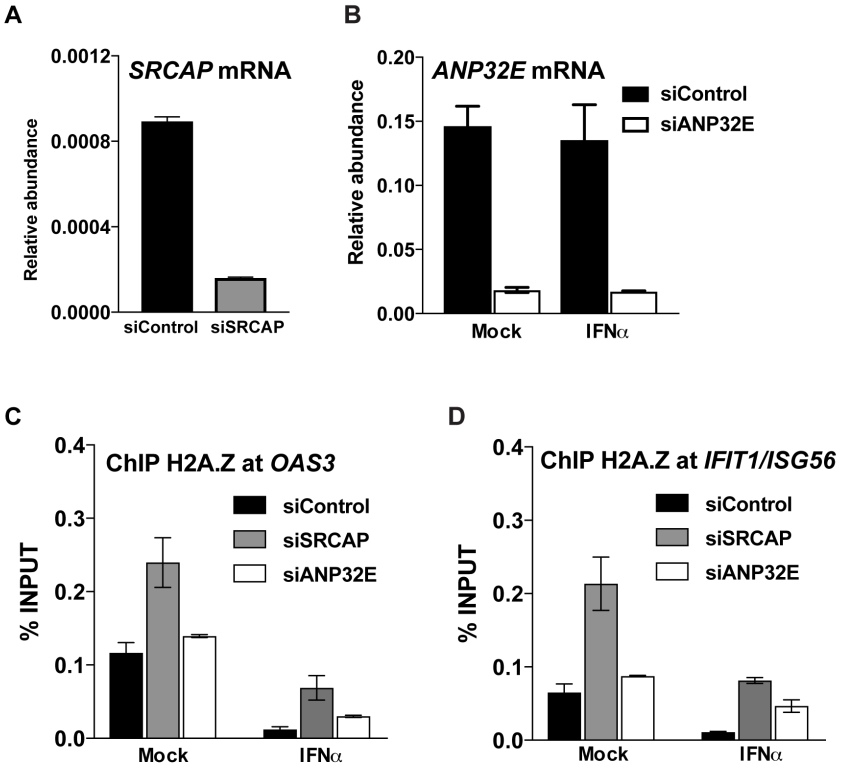

Figure 3.14: SRCAP and ANP32E are not required for IFN-induced H2A.Z loss

HeLa cells were transfected with siRNA against control (non-targeting sequence), SRCAP, or ANP32E. (A) *SRCAP* mRNA expression in control or SRCAP knockdown cells was measured with RT-qPCR and normalized to *GAPDH*. (B) *ANP32E* mRNA expression was measured with RT-qPCR and normalized to *GAPDH* in control or ANP32E knockdown cells following mock or IFN treatment. (C-D) ChIP assay of H2A.Z occupancy at C) *OAS3* and D) *IFIT1/ISG56* promoters in control, siSRCAP, or siANP32E knockdown cells mock-treated or treated with 3 hr IFNα. Error bars denote standard deviation of technical replicates. ChIP occupancy was computed as a percent of the input DNA.

SWI/SNF does not alter IFN-dependent H2A.Z removal

ISGF3, through STAT2, associates with the homologous yeast SWI/SNF and human BAF/pBAF remodeling complex through the ATPase subunit, BRG1 (Chi, 2004). BRG1 is required for the transcription of ISGs *IFI27* and *IFITM1/9-27,* but not *ISG15*, *IFI6*, *STAT1,* and *STAT2*. The mechanism underlying the differential requirement of BRG1 is unknown (Huang et al., 2002). However, BAF subunits BRG1 and BAF47 have been implicated in remodeling ISG, *IFITM1/9-27* and *IFITM3/1-8U,* promoter nucleosomes during IFN stimulation (Cui et al., 2004; Liu et al., 2002). These studies indicate the BAF/pBAF complex is recruited to remodel ISG promoter nucleosomes, which contain H2A.Z, and suggests the BAF complex may remodel H2A.Z-containing nucleosomes at ISG promoters. Furthermore, H2A.Z and the SWI/SNF remodeling complex are thought to be partially redundant in yeast, where deletion of H2A.Z increases the need for SWI/SNF (Santisteban et al., 2000). Here, interference of the SWI/SNF (BAF) complex with the BRG1/BRM inhibitor, PFI-3, potently inhibited ISG activation (Figure 3.15A). However, this treatment did not alter IFN-dependent H2A.Z removal (Figure 3.15B), indicating the role of BRG1 and the SWI/SNF complex in the IFN response is independent of H2A.Z dynamics.

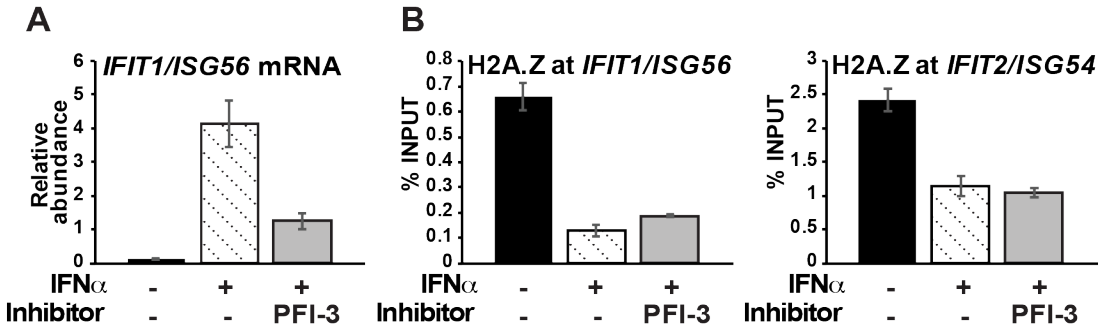

Figure 3.15: SWI/SNF (BRG1) does not alter IFN-induced H2A.Z loss

HeLa cells were mock-treated or IFNα-treated with or without PFI-3 (inhibits BRG1/SMARCA4) for 3 hr, then analyzed for (A) *IFIT1/ISG56* mRNA expression by RT-qPCR and (B) ChIP assays of H2A.Z occupancy at *IFIT1/ISG56* and *IFIT2/ISG54* promoters.

HDAC activity does not alter H2A.Z dynamics

Histone deacetylase (HDAC) activity is commonly associated with transcription repression (Delcuve et al., 2012; Grunstein, 1997), whereas for ISG transcription activation HDAC activity is absolutely required. Through experiments using HDAC inhibitors, trichostatin A (TSA) and sodium butyrate, ISG expression was globally inhibited or downregulated (Chang et al., 2004; Nusinzon and Horvath, 2003; Sakamoto et al., 2004). HDAC1 was specifically implicated in the process and interacts with STAT2 (Nusinzon and Horvath, 2003). However, HDAC inhibition did not affect IFN-induced STAT2 recruitment, but prevented Pol II recruitment to the *IFIT2/ISG54* promoter (Sakamoto et al., 2004). H2A.Z dynamic regulation is also under acetylation control (Sevilla and Binda, 2014), suggesting a potential relationship between the HDAC requirement for ISGs and IFN-induced H2A.Z removal. To evaluate the effect of HDAC inhibition on H2A.Z dynamics, cells were mock-treated or treated with IFN in the presence or absence of the HDAC inhibitor, TSA. Treatment with TSA potently inhibited ISGF3 transcriptional activity (Figure 3.16A), but no effect was observed for H2A.Z in the ChIP assay (Figure 3.16B), ruling out class I and II HDACs in this process.

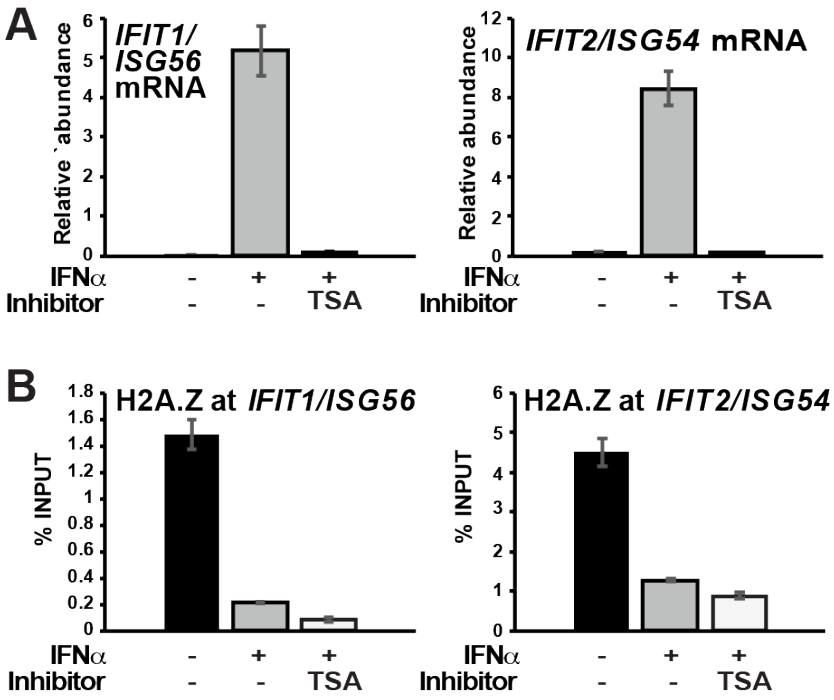

Figure 3.16: HDAC activity does not alter H2A.Z loss

HeLa cells were mock- or IFNα-treated for 3 hr with or without TSA (inhibits HDAC activity). (A) *IFIT1/ISG56* and *IFIT2/ISG54* mRNA expression in mock and 3 hr IFNα-treated cells measured by RT-qPCR. (B) ChIP assay of H2A.Z occupancy at *IFIT1/ISG56* and *IFIT2/ISG54* promoters in mock and 3 hr IFNα-treated cells with or without TSA. Error bars denote standard deviation of technical replicates. ChIP occupancy was computed as a percent of the input DNA.

GCN5, but not CBP, and BRD2 mediate IFN-induced H2A.Z removal

Histone H3 and H4 acetylation levels are altered in response to IFN stimulation and HAT activity is required for ISG expression (Nusinzon and Horvath, 2003; Paulson et al., 2002). The histone acetyltransferases (HATs), CBP/p300 and GCN5, interact with ISGF3 and participate in ISG transcription (Bhattacharya et al., 1996; Paulson et al., 2002). Genomic sites harboring CBP/p300 and H2A.Z have been correlated with specific binding of enhancers by pioneer transcription factors (Cauchy et al., 2017). To determine whether CBP mediates IFN-induced H2A.Z removal through its interaction with STAT2/ISGF3, cells containing shRNA targeting CBP or a non-silencing control were examined. Targeting CBP by lentiviral-packaged shRNA interfered with ISG transcription and reduced steady-state H2A.Z levels at ISG promoters, but H2A.Z was removed after IFN stimulation indicating CBP does not mediate IFN-induced H2A.Z removal (Figure 3.17).

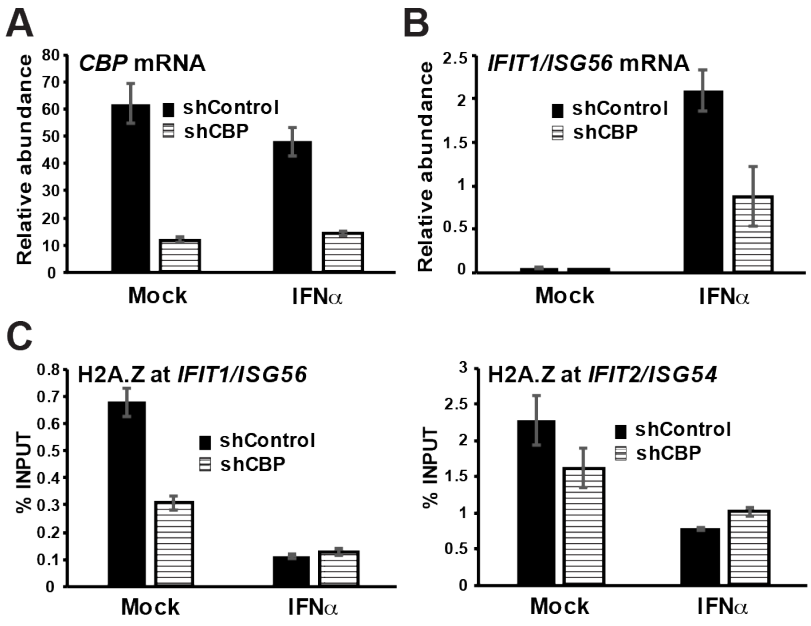

Figure 3.17: CBP does not alter H2A.Z loss

HeLa cells were transduced with shRNA vectors targeting *CBP* or control. (A) Gene expression of *CBP* in mock and 3 hr IFNα-treated cells containing shControl or shCBP was measured by RT-qPCR and normalized to *GAPDH*. (B) *IFIT1/ISG56* mRNA expression in mock and 3 hr IFNα-treated cells harboring shControl or shCBP was measured by RT-qPCR and normalized to *GAPDH*. (C) ChIP assay of H2A.Z occupancy at *IFIT1/ISG56* and *IFIT2/ISG54* promoters in mock and 2 hr IFNα-treated cells containing shControl or shCBP. Error bars denote standard deviation of technical replicates. ChIP occupancy was computed as a percent of the input DNA.

GCN5 is also required for ISG transcription and interacts with STAT2 (Paulson et al., 2002). Other studies have attributed acetylation of histones H2A.Z, H3, and H4 to GCN5 HAT activity (Anamika et al., 2010; Millar et al., 2006). To test whether GCN5 activity mediates IFN-induced H2A.Z loss, cells treated with IFN in the presence or absence of a GCN5 inhibitor, MB-3, were compared to mock-treated cells in RT-qPCR and ChIP assays. Inhibition with MB-3 not only downregulated ISG transcription (Figure 3.18A, C), but also abrogated IFN-induced H2A.Z loss in HeLa and 2fTGH cells (Figure 3.18B, D).

GCN5 or GCN5-containing HAT complexes have been shown to acetylate histones H3, H4, and H2A.Z, and these acetylated lysines can in turn be recognized by bromodomain-containing factors. Bromodomains in the BET family proteins, BRD2, BRD3, BRD4 and BRDT, recognize and bind to acetylated lysine residues on histones to execute histone chaperone activities and recruit transcriptional machinery (Taniguchi, 2016). In the IFN response, BRD4 is an adaptor used for recruitment of pTEFb and NELF/DSIF for ISG transcription elongation (Patel et al., 2013). While BRD2 has not previously been examined for a role in the IFN system, it has been shown to preferentially associate with H2A.Z-containing nucleosomes rather than H2A; moreover, its recruitment has been linked to H2A.Z and acetylated H4K12 (Draker et al., 2012). Both the BET inhibitor, JQ1 (targeting BRD4 and BRD2) and BIC1 (a more selective BRD2 inhibitor), were able to interfere with ISG transcription and prevent IFN-stimulated H2A.Z removal including acetylated H2A.Z (Figure 3.18-3.19). Together, these results demonstrate the

GCN5 histone acetyltransferase and BRD2 bromodomain binding activity are required to regulate IFN-induced H2A.Z removal.

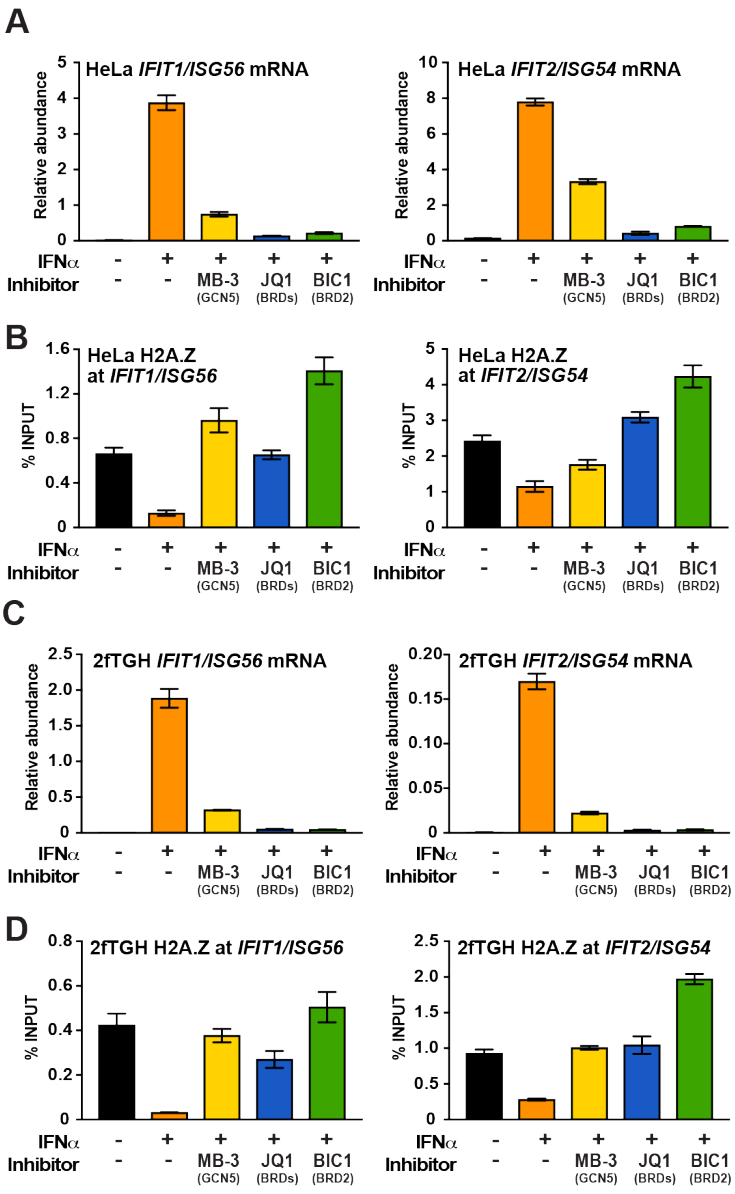

Figure 3.18: GCN5 and BRD2 are essential to IFN-induced H2A.Z loss

(A-B) HeLa cells were pretreated with MB-3 (inhibits KAT2A/GCN5) or BET inhibitors JQ1 (inhibits BRDs) or BIC1 (inhibits BRD2) for 1 hr, mock-treated or stimulated with IFNα for 3 hr, then analyzed for (A) *IFIT1/ISG56* and *IFIT2/ISG54* mRNA expression and (B) H2A.Z occupancy at *IFIT1/ISG56* and *IFIT2/ISG54*. Error bars denote mean ± SD of one representative experiment with technical triplicates. (C-D) Same as A-B except in 2fTGH cells.

A

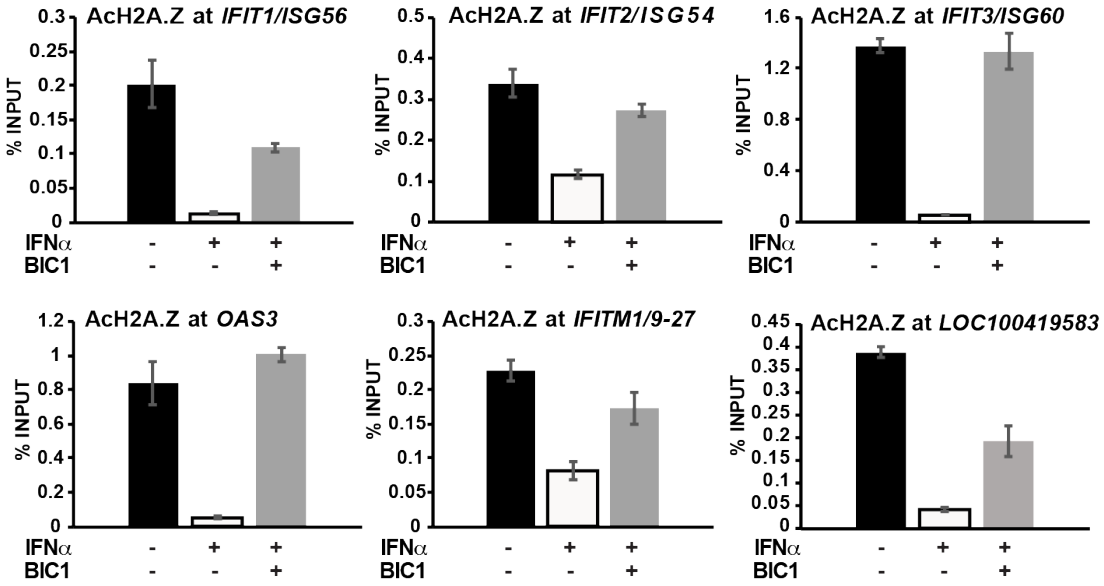

Figure 3.19: IFN-stimulated acetylated H2A.Z loss requires BRD2

(A) ChIP analysis of acetylated H2A.Z (AcH2A.Z; K4, K7, K11) after mock, 3 hr IFNα, or 1 hr pre-incubation with BIC1 followed by 3 hr IFNα/BIC1 treatment at the gene promoters of *IFIT1/ISG56*, *IFIT2/ISG54*, *IFIT3/ISG60*, *OAS3*, *IFITM1/9-27,* and *LOC100419583*. Normalized to percent (%) input. Error bars denote mean ± SD of a representative experiment with three technical replicates.

DISCUSSION

Direct examination of the histone composition of ISG promoters not only confirmed the IFN-induced nucleosome loss, but also identified an absence of histone H2A. In its place, the H2A variant H2A.Z was found to be enriched at or near the ISRE regions of most highly-responsive ISGs prior to IFN stimulation. H2A.Z presence at ISG promoters was found to be tightly but inversely correlated with IFN-stimulated STAT2 occupancy, and IFN stimulation induced acute and transient loss of H2A.Z at ISG promoters coinciding with the cycle of ISGF3 activation, inactivation, and transcription attenuation. H2A.Z removal requires ISGF3 components STAT1, STAT2, or IRF9, indicating a role for ISGF3 in recruiting and coordinating machinery for H2A.Z nucleosome eviction. Identification of H2A.Z at ISG promoters is in agreement with the general paradigm of H2A.Z nucleosome association with active or inducible gene promoters (Barski et al., 2007; Hu et al., 2013; Raisner et al., 2005). Here, H2A.Z colocalizes at steady state with the active histone modification mark, H3K4me3, but not the repressive H3K27me3 mark, and H3K4me3 is reduced after IFN. Additional studies will be required to examine other histone modifications that are present prior to or following IFN stimulation and their correlation with H2A.Z chromatin dynamics at ISG promoters.

To determine the factor(s) regulating H2A.Z loss, we examined a broad array of coactivators that were known to be associated with ISGF3 and ISG transcription, as well as those previously implicated in H2A.Z deposition or removal from other systems. In lower eukaryotes, SWR1 (SRCAP) was demonstrated to deposit H2A.Z, and knockdown of mammalian SRCAP did not alter IFN-induced H2A.Z removal. Although the INO80

remodeling complex is purported to be responsible for removing H2A.Z nucleosomes in lower eukaryotes (Lai and Pugh, 2017), results indicate neither RVB nor the INO80 components are necessary for IFN-induced H2A.Z removal in mammalian cells. Unexpectedly, interference with INO80 or RVB2 had no discernable effect on ISG transcription, though it is possible that RNA interference was insufficient to deplete stable protein activity. In contrast, RVB1 as well as CBP, BRG1/BRM, and HDACs were all found to be essential for ISG mRNA transcription, but their inhibition had no effect on IFN-stimulated H2A.Z removal. These proteins are otherwise required for ISG transcription, acting either through another remodeler such as SWI/SNF (BAF), or through distinct mechanisms. The increase of steady state H2A.Z in SRCAP and RVB1 knockdown cells suggests that the human SRCAP subunit/complex differs from its yeast homolog, which may not be surprising given the interferon/JAK-STAT system does not exist in yeast.

Instead, the histone acetyltransferase GCN5 was identified as being required for ISG transcription and as an essential component of H2A.Z eviction. Inhibition of GCN5 using MB-3 generally inhibited the IFN-induced H2A.Z removal at the ISG promoters examined in both HeLa and 2fTGH cell lines, but a smaller effect of GCN5 inhibition was observed at the *IFIT2/ISG54* promoter. We postulate that this might indicate redundancy in HAT activities or reflect heterogeneity at individual ISG loci. GCN5 or GCN5-containing HAT complexes have been shown to acetylate histones H3, H4, and H2A.Z, and these acetylated lysines are in turn recognized by BET family protein bromodomains (Anamika et al., 2010; Millar et al., 2006). The BET family protein BRD4 is a mediator of ISG transcriptional elongation by recruiting pTEFb and NELF/DSIF to paused polymerases

(Patel et al., 2013), and we find that BRD2 inhibition prevents both ISG transcription and H2A.Z removal. This finding is consistent with BRD2's preferential association with H2A.Z-containing nucleosomes (Draker et al., 2012; Punzeler et al., 2017; Surface et al., 2016).

Histones H2A.Z, H3, and H4 are acetylated at ISG promoters, and this acetyl-rich environment, catalyzed by GCN5, CBP, and potentially other unknown HATs, promotes bromodomain factors to bind. Recruitment of BRD2 along with other BRDs to ISG promoters drives the IFN-induced H2A.Z eviction. The interplay between H2A.Z and the intranucleosomal histones and PTMs can influence the role H2A.Z plays in gene regulation. For example, monoubiquitylation of H2B has been shown to antagonize H2A.Z eviction, while ubiquitylated H2A.Z prevents BRD2 binding (Segala et al., 2016; Surface et al., 2016). Similarly, acetylated histone H4 preferentially associates with H2A.Z-containing nucleosomes compared to H2A-containing nucleosomes (Draker et al., 2012), and when the BIC1 inhibitor binds to BRD2, this prevents BRD2 from interacting with the acetylated histone residue H4K12 (Ito et al., 2011). These findings suggest the association with repressive or active factors at H2A.Z-containing nucleosome could influence the dynamic role H2A.Z serves in chromatin accessibility and gene activation.

H2A.Z is thought to influence nucleosome stability and positioning, and consequently alter the ability of activating or repressing factors to make stable or transient contact with DNA. This general property of H2A.Z nucleosomes can result in both positive and negative regulation, depending on gene-specific, tissue-specific, and/or context-specific transcriptional responses (Marques et al., 2010; Subramanian et al., 2015). The

physical and regulatory properties of H2A.Z-containing nucleosomes have been widely studied, but the literature reflects a variety of roles. For example, in embryonic stem cell differentiation H2A.Z is important for facilitating recruitment of chromatin activators and repressors (Hu et al., 2013; Surface et al., 2016). H2A.Z has been associated with both transcription activation and transcription inhibition, and described as both an activator and repressor of gene expression (Hu et al., 2013; Ku et al., 2012; Schones et al., 2008; Surface et al., 2016; Zlatanova and Thakar, 2008). Although knocking down H2A.Z does not alter steady state ISG expression, loss of H2A.Z nucleosomes allows ISGF3 greater access to DNA, increases ISG expression, and produces a more effective innate antiviral response. The loss of H2A.Z and/or H2A.Z-nucleosomes did not induce complete loss of nucleosome(s) at ISGs based on either sustained or increased occupancy of histones H4 and H2A (Appendix Figure 4). Altogether, these results suggest a model where ISGF3 recruits GCN5 to acetylate histones leading to BRD2 engagement and to mediate remodeling/eviction of H2A.Z nucleosomes. Reduced H2A.Z relieves the need to remodel the nucleosomes at ISG promoters, enabling ISGF3 to bind and activate ISG expression more easily. This greater access translates into more potent antiviral activity.

Regulating ISG transcription is critical for cellular antiviral responses and for subsequent immune responses, and chronic IFN signaling can lead to inflammatory and autoimmune diseases (Rodero and Crow, 2016). Dysregulation of ISG transcription is also observed in tumors, and contributes to immunotherapy resistance (Benci et al., 2016). The combinatorial use of BET inhibitors or other epigenetic drugs with immunotherapy is a current strategy to improve treatment outcomes (Marazzi et al., 2017), and H2A.Z

expression is also associated with malignancies (Monteiro et al., 2014), suggesting an interrelated regulatory network that includes cytokine-activated transcription, nucleosome dynamics, and chromatin remodeling activities that can be exploited for augmenting therapeutic strategies.

RESEARCH CONTRIBUTIONS AND PUBLICATION

Dr. Curt M. Horvath and I designed and interpreted the experiments. I conducted all of the experiments and bioinformatic analyses. The major findings are published in the following manuscript:

Au-Yeung, N., and Horvath, C.M. (2018). Histone H2A.Z Suppression of Interferon-Stimulated Transcription and Antiviral Immunity is Modulated by GCN5 and BRD2. iScience *6*, 68-82.

CHAPTER 4.

PERSPECTIVE

CHROMATIN REGULATION OF IFN-STIMULATED GENE TRANSCRIPTION

The aim of this thesis project was to characterize the ISGF3-mediated chromatin dynamics at ISGs and the complementary ISG chromatin regulation during steady state and after IFN stimulation. Similar to other genes, ISGs are governed by the same chromatin structure, and consequently, many of the same rules for gene accessibility. Induction of ISGs during the IFN-JAK-STAT signaling response is rapid and necessary to establish a protective environment against virus infection (Stark and Darnell, 2012). Compared to other facets of the JAK-STAT signaling pathway, our understanding of the ISG chromatin landscape and ISGF3-mediated nucleosome dynamics in the IFN response is less comprehensive.

At the time of this thesis work, no high-resolution data on the changes in nucleosome positioning at ISGs undergoing IFN stimulation existed. The ISG nucleosome and chromatin landscape following IFN stimulation was largely a mystery. The thesis work described in Chapter 2 fills much of that gap with high-resolution ISG nucleosome maps during steady state and after multiple time points of IFN stimulation corresponding to ISGF3 activation and attenuation. In-depth examination of the nucleosome dynamics from Chapter 2 led to a previously unrecognized role for histone variant H2A.Z in ISG transcription regulation described in Chapter 3. Together, this thesis project not only identifies the positioned nucleosome dynamics at ISGs during steady state and after IFN stimulation, but also correlates it to ISGF3 recruitment. ChIP-Seq data from this thesis project of all three ISGF3 components STAT1, STAT2, and IRF9 provided the first genome-wide analysis of ISGF3 occupancy after IFN stimulation. This

work also led to the dissection of the histone composition at ISG promoter nucleosomes, revealing a mechanistic role for histone variant H2A.Z-containing nucleosomes in ISG transcriptional regulation in Chapter 3. On one hand, IFN-induced H2A.Z removal required ISGF3 and coactivators GCN5 and BRD2; and on the other hand, H2A.Z nucleosomes negatively regulated ISGF3 occupancy and ISG transcription. Examination of the interplay between ISGF3 and the ISG promoter nucleosomes is necessary to understand how ISGF3 interacts with ISG chromatin, and simultaneously, how chromatin regulates ISG transcription.

Expectations and deviations of ISGF3 recruitment at ISG promoters

Since several of the 20 ISGs examined were well-characterized and previously associated with ISGF3, the expected recruitment of the ISGF3 components STAT1, STAT2, and IRF9 following IFN stimulation was confirmed at most of the ISGs. However, two unexpected results were observed at the gene promoter region of *AIM2* and *STAT1. AIM2* is a member of the HIN-200 gene family, which includes *IFI16,* and was a latecomer to being recognized as an ISG (Landolfo et al., 1998). At the *AIM2* promoter, little to no recruitment of STAT1 and IRF9 was observed. STAT2 is also not highly recruited following IFN stimulation, however, the relatively higher STAT2 signal than STAT1 and IRF9 at *AIM2* likely reflects a more efficient STAT2 immunoprecipitation owing to the quality of the antibody. This data suggests *AIM2* is not highly targeted by ISGF3 during the primary IFN response, if at all, even though it is recognized as an ISG.

For the *STAT1* proximal promoter region, where an ISRE is present, very little STAT2 and IRF9 recruitment is observed. Interestingly, examination of the genomic region approximately 6000 bp upstream of the *STAT1* TSS, a strong recruitment of STAT1, STAT2, and IRF9 is apparent (Figure 4.1). This upstream site resembles a distal regulatory element approximately 5500 bp upstream of *STAT1* from a study in mouse 3T3 cells (Yuasa and Hijikata, 2016). The distal *STAT1* element from mouse 3T3 cells was found to interact with the core promoter of *STAT1* and enhanced *STAT1* luciferase reporter activity. Determining whether these sites in human and mice represent the same element and/or a long-range chromatin interaction site require further investigation.

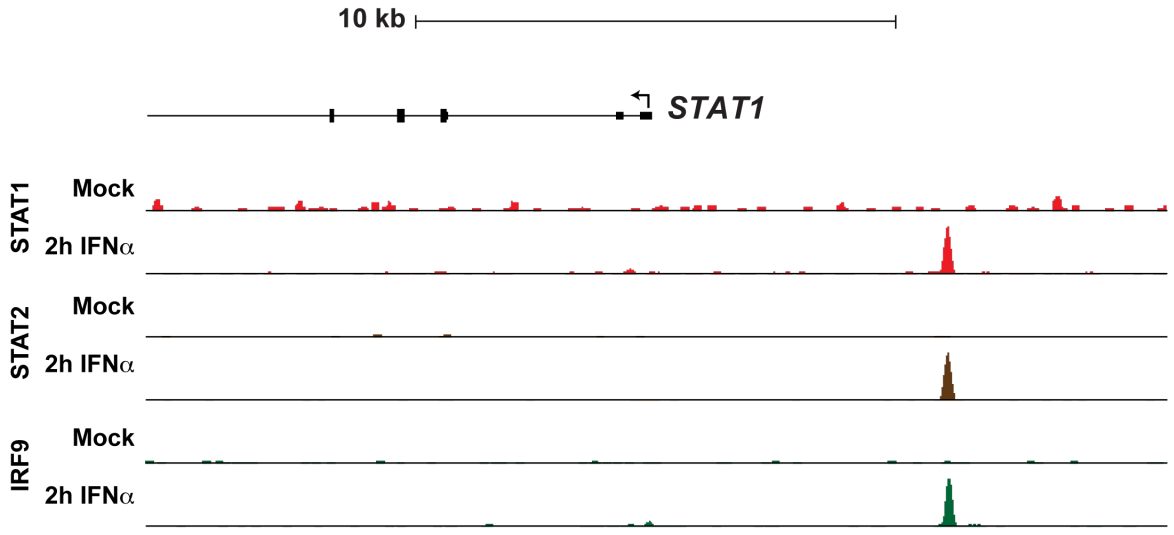

Figure 4.1 ISGF3 recruitment at *STAT1* is approximately 6000 bp upstream of TSS
Genome browser view of IFN-induced ISGF3 recruitment at *STAT1.* (From top to bottom) 10 kilobase (kb) pair scale bar. The arrow denotes the TSS of *STAT1* and the direction of transcription. The 5' end of *STAT1* is depicted by small black bars (untranslated region), large black bars (exon) and line (intron). ChIP-Seq density of STAT1, STAT2, and IRF9 occupancy after mock or 2 hr IFNα treatment in HeLa cells.

Differential ISG promoter nucleosome arrangements

ISGs are represented by hundreds of genes that are upregulated by IFN stimulation and transcriptionally activated by ISGF3. Despite the simultaneous gene activation of ISGs, examination of the 20 ISG promoter nucleosomes revealed differential patterns of nucleosome arrangement (Figure 2.7-2.9). This difference was observed even among ISG protein family members that are clustered closely together in the genome. These include the gene families of *OAS* (*1, 2, 3*), *IFIT* (*1, 2, 3, 5*), *IFITM* (*1, 2, 3, 5*), *MX* (*1, 2*) and HIN200 (*IFI16, AIM2)*. Among members of the same protein family, different dynamic schemes of -1 and +1 positioned nucleosomes were utilized. For example, in the *OAS* family, *OAS1* had the most apparent +1 positioned nucleosome which was subsequently lost after IFN treatment. Although *OAS2* also contains a well-positioned +1 nucleosome, its relative loss pattern was less dramatic. Finally, *OAS3* did not have an apparent +1 nucleosome, though this lack of signal may indicate a “fragile” nucleosome more susceptible to nuclease cleavage. Gene-specific patterns of nucleosome arrangements are observed across the 20 ISGs examined, even among genes from the same ISG family. Generally, the most apparent IFN-induced nucleosome loss accompanies the best recognized or classic ISGs, which tend to have robust ISGF3 recruitment and high gene expression.

Comparison with public ISG chromatin accessibility data

In addition to the BEM-seq method employed in the thesis work in Chapter 2, other methods coupled with next generation sequencing exist to examine chromatin

accessibility including DNase-seq and FAIRE-seq (Tsompana and Buck, 2014). Although these methods are unable to identify the position of an individual nucleosome or achieve the hundreds of fold higher resolution at an individual gene that BEM-seq can, data generated with comparable experimental conditions (i.e. cell type, treatment) from these methods allow for comparison between independent studies. Public domain data examining HeLa cells during steady state and after 4 hr IFNα treatment using alternative chromatin accessibility methods, FAIRE-seq and DNase-seq, are available. In Figure 4.2, a representative ISG *IFITM1/9-27* is used as an example to compare the BEM-seq data with comparable public domain data to further our understanding of the ISG chromatin landscape during the IFN response. Even though the 4 hr IFN treatment time used in the public data differs from the 2 hr IFNα treatment time used for the BEM-seq high-resolution nucleosome maps in Chapter 2, both time points are within a time frame when the IFN response and ISGF3 recruitment is highly active (Figure 2.1; Consortium, 2012). Parallel examination of the high-resolution nucleosome maps generated in this project and the public FAIRE-seq and DNase-seq data reveal a similar pattern of increased chromatin accessibility following IFN treatment at *IFITM1/9-27* (Figure 4.2). In particular, both nucleosome loss and chromatin accessibility increased at the promoter region following IFN treatment, coinciding with ISGF3 recruitment. Collectively, the BEM-seq, FAIRE-seq, and DNase-seq data support an increase in chromatin accessibility at ISG promoters in response to IFN stimulation and ISGF3-mediated nucleosome dynamics.

More recently, a study in mouse B cells following a 1.5 hr IFN treatment was examined with an alternative chromatin accessibility method, ATAC-seq (Mostafavi et al.,

2016). However, parallel examination with the ATAC-seq data from mice is not possible with the human BEM-seq nucleosome maps because of the genomic positioning difference between the human and mice genome. Nevertheless, a general trend of increased chromatin accessibility at mouse ISG promoters is observed and is not dissimilar to the general nucleosome loss from the BEM-seq nucleosome maps. Cumulatively, the various methods to interrogate chromatin and nucleosome dynamics at ISGs during steady and after IFN stimulation demonstrate a similar pattern of increased chromatin accessibility and nucleosome loss during the IFN response.

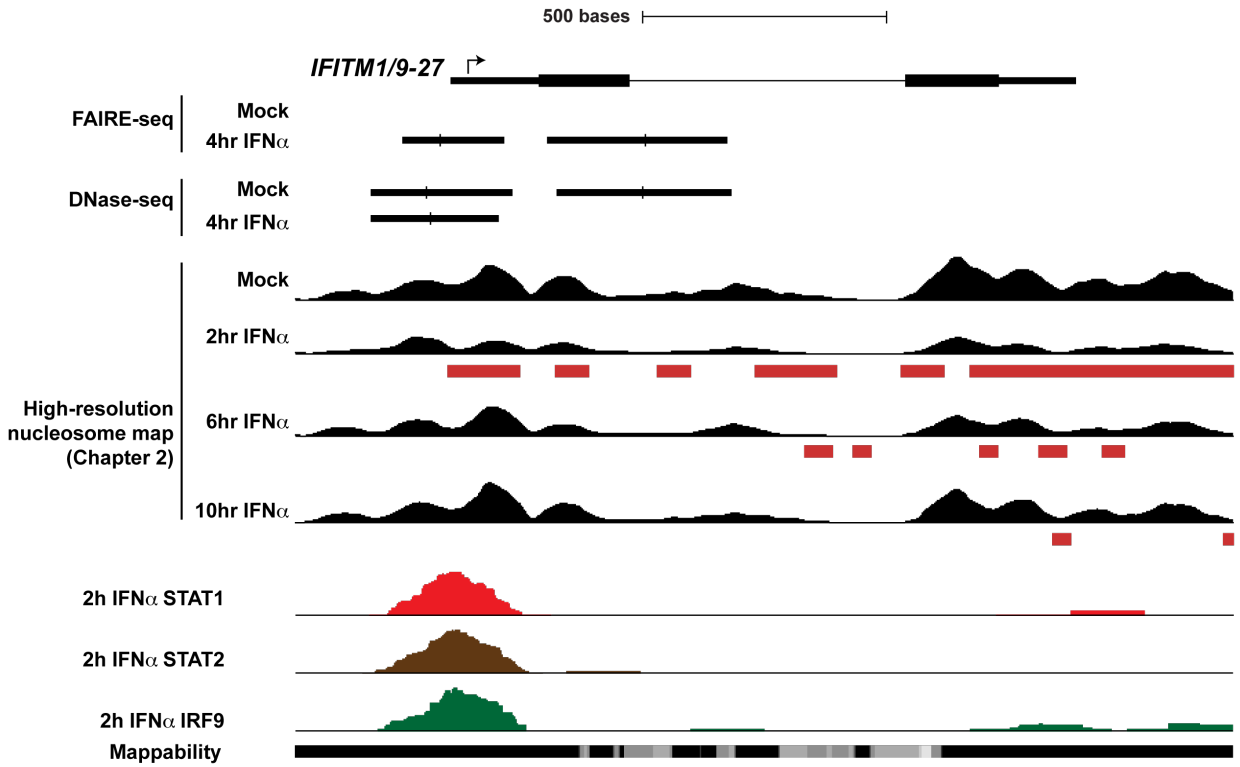

Figure 4.2 Comparison of high-resolution nucleosome data with public FAIRE-seq and DNase-seq data

Genome browser view of *IFITM1/9-27* from public domain FAIRE-seq and DNase-seq data compared with high-resolution nucleosome occupancy data and ISGF3 (STAT1, STAT2, IRF9) occupancy data described in Chapter 2. (From top to bottom) 500 base pair scale bar. Arrow denotes the TSS of *IFITM1/9-27* and the direction of transcription. The 5' end of *IFITM1/9-27* gene is depicted by small black bars (untranslated region), large black bars (exon), and line (intron). Chromatin accessible regions from FAIRE-seq data of mock or 4 hr IFNα treated HeLa cells. DNase-sensitive regions from DNase-seq data of mock or 4 hr IFNα treated HeLa cells. High-resolution maps of nucleosome occupancy after mock, 2 hr, 6 hr, or 10 hr IFNα treatment in HeLa cells. Red bars beneath nucleosome maps denote nucleosome loss due to 2 hr, 6 hr, or 10 hr IFNα treatment compared to mock (Poisson p-value ≤ $1x10^{-5}$). ChIP-Seq density of STAT1, STAT2, and IRF9 occupancy after 2 hr IFNα treatment in HeLa cells. Mappability depicts the uniqueness of reference genome from most (black) to least (gray).

HISTONE H2A.Z REGULATION AT IFN-STIMULATED GENES

H2A.Z occupancy and its role at ISG promoters

IFN stimulation results in ISG nucleosome loss and increased chromatin accessibility, particularly at ISG promoters. In the process of determining the histones contributing to the IFN-stimulated nucleosome loss, I uncovered that histone variant H2A.Z occupies ISG promoters, in lieu of the canonical and abundant core histone H2A during steady state. Following IFN stimulation, H2A.Z is removed from ISG promoter nucleosomes. The contrasting roles described for H2A.Z in organism viability, gene activation/repression and nucleosome stability/instability also represented an opportunity to examine its role at ISGs to understand its enigmatic function (Marques et al., 2010). More importantly, subunits of chromatin remodeling complexes connected with H2A.Z deposition and eviction were also required for ISG transcription (Gnatovskiy et al., 2013). The IFN-induced H2A.Z loss at ISG promoters and connection to H2A.Z-associated chromatin remodelers suggested H2A.Z-containing nucleosomes played a role in regulating ISG transcription.

The predominant transcription factor complex regulating ISG transcription is ISGF3. An inverse temporal relationship was observed between IFN-induced ISGF3 recruitment and IFN-induced H2A.Z loss at ISG promoters, suggesting a dynamic interplay between the two factors in regulating ISG transcription. With H2A.Z-deficient nucleosomes at the ISG promoter, an increase in STAT2/ISGF3 recruitment was observed and led to enhanced ISG expression. These data implicate H2A.Z as a suppressor of ISG transcription. Furthermore, the data suggest H2A.Z-containing

nucleosomes pose a barrier to ISGF3 docking to the ISRE DNA, which normally requires STAT2/ISGF3 recruitment of coactivators to remodel before it can bind. Therefore, under experimental conditions that lack H2A.Z-containing nucleosomes, the chromatin configuration at an ISG promoter enables ISGF3 to dock more efficiently, resulting in enhanced ISG transcription and potentiated antiviral protection.

In addition to H2A.Z-containing nucleosomes at human ISG promoters, a study in mouse NIH3T3 cells documented low levels of histone variant H3.3 at the ISG *IFIT1/ISG56* promoter region (Tamura et al., 2009). In the thesis work described in Chapter 3, histone H3 was found to be present at human ISG promoters including *IFIT1/ISG56*. Since the histone H3 antibody used in examining H3 occupancy in Chapter 3 may not distinguish between the core histone H3 or histone variant H3.3, it is not inconsistent with the mice NIH3T3 data. Nucleosomes containing both H2A.Z and H3.3 histone variants have been shown from literature to be enriched at nucleosome-depleted regions (NDR) (Henikoff, 2009). However, since the detection range of where the immunoprecipitated factor binds is typically within a few hundred base pairs using sonication to shear the genomic DNA, neither the H2A.Z data in Chapter 3 nor the H3.3 study in mice can assign the histone variant occupancy to a specific promoter nucleosome (Au-Yeung and Horvath, 2018; Lee et al., 2006; Tamura et al., 2009). Therefore, H2A.Z and H3.3 can both be found at an ISG promoter, but to determine whether they occupy the same nucleosome would require single nucleosome or base pair resolution.

Although it is well known that H2A.Z is enriched at ISG promoters, the role of H2A.Z in transcription regulation has been mysterious owing to its association with both positive and negative transcription in a context-dependent manner. One of the current hypotheses on the contrasting roles of H2A.Z in transcription is that its occupancy at the -1 and/or +1 nucleosome determines the gene activation or repression status (Domaschenz et al., 2017). In *Drosophila*, where H2A.Z is a hybrid of H2A.Z and H2A.X, the +1 nucleosome decorated with H2A.Z is regarded as having a positive role for Pol II elongation (Weber et al., 2014). In the epithelial-mesenchymal transition (EMT) in MDCK cells, epithelial genes with the H2A.Z-containing -1 nucleosome are active, whereas, mesenchymal genes featuring a +1 H2A.Z-nucleosome are repressed. Loss of the H2A.Z or replacement with a H2A +1 nucleosome enables activation of the mesenchymal genes. The *Drosophila* and EMT systems present opposing hypotheses regarding the associated gene outcome and the +1 or -1 nucleosome position. At several ISGs examined, the presence of a discrete -1 and +1 nucleosome can be found, but higher resolution H2A.Z occupancy data is needed to discern the specific nucleosome position it occupies to correlate with its negative role on ISG expression.

Another hypothesis on the contrasting role of H2A.Z in transcription is associated with its post-translational modification status (Sevilla and Binda, 2014). Acetylated H2A.Z (H2A.Zac) is associated with positive transcription, whereas ubiquitylated H2A.Z (H2A.Zub) is associated with transcription silencing. In mouse embryonic stem cells, H2A.Zub is thought to establish a poised chromatin environment and inability to establish that mark leads to derepression of the gene (Surface et al., 2016). ISG promoter

nucleosomes are comprised of the acetylated H2A.Z. Therefore, it would be interesting to test whether replacing the native H2A.Zac at ISG promoters with H2A.Zub would repress ISG transcription and abolish the associated antiviral protection based on this hypothesis. Whether these current hypotheses will apply generally across all systems containing H2A.Z-nucleosomes or continue to operate in a context-dependent manner will hopefully come to light with further information.

Collaboration of histone readers and histone writers in IFN-H2A.Z removal

In searching for the factor(s) responsible for IFN-induced H2A.Z loss, it was surprising that several previously implicated factors in the IFN and/or H2A.Z deposition/removal system were not responsible (Gnatovskiy et al., 2013; Mizuguchi et al., 2004; Obri et al., 2014; Papamichos-Chronakis et al., 2011). These included RVB1, RVB2, INO80, SRCAP, ANP32E, and BRG1. Instead, the activities from histone acetyltransferase (HAT), GCN5, and acetyl-binding bromodomain protein, BRD2, were required for IFN-stimulated H2A.Z eviction.

It is interesting to note that RVB1 and RVB2 were found to be required in ISG transcription and Pol II recruitment, but not for STAT2 recruitment. They are also common subunits in several chromatin remodeling complexes including INO80 and SRCAP, which are implicated in H2A.Z removal and deposition, respectively. These connections RVB1 and RVB2 had with both ISG transcription and H2A.Z made it surprising when they were discovered to not be involved in IFN-induced H2A.Z removal. Although interference with these two factors did not impact H2A.Z dynamics in the IFN system, knockdown of RVB1

did result in abrogation of ISG transcription in agreement with a prior study (Gnatovskiy et al., 2013). However, knockdown of RVB2 did not inhibit ISG transcription as expected. Disagreement of the RVB2 phenotype could be due to insufficient knockdown, protein instability or differences in the knockdown or cell system used between the two studies. Both RVB1 and RVB2 contain ATPase and helicase domains, though inconsistent reports of weak to no ATPase activity of these factors further confound their potential roles in the IFN response.

Another factor that was hypothesized to remove H2A.Z after IFN stimulation was ANP32E. In addition to its potential role as a histone chaperone to H2A.Z, ANP32E is related to PP32 (also termed ANP32A) in the ANP32 family of proteins (Reilly et al., 2014). PP32 was reported to interact with STAT2 and was required for maximal induction of ISG transcription. In that study, knockdown of PP32 reduced histone acetylation at ISG promoters (Kadota and Nagata, 2011). Based on the data in the PP32 study and the requirement for HAT and HDAC activity in the IFN response, the authors speculated that PP32 may assist in the recruitment of HATs. In considering ANP32E in IFN-induced H2A.Z removal, its familial relationship with PP32 suggested ANP32E could be recruited as a part of the PP32-STAT2 complex during IFN stimulation. However, knockdown of ANP32E described in Chapter 3 did not abolish H2A.Z loss during IFN stimulation. Thus, ANP32E was ruled out for having a role in IFN-induced H2A.Z removal.

Although HAT and HDAC activity in the IFN response remains to be fully elucidated, they are undoubtedly required for positive ISG transcription. My data show both the HAT, GCN5, and acetyl-binding bromodomain protein, BRD2, are required for IFN-induced

H2A.Z eviction. In yeast, GCN5 has been shown to acetylate H2A.Z and other histone proteins, notably histone H3. Acetylation of H2A.Z and other histones recruit binding of BRD2 and other bromodomain proteins to H2A.Z-containing nucleosomes. Inhibition of BRD2 activity prevents IFN-induced H2A.Z removal suggesting BRD2 association facilitates H2A.Z eviction, possibly through disrupting the histone interactions within a nucleosome. It is tempting to speculate that GCN5 acetylates H2A.Z, recruiting BRD2 to the ISG promoter, where it participates in H2A.Z removal.

MODEL FOR ISGF3-MEDIATED CHROMATIN AND TRANSCRIPTION DYNAMICS

Relatively little was known about chromatin regulation of ISGs at the beginning of this thesis project. Since most, if not all ISGs, are regulated by ISGF3, the focus was directed towards ISGF3-mediated chromatin dynamics. Data in the literature relevant to ISG promoter organization and dynamics are combined with the findings uncovered from this thesis work to generate a working model of ISGF3-mediated transcriptional regulation at ISGs that includes a promoter decorated with H2A.Z nucleosome(s) (Figure 4.3).

The top box illustrates what is known in the wild-type cell, with the ISG promoter containing a H2A.Z nucleosome(s), during steady state and following IFN stimulation. During steady state in wild-type cells, ISG promoter nucleosomes are present and demarcation of the -1 and +1 nucleosome position varies between ISGs based on data from Chapter 2. The nucleosome is comprised of acetylated H2A.Z in the homo- or heterodimers of H2A.Z-H2B accompanied with homo- or heterodimers of H3.3-H4 or H3-H4 based on data from Chapter 3 and literature (Tamura et al., 2009). No data has

determined whether the canonical histone H2B or H2B variants are used at ISG promoters. Histone H3 or H3.3 is trimethylated at lysine 4, likely alongside other histone marks associated with active promoters. Since no variant forms of histone H4 are known, the canonical H4 is present. Together, ISG promoter nucleosomes are comprised of histones H2A.Z, canonical H2B or H2B variants, canonical H3 or H3.3, and canonical H4 during steady state.

Following IFN stimulation, ISGF3 recruits GCN5 to acetylate histones H2A.Z, H3, and/or H4. This acetyl-rich environment promotes the association of bromodomain proteins BRD2, BRD4 and other bromodomain proteins. BRD2 preferentially localizes to H2A.Z nucleosomes and together with GCN5 acetylation drives the eviction of H2A.Z from ISG promoter nucleosomes (Draker et al., 2012). H2A.Z is presumed to be displaced as a H2A.Z-H2B dimer (Tamura et al., 2009). Histones H3.3/H3 and histone H4 decrease at ISG promoters following IFN stimulation, but remains present to some extent based on data in Chapter 2 and literature. At the same time, the H3K4 methylation mark is removed from histone H3 at ISG promoters. ISGF3 binds to the ISRE stably and its associated coactivators (i.e. HDACs, CBP, RVB1, RVB2, BRG1) continue to remodel the promoter region for recruitment of Mediator, transcription machinery and Pol II. BRD2 and BRD4 promote positive transcriptional elongation and ISG transcription until phosphatase activities dephosphorylates STAT1 and STAT2 (LeRoy et al., 2008; Patel et al., 2013). Dephosphorylated ISGF3 is exported from the nucleus and H2A.Z is recovered at ISG promoters, re-establishing the native steady state chromatin configuration.

The bottom box (Figure 4.3) depicts a cell harboring shRNA against H2A.Z, resulting in H2A.Z-deficient nucleosomes at ISG promoters during steady state. In cells with H2A.Z-deficient nucleosomes, ISG promoter nucleosomes contain histone H2A that has not been exchanged out owing to the lack of H2A.Z in the cell. Upon IFN stimulation, ISGF3 efficiently docks to the H2A.Z-deficient ISG promoter and activates maximal ISG transcription. Presumably H2A.Z-deficient nucleosomes support an optimal promoter configuration that enables ISGF3 to access ISG promoters more easily. In cells harboring shRNA targeting H2A.Z, the reduced H2A.Z relieves the need for chromatin remodeling and histone modifying activities that are normally required prior to or at the same time as ISGF3 docking. Relieving the need to remodel the H2A.Z nucleosome(s) at ISG promoters enables ISGF3 to bind and activate ISG expression more easily. This greater access to the ISRE translates into potentiated antiviral activity.

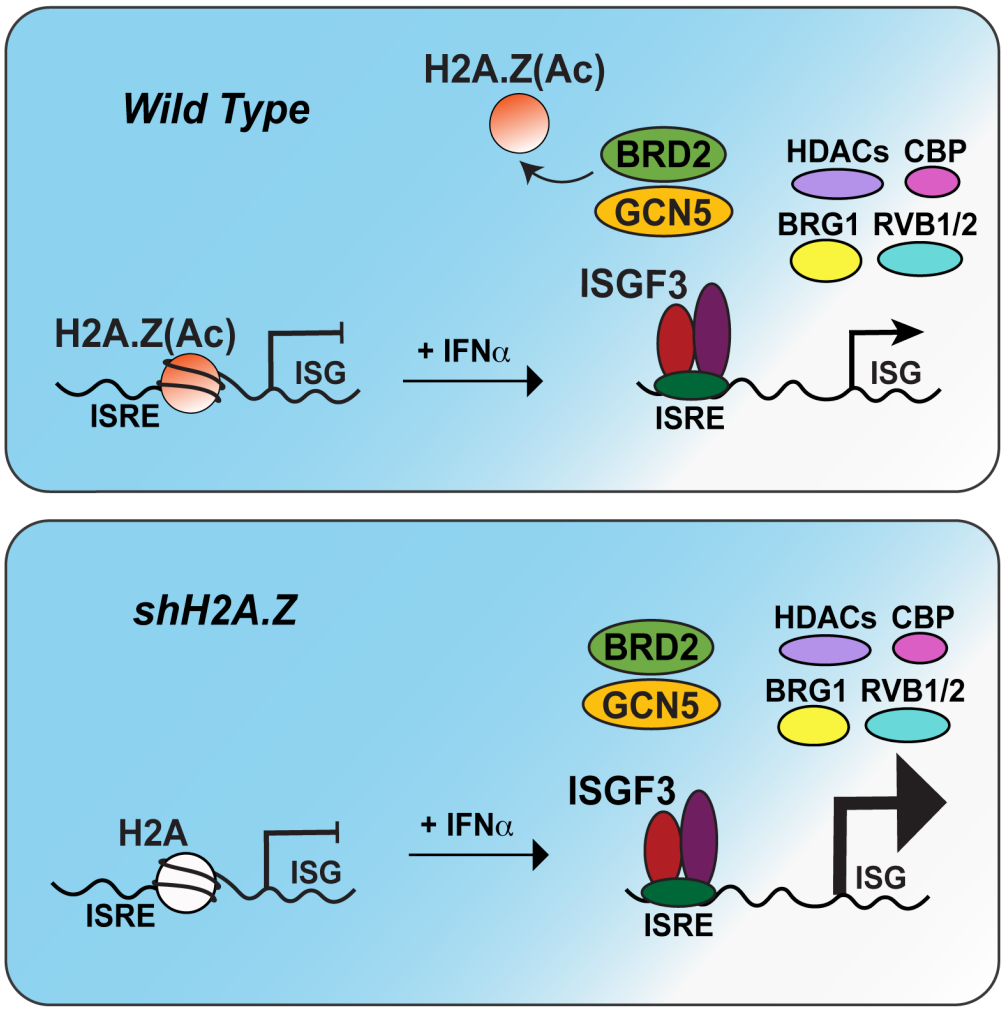

Figure 4.3 Model of ISGF3-mediated chromatin and transcription dynamics
Illustration of a working model of the ISGF3-mediated chromatin and transcription dynamics in a wild-type cell (top) and a cell harboring shRNA against H2A.Z resulting in H2A.Z-deficient nucleosomes (bottom). (Top) In the wild-type cell, non-acetylated or acetylated (Ac) H2A.Z nucleosomes are positioned at the ISG promoter during steady state. Following IFN stimulation, ISGF3 (STAT1, STAT2, IRF9) is recruited to ISG promoters where it interacts with co-activators, including GCN5, HDACs, CBP, BRG1, RVB1, and RVB2, and activates ISG transcription. Associated GCN5 and BRD2 activities promote the eviction of IFN-induced H2A.Z from the ISG promoter. (Bottom) In a cell harboring shRNA against H2A.Z, ISG promoter nucleosomes contain H2A during steady state. After IFNα treatment, ISGF3 binds to the ISRE at ISG promoters more easily with a lack of H2A.Z nucleosome(s) and recruits various co-activators as in the wild-type cell, resulting in enhanced ISG transcription.

CONCLUSION AND FUTURE DIRECTIONS

The role of ISGF3 in regulating ISG transcription activation remains undoubtedly important and data from this thesis demonstrate its regulatory role on ISG chromatin during the IFN response. In determining the nucleosome occupancy at ISGs, genomic sites occupied by ISGF3 coincided with the most prominent nucleosome loss spatially and temporally. I postulated that this loss was due to the loss of core histones; this hypothesis turned out to be true for the core histones H2B, H3, and H4. Unexpectedly, the major core histone H2A was absent, and instead, I discovered the histone variant H2A.Z was present at ISG promoters and removed following IFN stimulation. This result led me to hypothesize that H2A.Z-containing nucleosomes at ISG promoters play a role in regulating ISG expression. Initially, I hypothesized that the role of H2A.Z nucleosomes was to direct ISGF3 recruitment to ISG promoters by presenting a distinguishable histone variant, H2A.Z. However, this hypothesis was disproved since loss of H2A.Z enhanced ISG expression indicating ISGF3 recruitment was intact to activate ISG transcription.

Since deficiency in H2A.Z increased ISG expression and ISGF3 is the predominant transcription factor to activate ISG transcription, I hypothesized that the upregulated ISG transcription could result from heightened ISGF3 recruitment to ISG promoters. I had already uncovered a significant overlap of steady state H2A.Z at IFN-induced STAT2/ISGF3 target sites genome-wide; this result coupled with an inverse temporal relationship between the H2A.Z and STAT2/ISGF3 at ISG promoters supported the hypothesis that the presence of H2A.Z nucleosomes negatively regulated ISGF3 recruitment. Testing the recruitment of ISGF3 in H2A.Z-deficient cells demonstrated an

enhancement in the IFN-stimulated recruitment of STAT2/ISGF3 at ISG promoters. This result indicated that H2A.Z nucleosomes at ISG promoters suppress ISGF3 recruitment and loss of H2A.Z alleviates a barrier for ISGF3 binding, translating into enhanced ISG expression and robust antiviral protection. The mechanism on how loss of H2A.Z-containing nucleosomes shapes the promoter region to promote higher levels of ISGF3 at ISGs remains to be fully elucidated. However, these new findings not only advance our mechanistic understanding of ISG chromatin regulation, but offers insights in therapeutic developments including epigenetic-based therapies and cancer immunotherapy.

Several questions still remain though. On one hand, despite knowing that H2A.Z-deficient nucleosomes increase ISGF3 occupancy and enhance ISG transcription during the IFN response, the role of positioned H2A.Z nucleosomes at ISG promoters remains to be fully elucidated. On the other hand, IFN-induced H2A.Z removal requires ISGF3 and the activities of GCN5 and BRD2, yet how ISGF3 regulates H2A.Z removal through these activities are not completely understood. Furthermore, it is not known how the complementary functions of histone writer GCN5 and histone reader BRD2 mediate IFN-induced H2A.Z loss. Following IFN stimulation, ISGF3 associates with GCN5 through STAT2 and recruits GCN5 to the ISG promoter. GCN5 has been shown to acetylate specific residues in histones H3, H4, and H2A.Z (Anamika et al., 2010; Millar et al., 2006). ISG promoter nucleosomes are comprised of acetylated H2A.Z, which are postulated to be a product of GCN5 acetylation. However, further investigation is necessary to determine whether GCN5 acetylates H2A.Z and/or another histone comprising the ISG

promoter nucleosome, and thereby, promotes the BRD2 bromodomain association with acetylated H2A.Z.

In addition to the possibility that BRD2 is recruited through GCN5-acetylated histones during IFN stimulation, another hypothesis is BRD2 is recruited through an interaction with ISGF3. BRD2 has been observed to associate with another STAT factor, STAT3, during Th17 cell differentiation (Cheung et al., 2017). Therefore, testing whether BRD2 interacts with STAT1 or STAT2 during IFN induction would determine if ISGF3 associates with BRD2 and directs BRD2 to H2A.Z nucleosomes at ISG promoters. Therefore, examining how BRD2 is associated and whether its recruitment is related to GCN5 HAT activity to support IFN-induced H2A.Z loss are still required.

Conversely, positioned H2A.Z-containing nucleosomes at ISG promoters, which are subsequently removed after IFN stimulation, represent one of the ways that chromatin regulates transcription at ISG promoters. The consequence of positioning the histone variant H2A.Z as opposed to H2A at ISG promoter nucleosomes during steady state is still not well understood. One insight from the work in Chapter 3 on steady state H2A.Z at ISG promoters stems from the disruption of the chromatin remodeling subunit, RVB1. Knocking down RVB1 led to an increase in H2A.Z levels at ISG promoters. This result suggests that the loss of RVB1 disturbed the steady-state equilibrium of H2A.Z deposition and removal, albeit through an unknown mechanism. In addition to the implication of a role for RVB1 in basal H2A.Z establishment, this data suggests there is a balancing process to ensure homeostatic H2A.Z levels at ISG promoters during steady state.

Since H2A.Z-containing nucleosomes also contain the core histones or histone variants of H2B, H3, and H4, the interaction between the octamer histones drive the cumulative effects of a particular nucleosome on ISGF3 recruitment and ISG transcriptional activation. Therefore, to understand how the loss of H2A.Z from ISG promoter nucleosome(s) leads to an increase in ISGF3 occupancy, it is also necessary to determine the overall histone composition during steady state and after IFN stimulation at higher and single nucleosome resolution. Not only would a single nucleosome resolution analysis of all the possible histones identify the mutual existence between different histones, it would likely reveal whether the nucleosome exists as an octamer or other documented nucleosome forms such as hexameric nucleosomes (Ellison and Pulleyblank, 1983; Kulaeva and Studitsky, 2010). This task is undoubtedly challenging because the diverse histone population to survey is not limited to core histones and their variants, but also the numerous combinations of histone modifications possible. However, the collective data will provide a more complete description and mechanistic understanding of the interactions between ISGF3, co-regulators, and chromatin during the IFN response. These cumulative interactions not only drive the physiological antiviral biology that protects the cell against virus infection, but will enable us to further understand IFN-associated autoimmune and inflammatory diseases and develop improved therapeutic strategies.

REFERENCES

Aaronson, D.S., and Horvath, C.M. (2002). A road map for those who don't know JAK-STAT. Science *296*, 1653-1655.

Adelman, K., and Lis, J.T. (2012). Promoter-proximal pausing of RNA polymerase II: emerging roles in metazoans. Nat Rev Genet *13*, 720-731.

Afgan, E., Baker, D., van den Beek, M., Blankenberg, D., Bouvier, D., Cech, M., Chilton, J., Clements, D., Coraor, N., Eberhard, C.*, et al.* (2016). The Galaxy platform for accessible, reproducible and collaborative biomedical analyses: 2016 update. Nucleic Acids Res *44*, W3-W10.

Agalioti, T., Chen, G., and Thanos, D. (2002). Deciphering the transcriptional histone acetylation code for a human gene. Cell *111*, 381-392.

Agalioti, T., Lomvardas, S., Parekh, B., Yie, J., Maniatis, T., and Thanos, D. (2000). Ordered recruitment of chromatin modifying and general transcription factors to the IFN-beta promoter. Cell *103*, 667-678.

Alatwi, H.E., and Downs, J.A. (2015). Removal of H2A.Z by INO80 promotes homologous recombination. EMBO Rep *16*, 986-994.

Anamika, K., Krebs, A.R., Thompson, J., Poch, O., Devys, D., and Tora, L. (2010). Lessons from genome-wide studies: an integrated definition of the coactivator function of histone acetyl transferases. Epigenetics Chromatin *3*, 18.

Au-Yeung, N., and Horvath, C.M. (2018). Histone H2A.Z Suppression of Interferon-Stimulated Transcription and Antiviral Immunity is Modulated by GCN5 and BRD2. iScience *6*, 68-82.

Au-Yeung, N., Mandhana, R., and Horvath, C.M. (2013). Transcriptional regulation by STAT1 and STAT2 in the interferon JAK-STAT pathway. JAKSTAT *2*, e23931.

Banninger, G., and Reich, N.C. (2004). STAT2 nuclear trafficking. J Biol Chem *279*, 39199-39206.

Barski, A., Cuddapah, S., Cui, K., Roh, T.Y., Schones, D.E., Wang, Z., Wei, G., Chepelev, I., and Zhao, K. (2007). High-resolution profiling of histone methylations in the human genome. Cell *129*, 823-837.

Bartlett, D.W., and Davis, M.E. (2006). Insights into the kinetics of siRNA-mediated gene silencing from live-cell and live-animal bioluminescent imaging. Nucleic Acids Res *34*, 322-333.

Bell, O., Tiwari, V.K., Thoma, N.H., and Schubeler, D. (2011). Determinants and dynamics of genome accessibility. Nat Rev Genet *12*, 554-564.

Benci, J.L., Xu, B., Qiu, Y., Wu, T.J., Dada, H., Twyman-Saint Victor, C., Cucolo, L., Lee, D.S.M., Pauken, K.E., Huang, A.C.*, et al.* (2016). Tumor Interferon Signaling Regulates a Multigenic Resistance Program to Immune Checkpoint Blockade. Cell *167*, 1540-1554 e1512.

Bhattacharya, S., Eckner, R., Grossman, S., Oldread, E., Arany, Z., D'Andrea, A., and Livingston, D.M. (1996). Cooperation of Stat2 and p300/CBP in signalling induced by interferon-alpha. Nature *383*, 344-347.

Billon, P., and Cote, J. (2013). Precise deposition of histone H2A.Z in chromatin for genome expression and maintenance. Biochim Biophys Acta *1819*, 290-302.

Bluyssen, H.A., and Levy, D.E. (1997). Stat2 is a transcriptional activator that requires sequence-specific contacts provided by stat1 and p48 for stable interaction with DNA. J Biol Chem *272*, 4600-4605.

Bonisch, C., and Hake, S.B. (2012). Histone H2A variants in nucleosomes and chromatin: more or less stable? Nucleic Acids Res *40*, 10719-10741.

Borden, E.C., Sen, G.C., Uze, G., Silverman, R.H., Ransohoff, R.M., Foster, G.R., and Stark, G.R. (2007). Interferons at age 50: past, current and future impact on biomedicine. Nat Rev Drug Discov *6*, 975-990.

Bowman, G.D., and Poirier, M.G. (2015). Post-translational modifications of histones that influence nucleosome dynamics. Chem Rev *115*, 2274-2295.

Brickner, D.G., Cajigas, I., Fondufe-Mittendorf, Y., Ahmed, S., Lee, P.C., Widom, J., and Brickner, J.H. (2007). H2A.Z-mediated localization of genes at the nuclear periphery confers epigenetic memory of previous transcriptional state. PLoS Biol *5*, e81.

Bruns, A.M., and Horvath, C.M. (2012). Activation of RIG-I-like receptor signal transduction. Crit Rev Biochem Mol Biol *47*, 194-206.

Buschbeck, M., and Hake, S.B. (2017). Variants of core histones and their roles in cell fate decisions, development and cancer. Nat Rev Mol Cell Biol *18*, 299-314.

Cauchy, P., Koch, F., and Andrau, J.C. (2017). Two possible modes of pioneering associated with combinations of H2A.Z and p300/CBP at nucleosome-occupied enhancers. Transcription *8*, 179-184.

Chang, H.M., Paulson, M., Holko, M., Rice, C.M., Williams, B.R., Marie, I., and Levy, D.E. (2004). Induction of interferon-stimulated gene expression and antiviral responses require protein deacetylase activity. Proc Natl Acad Sci U S A *101*, 9578-9583.

Chen, K., Liu, J., Liu, S., Xia, M., Zhang, X., Han, D., Jiang, Y., Wang, C., and Cao, X. (2017). Methyltransferase SETD2-Mediated Methylation of STAT1 Is Critical for Interferon Antiviral Activity. Cell *170*, 492-506 e414.

Chen, K., Xi, Y., Pan, X., Li, Z., Kaestner, K., Tyler, J., Dent, S., He, X., and Li, W. (2013). DANPOS: dynamic analysis of nucleosome position and occupancy by sequencing. Genome Res *23*, 341-351.

Cheung, K.L., Zhang, F., Jaganathan, A., Sharma, R., Zhang, Q., Konuma, T., Shen, T., Lee, J.Y., Ren, C., Chen, C.H.*, et al.* (2017). Distinct Roles of Brd2 and Brd4 in Potentiating the Transcriptional Program for Th17 Cell Differentiation. Mol Cell *65*, 1068-1080 e1065.

Chi, T. (2004). A BAF-centred view of the immune system. Nat Rev Immunol *4*, 965-977.

Cimica, V., and Reich, N.C. (2013). Nuclear trafficking of STAT proteins visualized by live cell imaging. Methods Mol Biol *967*, 189-202.

Clarkson, M.J., Wells, J.R., Gibson, F., Saint, R., and Tremethick, D.J. (1999). Regions of variant histone His2AvD required for Drosophila development. Nature *399*, 694-697.

Consortium, E.P. (2012). An integrated encyclopedia of DNA elements in the human genome. Nature *489*, 57-74.

Cui, K., Tailor, P., Liu, H., Chen, X., Ozato, K., and Zhao, K. (2004). The chromatin-remodeling BAF complex mediates cellular antiviral activities by promoter priming. Mol Cell Biol *24*, 4476-4486.

Dai, X., Bai, Y., Zhao, L., Dou, X., Liu, Y., Wang, L., Li, Y., Li, W., Hui, Y., Huang, X.*, et al.* (2017). H2A.Z Represses Gene Expression by Modulating Promoter Nucleosome Structure and Enhancer Histone Modifications in Arabidopsis. Mol Plant *10*, 1274-1292.

Decker, T., Lew, D.J., and Darnell, J.E., Jr. (1991). Two distinct alpha-interferon-dependent signal transduction pathways may contribute to activation of transcription of the guanylate-binding protein gene. Mol Cell Biol *11*, 5147-5153.

Delcuve, G.P., Khan, D.H., and Davie, J.R. (2012). Roles of histone deacetylases in epigenetic regulation: emerging paradigms from studies with inhibitors. Clin Epigenetics *4*, 5.

Dhillon, N., and Kamakaka, R.T. (2000). A histone variant, Htz1p, and a Sir1p-like protein, Esc2p, mediate silencing at HMR. Mol Cell *6*, 769-780.

Domaschenz, R., Kurscheid, S., Nekrasov, M., Han, S., and Tremethick, D.J. (2017). The Histone Variant H2A.Z Is a Master Regulator of the Epithelial-Mesenchymal Transition. Cell Rep *21*, 943-952.

Dovey, O.M., Foster, C.T., and Cowley, S.M. (2010). Emphasizing the positive: A role for histone deacetylases in transcriptional activation. Cell Cycle *9*, 2700-2701.

Draker, R., Ng, M.K., Sarcinella, E., Ignatchenko, V., Kislinger, T., and Cheung, P. (2012). A combination of H2A.Z and H4 acetylation recruits Brd2 to chromatin during transcriptional activation. PLoS Genet *8*, e1003047.

Ellison, M.J., and Pulleyblank, D.E. (1983). The assembly of an H2A2,H2B2,H3,H4 hexamer onto DNA under conditions of physiological ionic strength. J Biol Chem *258*, 13307-13313.

Faast, R., Thonglairoam, V., Schulz, T.C., Beall, J., Wells, J.R., Taylor, H., Matthaei, K., Rathjen, P.D., Tremethick, D.J., and Lyons, I. (2001). Histone variant H2A.Z is required for early mammalian development. Curr Biol *11*, 1183-1187.

Fan, J.Y., Rangasamy, D., Luger, K., and Tremethick, D.J. (2004). H2A.Z alters the nucleosome surface to promote HP1alpha-mediated chromatin fiber folding. Mol Cell *16*, 655-661.

Freaney, J.E., Kim, R., Mandhana, R., and Horvath, C.M. (2013). Extensive cooperation of immune master regulators IRF3 and NFkappaB in RNA Pol II recruitment and pause release in human innate antiviral transcription. Cell Rep *4*, 959-973.

Freaney, J.E., Zhang, Q., Yigit, E., Kim, R., Widom, J., Wang, J.P., and Horvath, C.M. (2014). High-density nucleosome occupancy map of human chromosome 9p21-22 reveals chromatin organization of the type I interferon gene cluster. J Interferon Cytokine Res *34*, 676-685.

Fu, X.Y., Kessler, D.S., Veals, S.A., Levy, D.E., and Darnell, J.E., Jr. (1990). ISGF3, the transcriptional activator induced by interferon alpha, consists of multiple interacting polypeptide chains. Proc Natl Acad Sci U S A *87*, 8555-8559.

Garcia-Sastre, A. (2017). Ten Strategies of Interferon Evasion by Viruses. Cell Host Microbe *22*, 176-184.

GENCODE (2017). Statistics about the current Human GENCODE Release (version 28).

George, C.X., and Samuel, C.E. (1999). Characterization of the 5'-flanking region of the human RNA-specific adenosine deaminase ADAR1 gene and identification of an interferon-inducible ADAR1 promoter. Gene *229*, 203-213.

Gevry, N., Chan, H.M., Laflamme, L., Livingston, D.M., and Gaudreau, L. (2007). p21 transcription is regulated by differential localization of histone H2A.Z. Genes Dev *21*, 1869-1881.

Gevry, N., Hardy, S., Jacques, P.E., Laflamme, L., Svotelis, A., Robert, F., and Gaudreau, L. (2009). Histone H2A.Z is essential for estrogen receptor signaling. Genes Dev *23*, 1522-1533.

Gnatovskiy, L., Mita, P., and Levy, D.E. (2013). The human RVB complex is required for efficient transcription of type I interferon-stimulated genes. Mol Cell Biol *33*, 3817-3825.

Gongora, C., Degols, G., Espert, L., Hua, T.D., and Mechti, N. (2000). A unique ISRE, in the TATA-less human Isg20 promoter, confers IRF-1-mediated responsiveness to both interferon type I and type II. Nucleic Acids Res *28*, 2333-2341.

Gonzalez-Navajas, J.M., Lee, J., David, M., and Raz, E. (2012). Immunomodulatory functions of type I interferons. Nat Rev Immunol *12*, 125-135.

Grandvaux, N., Servant, M.J., tenOever, B., Sen, G.C., Balachandran, S., Barber, G.N., Lin, R., and Hiscott, J. (2002). Transcriptional profiling of interferon regulatory factor 3 target genes: direct involvement in the regulation of interferon-stimulated genes. J Virol *76*, 5532-5539.

Grunstein, M. (1997). Histone acetylation in chromatin structure and transcription. Nature *389*, 349-352.

Guillemette, B., Bataille, A.R., Gevry, N., Adam, M., Blanchette, M., Robert, F., and Gaudreau, L. (2005). Variant histone H2A.Z is globally localized to the promoters of inactive yeast genes and regulates nucleosome positioning. PLoS Biol *3*, e384.

Guillemette, B., and Gaudreau, L. (2006). Reuniting the contrasting functions of H2A.Z. Biochem Cell Biol *84*, 528-535.

Hartman, S.E., Bertone, P., Nath, A.K., Royce, T.E., Gerstein, M., Weissman, S., and Snyder, M. (2005). Global changes in STAT target selection and transcription regulation upon interferon treatments. Genes Dev *19*, 2953-2968.

Heinz, S., Benner, C., Spann, N., Bertolino, E., Lin, Y.C., Laslo, P., Cheng, J.X., Murre, C., Singh, H., and Glass, C.K. (2010). Simple combinations of lineage-determining transcription factors prime cis-regulatory elements required for macrophage and B cell identities. Mol Cell *38*, 576-589.

Henikoff, S. (2009). Labile H3.3+H2A.Z nucleosomes mark 'nucleosome-free regions'. Nat Genet *41*, 865-866.

Hoffmann, H.H., Schneider, W.M., and Rice, C.M. (2015). Interferons and viruses: an evolutionary arms race of molecular interactions. Trends Immunol *36*, 124-138.

Horvath, C.M., Stark, G.R., Kerr, I.M., and Darnell, J.E., Jr. (1996). Interactions between STAT and non-STAT proteins in the interferon-stimulated gene factor 3 transcription complex. Mol Cell Biol *16*, 6957-6964.

Hu, G., Cui, K., Northrup, D., Liu, C., Wang, C., Tang, Q., Ge, K., Levens, D., Crane-Robinson, C., and Zhao, K. (2013). H2A.Z facilitates access of active and repressive complexes to chromatin in embryonic stem cell self-renewal and differentiation. Cell Stem Cell *12*, 180-192.

Huang, M., Qian, F., Hu, Y., Ang, C., Li, Z., and Wen, Z. (2002). Chromatin-remodelling factor BRG1 selectively activates a subset of interferon-alpha-inducible genes. Nat Cell Biol *4*, 774-781.

Huang, Y., Krein, P.M., and Winston, B.W. (2001). Characterization of IFN-gamma regulation of the complement factor B gene in macrophages. Eur J Immunol *31*, 3676-3686.

Huen, J., Kakihara, Y., Ugwu, F., Cheung, K.L., Ortega, J., and Houry, W.A. (2010). Rvb1-Rvb2: essential ATP-dependent helicases for critical complexes. Biochem Cell Biol *88*, 29-40.

Huminiecki, L., and Horbanczuk, J. (2017). Can We Predict Gene Expression by Understanding Proximal Promoter Architecture? Trends Biotechnol *35*, 530-546.

Iouzalen, N., Moreau, J., and Mechali, M. (1996). H2A.ZI, a new variant histone expressed during Xenopus early development exhibits several distinct features from the core histone H2A. Nucleic Acids Res *24*, 3947-3952.

Isaacs, A., and Lindenmann, J. (1957). Virus interference. I. The interferon. Proc R Soc Lond B Biol Sci *147*, 258-267.

Ito, T., Umehara, T., Sasaki, K., Nakamura, Y., Nishino, N., Terada, T., Shirouzu, M., Padmanabhan, B., Yokoyama, S., Ito, A.*, et al.* (2011). Real-time imaging of histone H4K12-specific acetylation determines the modes of action of histone deacetylase and bromodomain inhibitors. Chem Biol *18*, 495-507.

Ivashkiv, L.B., and Donlin, L.T. (2014). Regulation of type I interferon responses. Nat Rev Immunol *14*, 36-49.

Jackson, J.D., and Gorovsky, M.A. (2000). Histone H2A.Z has a conserved function that is distinct from that of the major H2A sequence variants. Nucleic Acids Res *28*, 3811-3816.

Jamieson, A.M., Farlik, M., and Decker, T. (2012). How Stats Interact with the Molecular Machinery of Transcriptional Activation. Jak-Stat Signaling: From Basics to Disease, 65-89.

Jeronimo, C., Watanabe, S., Kaplan, C.D., Peterson, C.L., and Robert, F. (2015). The Histone Chaperones FACT and Spt6 Restrict H2A.Z from Intragenic Locations. Mol Cell *58*, 1113-1123.

Jha, S., and Dutta, A. (2009). RVB1/RVB2: running rings around molecular biology. Mol Cell *34*, 521-533.

Jin, C., and Felsenfeld, G. (2007). Nucleosome stability mediated by histone variants H3.3 and H2A.Z. Genes Dev *21*, 1519-1529.

John, J., McKendry, R., Pellegrini, S., Flavell, D., Kerr, I.M., and Stark, G.R. (1991). Isolation and characterization of a new mutant human cell line unresponsive to alpha and beta interferons. Mol Cell Biol *11*, 4189-4195.

Kadota, S., and Nagata, K. (2011). pp32, an INHAT component, is a transcription machinery recruiter for maximal induction of IFN-stimulated genes. J Cell Sci *124*, 892-899.

Kadota, S., and Nagata, K. (2014). Silencing of IFN-stimulated gene transcription is regulated by histone H1 and its chaperone TAF-I. Nucleic Acids Res *42*, 7642-7653.

Kaplan, N., Moore, I.K., Fondufe-Mittendorf, Y., Gossett, A.J., Tillo, D., Field, Y., LeProust, E.M., Hughes, T.R., Lieb, J.D., Widom, J.*, et al.* (2009). The DNA-encoded nucleosome organization of a eukaryotic genome. Nature *458*, 362-366.

Kchou, M., Gibrat, J.-F., and Elloumi, M. (2017). Generations of Sequencing Technologies: From First to Next Generation. Biology and Medicine *9*.

Kelly, R.D., and Cowley, S.M. (2013). The physiological roles of histone deacetylase (HDAC) 1 and 2: complex co-stars with multiple leading parts. Biochem Soc Trans *41*, 741-749.

Kent, W.J., Sugnet, C.W., Furey, T.S., Roskin, K.M., Pringle, T.H., Zahler, A.M., and Haussler, D. (2002). The human genome browser at UCSC. Genome Res *12*, 996-1006.

Kimura, H. (2013). Histone modifications for human epigenome analysis. J Hum Genet *58*, 439-445.

Kobor, M.S., Venkatasubrahmanyam, S., Meneghini, M.D., Gin, J.W., Jennings, J.L., Link, A.J., Madhani, H.D., and Rine, J. (2004). A protein complex containing the conserved Swi2/Snf2-related ATPase Swr1p deposits histone variant H2A.Z into euchromatin. PLoS Biol *2*, E131.

Konan, K.V., and Taylor, M.W. (1996). Importance of the two interferon-stimulated response element (ISRE) sequences in the regulation of the human indoleamine 2,3-dioxygenase gene. J Biol Chem *271*, 19140-19145.

Krogan, N.J., Keogh, M.C., Datta, N., Sawa, C., Ryan, O.W., Ding, H., Haw, R.A., Pootoolal, J., Tong, A., Canadien, V.*, et al.* (2003). A Snf2 family ATPase complex required for recruitment of the histone H2A variant Htz1. Mol Cell *12*, 1565-1576.

Ku, M., Jaffe, J.D., Koche, R.P., Rheinbay, E., Endoh, M., Koseki, H., Carr, S.A., and Bernstein, B.E. (2012). H2A.Z landscapes and dual modifications in pluripotent and multipotent stem cells underlie complex genome regulatory functions. Genome Biol *13*, R85.

Kubik, S., Bruzzone, M.J., Jacquet, P., Falcone, J.L., Rougemont, J., and Shore, D. (2015). Nucleosome Stability Distinguishes Two Different Promoter Types at All Protein-Coding Genes in Yeast. Mol Cell *60*, 422-434.

Kulaeva, O.I., and Studitsky, V.M. (2010). Mechanism of histone survival during transcription by RNA polymerase II. Transcription *1*, 85-88.

Lai, W.K.M., and Pugh, B.F. (2017). Understanding nucleosome dynamics and their links to gene expression and DNA replication. Nat Rev Mol Cell Biol *18*, 548-562.

Landolfo, S., Gariglio, M., Gribaudo, G., and Lembo, D. (1998). The Ifi 200 genes: an emerging family of IFN-inducible genes. Biochimie *80*, 721-728.

Langmead, B., Trapnell, C., Pop, M., and Salzberg, S.L. (2009). Ultrafast and memory-efficient alignment of short DNA sequences to the human genome. Genome Biol *10*, R25.

Larner, A.C., Jonak, G., Cheng, Y.S., Korant, B., Knight, E., and Darnell, J.E., Jr. (1984). Transcriptional induction of two genes in human cells by beta interferon. Proc Natl Acad Sci U S A *81*, 6733-6737.

Lau, J.F., Nusinzon, I., Burakov, D., Freedman, L.P., and Horvath, C.M. (2003). Role of metazoan mediator proteins in interferon-responsive transcription. Mol Cell Biol *23*, 620-628.

Lau, J.F., Parisien, J.P., and Horvath, C.M. (2000). Interferon regulatory factor subcellular localization is determined by a bipartite nuclear localization signal in the DNA-binding domain and interaction with cytoplasmic retention factors. Proc Natl Acad Sci U S A *97*, 7278-7283.

Lee, C.K., Bluyssen, H.A., and Levy, D.E. (1997). Regulation of interferon-alpha responsiveness by the duration of Janus kinase activity. J Biol Chem *272*, 21872-21877.

Lee, T.I., Johnstone, S.E., and Young, R.A. (2006). Chromatin immunoprecipitation and microarray-based analysis of protein location. Nat Protoc *1*, 729-748.

Lee, W., Tillo, D., Bray, N., Morse, R.H., Davis, R.W., Hughes, T.R., and Nislow, C. (2007). A high-resolution atlas of nucleosome occupancy in yeast. Nat Genet *39*, 1235-1244.

LeRoy, G., Rickards, B., and Flint, S.J. (2008). The double bromodomain proteins Brd2 and Brd3 couple histone acetylation to transcription. Mol Cell *30*, 51-60.

Leung, S., Qureshi, S.A., Kerr, I.M., Darnell, J.E., Jr., and Stark, G.R. (1995). Role of STAT2 in the alpha interferon signaling pathway. Mol Cell Biol *15*, 1312-1317.

Levy, D.E., Kessler, D.S., Pine, R., and Darnell, J.E., Jr. (1989). Cytoplasmic activation of ISGF3, the positive regulator of interferon-alpha-stimulated transcription, reconstituted in vitro. Genes Dev *3*, 1362-1371.

Levy, D.E., Kessler, D.S., Pine, R., Reich, N., and Darnell, J.E., Jr. (1988). Interferon-induced nuclear factors that bind a shared promoter element correlate with positive and negative transcriptional control. Genes Dev *2*, 383-393.

Lewin, A.R., Reid, L.E., McMahon, M., Stark, G.R., and Kerr, I.M. (1991). Molecular analysis of a human interferon-inducible gene family. Eur J Biochem *199*, 417-423.

Lim, C.P., and Cao, X. (2006). Structure, function, and regulation of STAT proteins. Mol Biosyst *2*, 536-550.

Liu, H., Kang, H., Liu, R., Chen, X., and Zhao, K. (2002). Maximal induction of a subset of interferon target genes requires the chromatin-remodeling activity of the BAF complex. Mol Cell Biol *22*, 6471-6479.

Liu, X., Li, B., and GorovskyMa (1996). Essential and nonessential histone H2A variants in Tetrahymena thermophila. Mol Cell Biol *16*, 4305-4311.

Lomvardas, S., and Thanos, D. (2002). Modifying gene expression programs by altering core promoter chromatin architecture. Cell *110*, 261-271.

Luger, K., Dechassa, M.L., and Tremethick, D.J. (2012). New insights into nucleosome and chromatin structure: an ordered state or a disordered affair? Nat Rev Mol Cell Biol *13*, 436-447.

Luger, K., Mader, A.W., Richmond, R.K., Sargent, D.F., and Richmond, T.J. (1997). Crystal structure of the nucleosome core particle at 2.8 A resolution. Nature *389*, 251-260.

Luo, M., Pang, C.W., Gerken, A.E., and Brock, T.G. (2004). Multiple nuclear localization sequences allow modulation of 5-lipoxygenase nuclear import. Traffic *5*, 847-854.

Malik, S., and Roeder, R.G. (2005). Dynamic regulation of pol II transcription by the mammalian Mediator complex. Trends Biochem Sci *30*, 256-263.

Manry, J., Laval, G., Patin, E., Fornarino, S., Itan, Y., Fumagalli, M., Sironi, M., Tichit, M., Bouchier, C., Casanova, J.L.*, et al.* (2011). Evolutionary genetic dissection of human interferons. J Exp Med *208*, 2747-2759.

Marazzi, I., Greenbaum, B.D., Low, D.H.P., and Guccione, E. (2017). Chromatin dependencies in cancer and inflammation. Nat Rev Mol Cell Biol.

Marques, M., Laflamme, L., Gervais, A.L., and Gaudreau, L. (2010). Reconciling the positive and negative roles of histone H2A.Z in gene transcription. Epigenetics *5*, 267-272.

Matsuda, R., Hori, T., Kitamura, H., Takeuchi, K., Fukagawa, T., and Harata, M. (2010). Identification and characterization of the two isoforms of the vertebrate H2A.Z histone variant. Nucleic Acids Res *38*, 4263-4273.

McKendry, R., John, J., Flavell, D., Muller, M., Kerr, I.M., and Stark, G.R. (1991). High-frequency mutagenesis of human cells and characterization of a mutant unresponsive to both alpha and gamma interferons. Proc Natl Acad Sci U S A *88*, 11455-11459.

Mechta-Grigoriou, F., Gerald, D., and Yaniv, M. (2001). The mammalian Jun proteins: redundancy and specificity. Oncogene *20*, 2378-2389.

Melen, K., Fagerlund, R., Franke, J., Kohler, M., Kinnunen, L., and Julkunen, I. (2003). Importin alpha nuclear localization signal binding sites for STAT1, STAT2, and influenza A virus nucleoprotein. J Biol Chem *278*, 28193-28200.

Meneghini, M.D., Wu, M., and Madhani, H.D. (2003). Conserved histone variant H2A.Z protects euchromatin from the ectopic spread of silent heterochromatin. Cell *112*, 725-736.

Millar, C.B. (2013). Organizing the genome with H2A histone variants. Biochem J *449*, 567-579.

Millar, C.B., Xu, F., Zhang, K., and Grunstein, M. (2006). Acetylation of H2AZ Lys 14 is associated with genome-wide gene activity in yeast. Genes Dev *20*, 711-722.

Mizuguchi, G., Shen, X., Landry, J., Wu, W.H., Sen, S., and Wu, C. (2004). ATP-driven exchange of histone H2AZ variant catalyzed by SWR1 chromatin remodeling complex. Science *303*, 343-348.

Monteiro, F.L., Baptista, T., Amado, F., Vitorino, R., Jeronimo, C., and Helguero, L.A. (2014). Expression and functionality of histone H2A variants in cancer. Oncotarget *5*, 3428-3443.

Mostafavi, S., Yoshida, H., Moodley, D., LeBoite, H., Rothamel, K., Raj, T., Ye, C.J., Chevrier, N., Zhang, S.Y., Feng, T.*, et al.* (2016). Parsing the Interferon Transcriptional Network and Its Disease Associations. Cell *164*, 564-578.

Nusinzon, I., and Horvath, C.M. (2003). Interferon-stimulated transcription and innate antiviral immunity require deacetylase activity and histone deacetylase 1. Proc Natl Acad Sci U S A *100*, 14742-14747.

Obri, A., Ouararhni, K., Papin, C., Diebold, M.L., Padmanabhan, K., Marek, M., Stoll, I., Roy, L., Reilly, P.T., Mak, T.W.*, et al.* (2014). ANP32E is a histone chaperone that removes H2A.Z from chromatin. Nature *505*, 648-653.

Papamichos-Chronakis, M., Watanabe, S., Rando, O.J., and Peterson, C.L. (2011). Global regulation of H2A.Z localization by the INO80 chromatin-remodeling enzyme is essential for genome integrity. Cell *144*, 200-213.

Parker, B.S., Rautela, J., and Hertzog, P.J. (2016). Antitumour actions of interferons: implications for cancer therapy. Nat Rev Cancer *16*, 131-144.

Patel, M.C., Debrosse, M., Smith, M., Dey, A., Huynh, W., Sarai, N., Heightman, T.D., Tamura, T., and Ozato, K. (2013). BRD4 coordinates recruitment of pause release factor P-TEFb and the pausing complex NELF/DSIF to regulate transcription elongation of interferon-stimulated genes. Mol Cell Biol *33*, 2497-2507.

Paulson, M., Press, C., Smith, E., Tanese, N., and Levy, D.E. (2002). IFN-Stimulated transcription through a TBP-free acetyltransferase complex escapes viral shutoff. Nat Cell Biol *4*, 140-147.

Porter, A.C., Chernajovsky, Y., Dale, T.C., Gilbert, C.S., Stark, G.R., and Kerr, I.M. (1988). Interferon response element of the human gene 6-16. EMBO J *7*, 85-92.

Punzeler, S., Link, S., Wagner, G., Keilhauer, E.C., Kronbeck, N., Spitzer, R.M., Leidescher, S., Markaki, Y., Mentele, E., Regnard, C.*, et al.* (2017). Multivalent binding of

PWWP2A to H2A.Z regulates mitosis and neural crest differentiation. EMBO J *36*, 2263-2279.

Qureshi, S.A., Salditt-Georgieff, M., and Darnell, J.E., Jr. (1995). Tyrosine-phosphorylated Stat1 and Stat2 plus a 48-kDa protein all contact DNA in forming interferon-stimulated-gene factor 3. Proc Natl Acad Sci U S A *92*, 3829-3833.

Radman-Livaja, M., and Rando, O.J. (2010). Nucleosome positioning: how is it established, and why does it matter? Dev Biol *339*, 258-266.

Raisner, R.M., Hartley, P.D., Meneghini, M.D., Bao, M.Z., Liu, C.L., Schreiber, S.L., Rando, O.J., and Madhani, H.D. (2005). Histone variant H2A.Z marks the 5' ends of both active and inactive genes in euchromatin. Cell *123*, 233-248.

Reder, A.T., and Feng, X. (2014). How type I interferons work in multiple sclerosis and other diseases: some unexpected mechanisms. J Interferon Cytokine Res *34*, 589-599.

Redon, C., Pilch, D., Rogakou, E., Sedelnikova, O., Newrock, K., and Bonner, W. (2002). Histone H2A variants H2AX and H2AZ. Curr Opin Genet Dev *12*, 162-169.

Reich, N., Evans, B., Levy, D., Fahey, D., Knight, E., Jr., and Darnell, J.E., Jr. (1987). Interferon-induced transcription of a gene encoding a 15-kDa protein depends on an upstream enhancer element. Proc Natl Acad Sci U S A *84*, 6394-6398.

Reich, N.C. (2013). STATs get their move on. JAKSTAT *2*, e27080.

Reid, L.E., Brasnett, A.H., Gilbert, C.S., Porter, A.C., Gewert, D.R., Stark, G.R., and Kerr, I.M. (1989). A single DNA response element can confer inducibility by both alpha- and gamma-interferons. Proc Natl Acad Sci U S A *86*, 840-844.

Reilly, P.T., Yu, Y., Hamiche, A., and Wang, L. (2014). Cracking the ANP32 whips: important functions, unequal requirement, and hints at disease implications. Bioessays *36*, 1062-1071.

Rengachari, S., Groiss, S., Devos, J.M., Caron, E., Grandvaux, N., and Panne, D. (2018). Structural basis of STAT2 recognition by IRF9 reveals molecular insights into ISGF3 function. Proc Natl Acad Sci U S A *115*, E601-E609.

Richmond, T.J., and Davey, C.A. (2003). The structure of DNA in the nucleosome core. Nature *423*, 145-150.

Ridgway, P., Brown, K.D., Rangasamy, D., Svensson, U., and Tremethick, D.J. (2004). Unique residues on the H2A.Z containing nucleosome surface are important for Xenopus laevis development. J Biol Chem *279*, 43815-43820.

Robertson, G., Hirst, M., Bainbridge, M., Bilenky, M., Zhao, Y., Zeng, T., Euskirchen, G., Bernier, B., Varhol, R., Delaney, A.*, et al.* (2007). Genome-wide profiles of STAT1 DNA association using chromatin immunoprecipitation and massively parallel sequencing. Nat Methods *4*, 651-657.

Rodero, M.P., and Crow, Y.J. (2016). Type I interferon-mediated monogenic autoinflammation: The type I interferonopathies, a conceptual overview. J Exp Med *213*, 2527-2538.

Ronni, T., Matikainen, S., Lehtonen, A., Palvimo, J., Dellis, J., Van Eylen, F., Goetschy, J.F., Horisberger, M., Content, J., and Julkunen, I. (1998). The proximal interferon-stimulated response elements are essential for interferon responsiveness: a promoter analysis of the antiviral MxA gene. J Interferon Cytokine Res *18*, 773-781.

Rosenbloom, K.R., Sloan, C.A., Malladi, V.S., Dreszer, T.R., Learned, K., Kirkup, V.M., Wong, M.C., Maddren, M., Fang, R., Heitner, S.G.*, et al.* (2013). ENCODE data in the UCSC Genome Browser: year 5 update. Nucleic Acids Res *41*, D56-63.

Rutherford, M.N., Hannigan, G.E., and Williams, B.R. (1988). Interferon-induced binding of nuclear factors to promoter elements of the 2-5A synthetase gene. EMBO J *7*, 751-759.

Sakamoto, S., Potla, R., and Larner, A.C. (2004). Histone deacetylase activity is required to recruit RNA polymerase II to the promoters of selected interferon-stimulated early response genes. J Biol Chem *279*, 40362-40367.

Santisteban, M.S., Kalashnikova, T., and Smith, M.M. (2000). Histone H2A.Z regulats transcription and is partially redundant with nucleosome remodeling complexes. Cell *103*, 411-422.

Schmidt, D., Wilson, M.D., Ballester, B., Schwalie, P.C., Brown, G.D., Marshall, A., Kutter, C., Watt, S., Martinez-Jimenez, C.P., Mackay, S.*, et al.* (2010). Five-vertebrate ChIP-seq reveals the evolutionary dynamics of transcription factor binding. Science *328*, 1036-1040.

Schneider, W.M., Chevillotte, M.D., and Rice, C.M. (2014). Interferon-stimulated genes: a complex web of host defenses. Annu Rev Immunol *32*, 513-545.

Schoggins, J.W., and Rice, C.M. (2011). Interferon-stimulated genes and their antiviral effector functions. Curr Opin Virol *1*, 519-525.

Schones, D.E., Cui, K., Cuddapah, S., Roh, T.Y., Barski, A., Wang, Z., Wei, G., and Zhao, K. (2008). Dynamic regulation of nucleosome positioning in the human genome. Cell *132*, 887-898.

Segala, G., Bennesch, M.A., Pandey, D.P., Hulo, N., and Picard, D. (2016). Monoubiquitination of Histone H2B Blocks Eviction of Histone Variant H2A.Z from Inducible Enhancers. Mol Cell *64*, 334-346.

Sevilla, A., and Binda, O. (2014). Post-translational modifications of the histone variant H2AZ. Stem Cell Res *12*, 289-295.

Soutourina, J. (2018). Transcription regulation by the Mediator complex. Nat Rev Mol Cell Biol *19*, 262-274.

Stark, G.R., and Darnell, J.E., Jr. (2012). The JAK-STAT pathway at twenty. Immunity *36*, 503-514.

Struhl, K. (1998). Histone acetylation and transcriptional regulatory mechanisms. Genes Dev *12*, 599-606.

Subramanian, V., Fields, P.A., and Boyer, L.A. (2015). H2A.Z: a molecular rheostat for transcriptional control. F1000Prime Rep *7*, 01.

Subramanian, V., Mazumder, A., Surface, L.E., Butty, V.L., Fields, P.A., Alwan, A., Torrey, L., Thai, K.K., Levine, S.S., Bathe, M.*, et al.* (2013). H2A.Z acidic patch couples chromatin dynamics to regulation of gene expression programs during ESC differentiation. PLoS Genet *9*, e1003725.

Sudhakar, A. (2009). History of Cancer, Ancient and Modern Treatment Methods. J Cancer Sci Ther *1*, 1-4.

Surface, L.E., Fields, P.A., Subramanian, V., Behmer, R., Udeshi, N., Peach, S.E., Carr, S.A., Jaffe, J.D., and Boyer, L.A. (2016). H2A.Z.1 Monoubiquitylation Antagonizes BRD2 to Maintain Poised Chromatin in ESCs. Cell Rep *14*, 1142-1155.

Tamura, T., Smith, M., Kanno, T., Dasenbrock, H., Nishiyama, A., and Ozato, K. (2009). Inducible deposition of the histone variant H3.3 in interferon-stimulated genes. J Biol Chem *284*, 12217-12225.

Tamura, T., Yanai, H., Savitsky, D., and Taniguchi, T. (2008). The IRF family transcription factors in immunity and oncogenesis. Annu Rev Immunol *26*, 535-584.

Taniguchi, Y. (2016). The Bromodomain and Extra-Terminal Domain (BET) Family: Functional Anatomy of BET Paralogous Proteins. Int J Mol Sci *17*.

Tenoever, B.R., Ng, S.L., Chua, M.A., McWhirter, S.M., Garcia-Sastre, A., and Maniatis, T. (2007). Multiple functions of the IKK-related kinase IKKepsilon in interferon-mediated antiviral immunity. Science *315*, 1274-1278.

Thanos, D., and Maniatis, T. (1995). Virus induction of human IFN beta gene expression requires the assembly of an enhanceosome. Cell *83*, 1091-1100.

Tramantano, M., Sun, L., Au, C., Labuz, D., Liu, Z., Chou, M., Shen, C., and Luk, E. (2016). Constitutive turnover of histone H2A.Z at yeast promoters requires the preinitiation complex. Elife *5*.

Trinchieri, G. (2010). Type I interferon: friend or foe? J Exp Med *207*, 2053-2063.

Tsompana, M., and Buck, M.J. (2014). Chromatin accessibility: a window into the genome. Epigenetics Chromatin *7*, 33.

Valouev, A., Johnson, S.M., Boyd, S.D., Smith, C.L., Fire, A.Z., and Sidow, A. (2011). Determinants of nucleosome organization in primary human cells. Nature *474*, 516-520.

van Daal, A., and Elgin, S.C. (1992). A histone variant, H2AvD, is essential in Drosophila melanogaster. Mol Biol Cell *3*, 593-602.

Venters, B.J., and Pugh, B.F. (2009). How eukaryotic genes are transcribed. Crit Rev Biochem Mol Biol *44*, 117-141.

Verdin, E., and Ott, M. (2015). 50 years of protein acetylation: from gene regulation to epigenetics, metabolism and beyond. Nat Rev Mol Cell Biol *16*, 258-264.

Voong, L.N., Xi, L., Sebeson, A.C., Xiong, B., Wang, J.P., and Wang, X. (2016). Insights into Nucleosome Organization in Mouse Embryonic Stem Cells through Chemical Mapping. Cell *167*, 1555-1570 e1515.

Weber, C.M., Ramachandran, S., and Henikoff, S. (2014). Nucleosomes are context-specific, H2A.Z-modulated barriers to RNA polymerase. Mol Cell *53*, 819-830.

Yan, Z., Cui, K., Murray, D.M., Ling, C., Xue, Y., Gerstein, A., Parsons, R., Zhao, K., and Wang, W. (2005). PBAF chromatin-remodeling complex requires a novel specificity subunit, BAF200, to regulate expression of selective interferon-responsive genes. Genes Dev *19*, 1662-1667.

Yen, K., Vinayachandran, V., and Pugh, B.F. (2013). SWR-C and INO80 chromatin remodelers recognize nucleosome-free regions near +1 nucleosomes. Cell *154*, 1246-1256.

Yigit, E., Zhang, Q., Xi, L., Grilley, D., Widom, J., Wang, J.P., Rao, A., and Pipkin, M.E. (2013). High-resolution nucleosome mapping of targeted regions using BAC-based enrichment. Nucleic Acids Res *41*, e87.

Yuasa, K., and Hijikata, T. (2016). Distal regulatory element of the STAT1 gene potentially mediates positive feedback control of STAT1 expression. Genes Cells *21*, 25-40.

Zanton, S.J., and Pugh, B.F. (2006). Full and partial genome-wide assembly and disassembly of the yeast transcription machinery in response to heat shock. Genes Dev *20*, 2250-2265.

Zeng, L., and Zhou, M.M. (2002). Bromodomain: an acetyl-lysine binding domain. FEBS Lett *513*, 124-128.

Zhang, Y., Liu, T., Meyer, C.A., Eeckhoute, J., Johnson, D.S., Bernstein, B.E., Nusbaum, C., Myers, R.M., Brown, M., Li, W.*, et al.* (2008). Model-based analysis of ChIP-Seq (MACS). Genome Biol *9*, R137.

Zitvogel, L., Galluzzi, L., Kepp, O., Smyth, M.J., and Kroemer, G. (2015). Type I interferons in anticancer immunity. Nat Rev Immunol *15*, 405-414.

Zlatanova, J., and Thakar, A. (2008). H2A.Z: view from the top. Structure *16*, 166-179.

APPENDIX A. SUPPLEMENTAL FIGURES

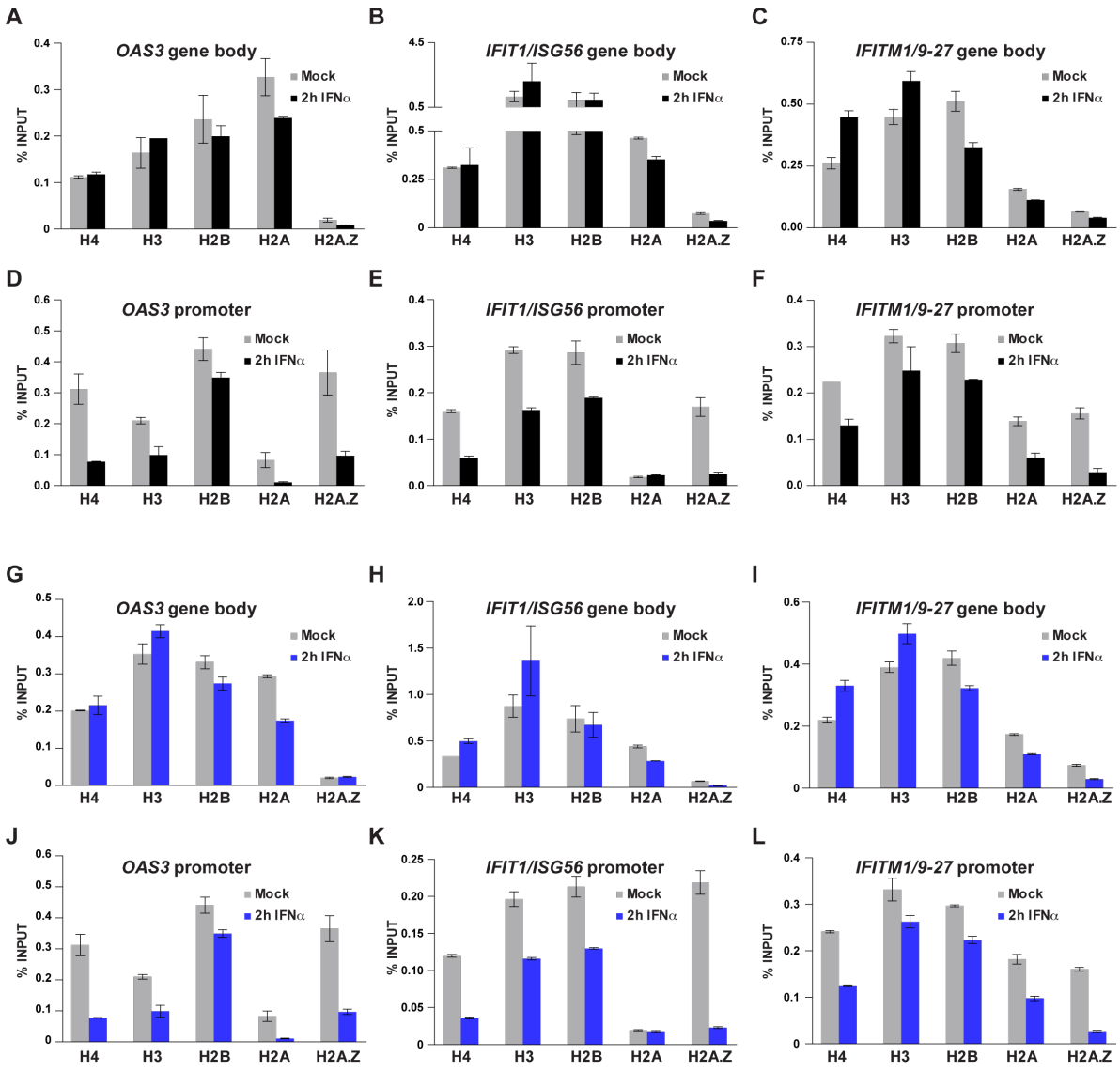

Appendix Figure 1. IFN-stimulated loss of histones H2A.Z, H2B, H3, and H4 at ISG promoters, Related to Figure 3.1

(A-F) Biological replicate for ChIP analysis of histones H4, H3, H2B, H2A, and H2A.Z occupancy at the gene body (A-C) or gene promoter (D-F) of *OAS3*, *IFIT1/ISG56*, and *IFITM1/9-27* during steady state and after 2 hr IFNα stimulation. Error bars denote standard deviation of technical replicates. (G-L) The mean computed from biological replicates in Figure 3.1 and Appendix Figure 1A-F. Error bars denote standard error of mean.

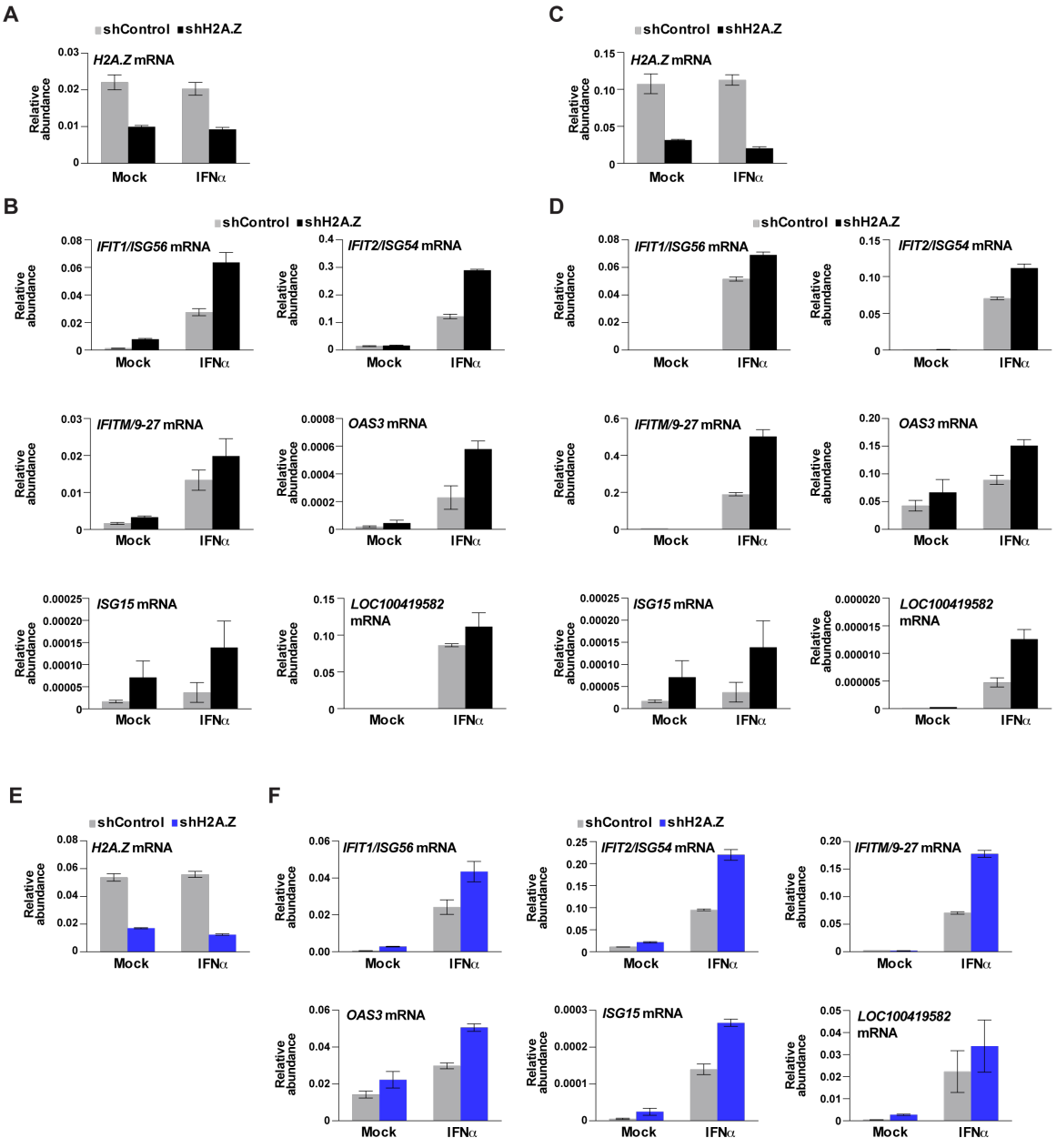

Appendix Figure 2: H2A.Z suppresses ISG mRNA expression, Related to Figure 3.8

(A-D) Biological replicates of HeLa cells transduced with an shRNA vector targeting H2A.Z or a non-targeting control. (A, C) Biological replicate of H2A.Z mRNA levels quantified by RT-qPCR in unstimulated and 10 hr IFNα-stimulated H2A.Z knockdown or control cells. (B, D) Biological replicates of the ISG mRNA expression of *IFIT1/ISG56*, *IFIT2/ISG54*, *IFITM1/9-27*, *OAS3*, *ISG15*, and *LOC100419583.* Error bars denote standard deviation of technical replicates. (E-F) The mean computed from biological replicates in Figure 3.8 and Appendix Figure 2A-D. Error bars denote standard error of mean.

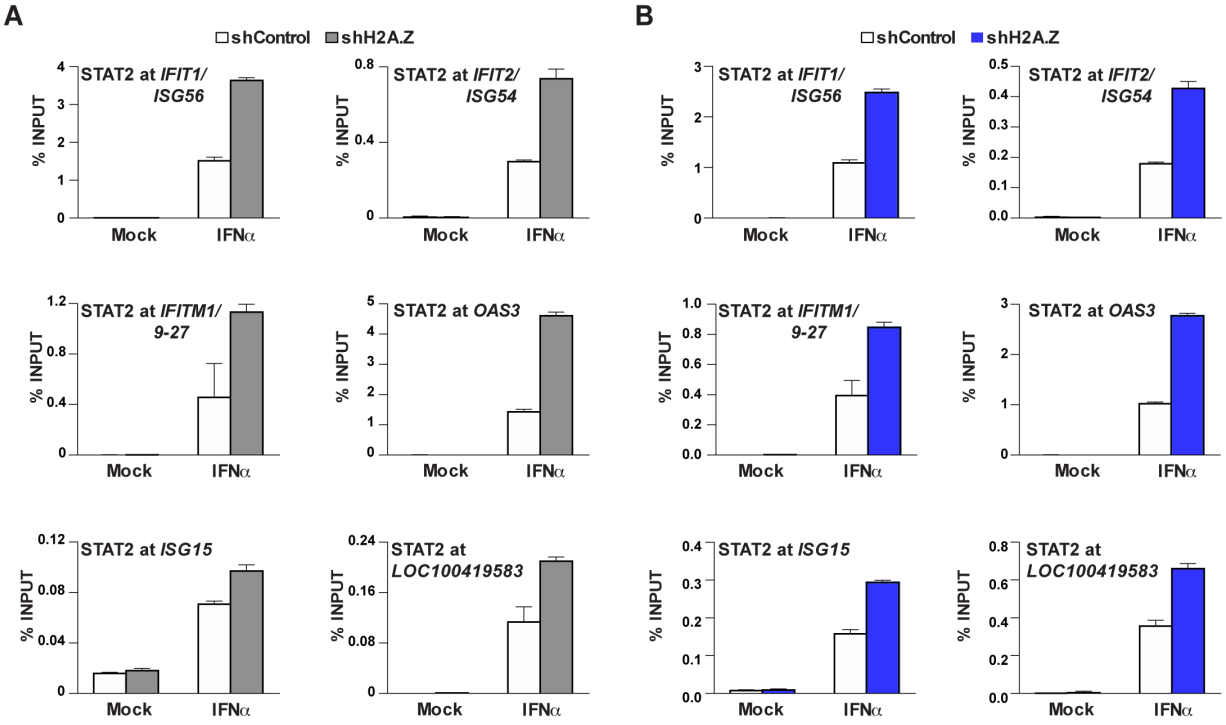

Appendix Figure 3: H2A.Z suppresses ISGF3 occupancy, Related to Figure 3.9
HeLa cells transduced with an shRNA vector targeting H2A.Z or a non-targeting control. (A) Biological replicate of the ChIP analysis of STAT2 occupancy in H2A.Z knockdown or control HeLa cells with or without 1 hr IFNα stimulation at promoters of *IFIT1/ISG56*, *IFIT2/ISG54*, *IFITM1/9-27*, *OAS3*, *ISG15*, and *LOC100419583*. Error bars denote standard deviation of technical replicates. (B) The mean computed from biological replicates in Figure 3.9 and Appendix Figure 3A. Error bars denote standard error of mean.

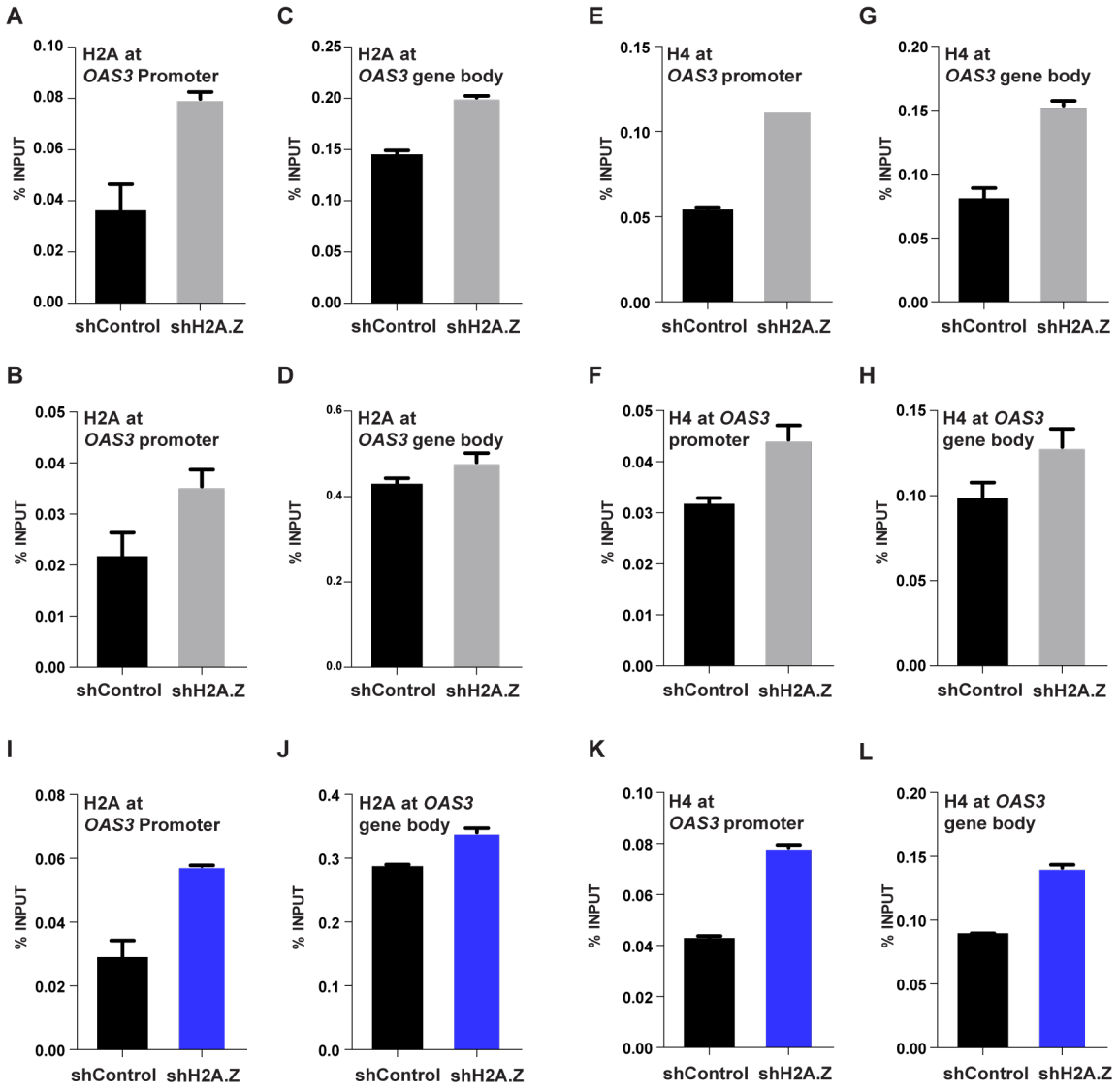

Appendix Figure 4: Histones H2A and H4 occupancy at ISGs in H2A.Z knockdown cells, Related to Figures 3.7-3.10.
HeLa cells transduced with an shRNA vector targeting H2A.Z or a non-targeting control. (A-D) Biological replicates of the ChIP analysis of histone H2A at the OAS3 promoter (A-B) and gene body (C-D) in unstimulated control and H2A.Z knockdown cells. (E-H) Same as A-D, but for histone H4. Error bars denote the standard deviation of technical replicates. (I-L) The mean computed from biological replicates in Appendix Figure 4A-D for histone H2A (I-J) or histone H4 (K-L). Error bars denote standard error of mean.

APPENDIX B. HISTONE ACETYLATION AND OTHER POST-TRANSLATIONAL MODIFICATIONS IN THE IFN RESPONSE

INTRODUCTION

Histone post-translational modifications (PTMs) contribute to the diversity and dynamics of the chromatin landscape by affecting the chromatin structure and the affinity to which coactivators bind histones (Kimura, 2013). Histone acetylation (HAT) is commonly associated with transcription activation, while histone deacetylation (HDAC) is linked to transcription repression (Dovey et al., 2010; Struhl, 1998). Surprisingly, for transcriptional activation of ISGs, both HAT and HDAC activity are required (Chang et al., 2004; Nusinzon and Horvath, 2003; Paulson et al., 2002).

The requirement for HDAC activity in ISG transcriptional activation was unexpected, as HDACs are often affiliated with transcription repression (Chang et al., 2004; Nusinzon and Horvath, 2003; Sakamoto et al., 2004). Stimulation with IFN and a HDAC inhibitor trichostatin A (TSA) abolished ISG transcription, indicating HDAC activity is essential to ISG activation (Nusinzon and Horvath, 2003). Since this initial discovery in our lab (Nusinzon and Horvath, 2003), several other groups have observed the same phenomenon, where HDAC activity is required for the transcription of ISGs (Chang et al., 2004; Sakamoto et al., 2004). Various aspects of the JAK-STAT signaling cascade had been examined to identify the mechanistic requirement of HDAC activity during the IFN response including phosphorylation of STAT1 and STAT2 and nuclear translocation of ISGF3; these experiments have ruled out ISGF3 activation and nuclear translocation as being affected by HDAC inhibition (Chang et al., 2004; Nusinzon and Horvath, 2003; Sakamoto et al., 2004).

ISGF3 was found to interact with HDAC1 through STAT2, and little to no association with HDAC4 and HDAC5. Yet, treatment with IFN and HDAC inhibitors TSA and SAHA did not affect the STAT2-HDAC1 interaction. Pol II and STAT2/ISGF3 recruitment to ISG promoters was also evaluated and while STAT2/ISGF3 recruitment remained intact in the presence of IFN and TSA treatment, Pol II recruitment was inhibited. This finding indicated HDAC activity was required following STAT2/ISGF3 recruitment, but prior to Pol II assembly at the ISG promoter.

The role of HDAC in regulating ISG transcription remains to be fully elucidated, but the accumulated data suggests HDAC regulation is required at the interface of ISGF3 and Pol II recruitment to ISGs. Although a commonly associated role of HDACs is to deacetylate histone substrates, no specific acetylated histone residue(s) have been implicated. To continue the investigation of the HDAC requirement for ISG transcription, ChIP-qPCR assays examining STAT2/ISGF3 and Pol II were performed to confirm the ISG requirement for HDAC activity occurs after ISGF3 recruitment and prior to Pol II assembly. Additionally, as a preliminary study to identify acetylated histone target(s) that are subject to deacetylation during the IFN response, the IFN-induced global histone modification profile was evaluated using an epiproteomic screen through the Northwestern Proteomic Core. These experiments provide additional insights into the investigation of the HDAC requirement and regulation in the IFN response.

RESULTS AND DISCUSSION

HDAC inhibition prevents ISGF3 recruitment to ISG promoters

The absolute requirement of HDAC activity for global ISG expression was found to prevent Pol II recruitment to the *IFIT1/ISG54* promoter, but not STAT2/ISGF3. The mechanism as to how HDAC activity is required for ISG transcriptional activity and IFN-stimulated Pol II recruitment remains unknown to date, but indicates HDAC function is required after STAT2/ISGF3 associates with the ISG promoter. To continue this line of investigation, ChIP assays of STAT2 and Pol II were performed to verify the HDAC requirement for ISG transcription occurs after STAT2/ISGF3 recruitment and prior to Pol II assembly at ISG promoters. ChIP analysis of RNA Pol II CTD was performed using mock-treated, 3 hr IFN-treated or 3 hr IFN- and TSA-treated HeLa cells (Appendix Figure 5A-B). As expected, RNA Pol II CTD was recruited to both *IFIT2/ISG54* and *OAS3* promoters after 3 hr IFN stimulation, and this process was inhibited in the presence of 3 hr IFN plus TSA.

To confirm STAT2/ISGF3 recruitment was intact during HDAC inhibition, STAT2 ChIP assays in HeLa cells mock-treated or treated with either 3 hr or 6 hr of IFN (+/- TSA) were examined (Appendix Figure 5C-D). IFN-induced STAT2 recruitment was observed following 3 hr IFN treatment and attenuated by 6 hr, corresponding to the ISGF3 recruitment time course in Chapter 2 (Figure 2.1). Unexpectedly, recruitment of STAT2 was inhibited after 3 hr IFN and TSA treatment at both *IFIT2/ISG54* and *OAS3* promoters (Appendix Figure 5C-D). On the other hand, STAT2 occupancy levels were similar after 6 hr IFN with or without TSA treatment. These results contrasted the previous finding that

STAT2 recruitment was unaffected, and instead, indicates STAT2 recruitment is impacted by HDAC inhibition. Moreover, it suggests the effects of HDAC operate upstream of ISGF3 recruitment and binding to ISG targets.

It was surprising to discover the data in Appendix Figure 5C-D disagreed with previous studies (Chang et al., 2004; Sakamoto et al., 2004). However, closer examination of the experimental conditions in these previous studies showed those observations were performed at different IFN time points and not at times with abundant ISGF3 present at an ISG promoter. In one experiment, 30 min of IFN +/- TSA was used, while in another study 6 hr of IFN +/- TSA was used. Based on the IFN-stimulated STAT2/ISGF3 recruitment profile over time, IFN treatment for 30 min or 6 hr represents the early ISGF3 recruitment and late ISGF3 attenuation. Consequently, examination of STAT2 at 30 min or 6 hr would correspond to little or no STAT2/ISGF3 present at an ISG promoter (Figure 2.1). Based on the finding that HDAC activity is required for STAT2/ISGF3 recruitment to ISGs, future examination of the HDAC requirement for ISG transcription should evaluate activities upstream of ISGF3 recruitment or at the interface of ISGF3 interactions with the ISG promoter nucleosomes.

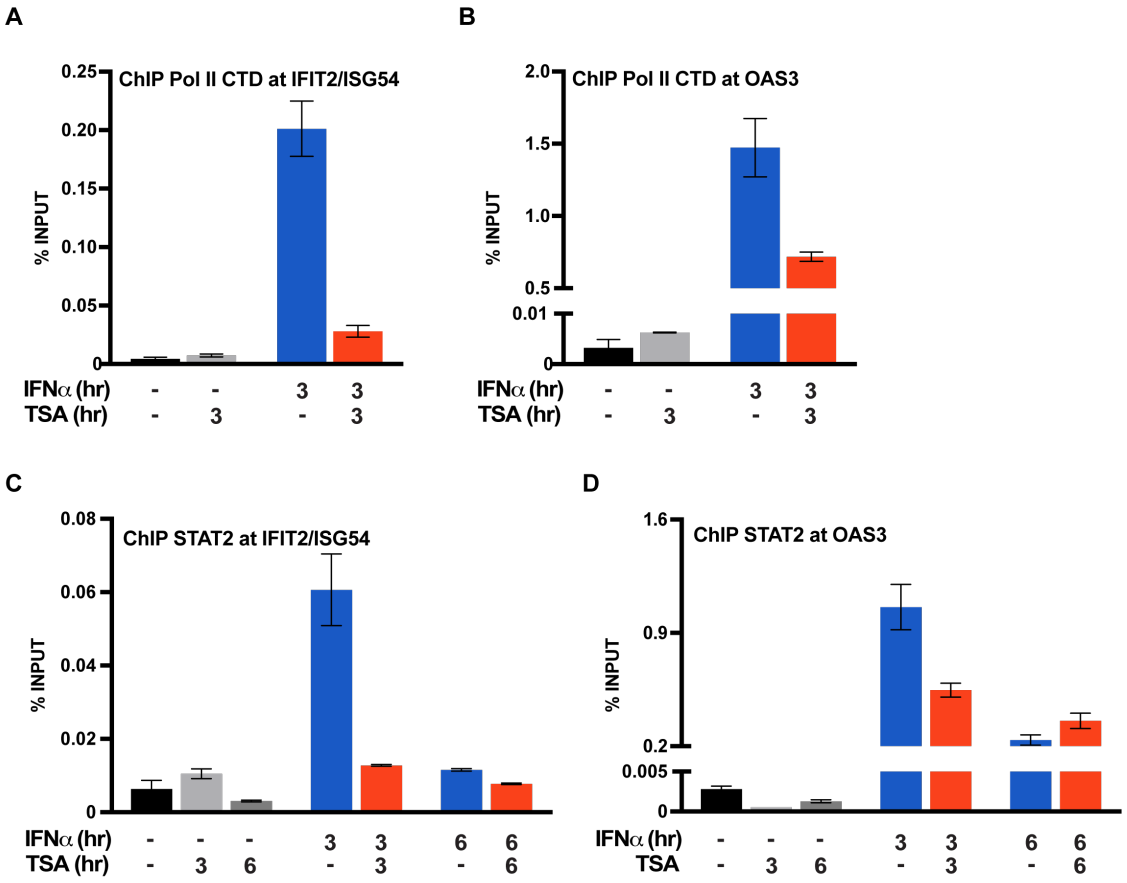

Appendix Figure 5: TSA treatment inhibits STAT2 recruitment to ISG promoters
(A-B) ChIP-qPCR assay of Pol II C-terminal domain at (A) *IFIT2/ISG56* and (B) *OAS3* promoters in HeLa cells mock-treated, treated with 3 hr IFNα or 3 hr IFNα + TSA. (C-D) ChIP-qPCR assay of STAT2 at (C) *IFIT2/ISG56* and (D) *OAS3* promoters in HeLa cells mock-treated, treated with either 3 hr or 6 hr IFNα ± TSA. IFN-stimulated global histone modifications

Examination of global IFN- and IFN-TSA-stimulated histone modifications

Transcriptional activation of ISGs depend on both HAT and HDAC activities (Chang et al., 2004; Nusinzon and Horvath, 2003; Paulson et al., 2002). The unexpected HDAC requirement for ISG transcription remains to be fully elucidated, however, HDAC activity is necessary for STAT2/ISGF3 recruitment to ISG promoters (Appendix Figure 5). During the IFN response, ISGF3 associates with coactivators that remodel chromatin and modify histones, including HATs and HDACs, to regulate ISG transcription activation. HATs and HDACs catalyze the acetylation and deacetylation of histone proteins that comprise the nucleosomes throughout the genome including at ISGs. However, little information on the histone acetylation status of ISGs during steady state and following IFN stimulation is known.

Histone PTMs have been associated with transcription activation or repression and can influence interactions with other factors during transcription (Bowman and Poirier, 2015). As a preliminary study to identify candidate histone residue(s) dynamically regulated in response to IFN stimulation by acetylation and deacetylation, a histone modification profiling screen was performed. The histone profiling screen is based on a "targeted quantitative peptide proteomics" method, which determines the relative percent abundance of the unmodified and modified forms of a specific histone residue. For example, global evaluation of the total H3K4 population would consist of the unmodified, mono-methylated (me1), di-methylated (me2), tri-methylated (me3), and acetylated (ac) forms and together they would total 100 percent.

The histone profiling screen was performed over an IFN treatment time course with and without the HDAC inhibitor TSA. HeLa cells were mock-treated or treated with IFN or IFN and TSA for 15 min, 1 hr, 2 hr, 4 hr or 10 hr, then harvested. The nuclei was isolated and histones were extracted for targeted liquid chromatography-coupled mass spectrometry (LC-MS). Surveyed histone modifications include those that are a part of the Epiproteomic Histone Modification Panel B from the Northwestern University Proteomic Core (Appendix Figure 6). The Histone Modification Panel B identifies both acetylation and methylation modification forms. The analysis focused on the histone acetylation dynamics during the IFN response, but all of the data is included and deposited in the Horvath lab NU Box repository.

Generally, the relative abundance of an acetylated histone residue in samples that were treated with both TSA and IFN were higher in abundance than samples treated with IFN only (Appendix Figure 7). Among the histone modifications surveyed with IFN treatment only, histone residues with notable changes in acetylation levels included H3.3K36, H3K23, H4K8, H4K12, and H2AK9 (Appendix Figure 7). Most of these histone residues exhibited an increase in acetylation following IFN stimulation except histone variant residue H3.3K36 (Appendix Figure 7A,F). It was the only histone residue from this screen that exhibited a decrease in acetylation following IFN treatment (Appendix Figure 7F). A decrease in H3.3.K36ac following IFN stimulation indicated the H3.3K36 residue is subject to HDAC activity during the IFN response.

Previous studies have demonstrated a role for histone variant H3.3 in ISG transcription (Chen et al., 2017; Tamura et al., 2009). IFN induces deposition of histone

variant H3.3 at distal regions of ISG, *IFIT1/ISG56*, increasing its abundance in the gene body, and H3.3 knockdown decreases ISG transcript expression. Thus, far, acetylated H3.3K36 has not been linked to ISG transcription regulation, while methylation of the H3.3K36 residue has been associated with ISG regulation following IFN stimulation (Chen et al., 2017; Patel et al., 2013). Based on this preliminary screen, H3.3K36 is a potential candidate to investigate to determine whether it is a specific target of HDAC(s) employed during the IFN response. Additional histone residues that exhibited little to no difference over the IFN treatment time course or following IFN and TSA treatment are included in Appendix Table 1.

A

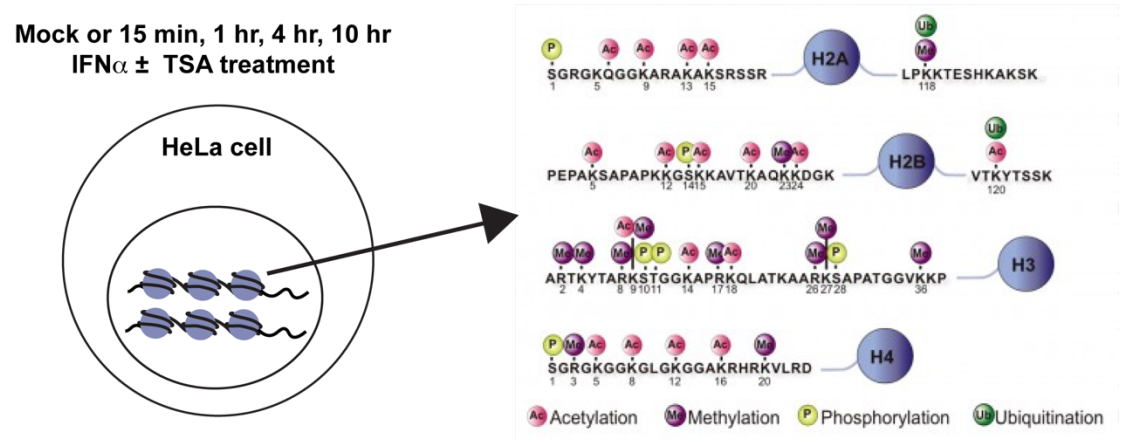

B

H1.4: K25UN	H1.4: K25AC	H1.4: K25ME1	H1.4: K25ME2	H1.4: K25ME3	H2A: K5UN	H2A: K5AC	H2A: K9UN	H2A: K9AC
H2A: K36UN	H2A: K36AC	H2A1: K13UN	H2A1: K13AC	H2A1: K15UN	H2A1: K15AC*	H2A1: K15UB*	H2A3: K13UN	H2A3: K13AC
H2A3: K15UN	H2A3: K15AC	H2A3: K15UB*	H3R2UN: K4UN	H3R2UN: K4AC	H3R2UN: K4ME1	H3R2UN: K4ME2	H3R2UN: K4ME3	H3R2UN: Q5UN
H3R2UN: Q5ME1	H3: K9UN	H3: K9AC	H3: K9ME1	H3: K9ME2	H3: K9ME3	H3: K14UN	H3: K14AC	H3: K18UN
H3: K18AC	H3: K18ME1	H3: Q19UN	H3: Q19ME1	H3: K23UN	H3: K23AC	H3: K23ME1	H3: R42UN	H3: R42ME2*
H3: R49UN	H3: R49ME2*	H3: Q55UN	H3: Q55ME1*	H3: K56UN	H3: K56AC	H3: K64UN	H3: K64AC	H3: K79UN
H3: K79AC	H3: K79ME1	H3: K79ME2	H3: K79ME3	H3: K122UN	H3: K122AC	H3.1: K27UN	H3.1: K27AC	H3.1: K27ME1
H3.1: K27ME2	H3.1: K27ME3	H3.1: K36UN	H3.1: K36AC	H3.1: K36ME1	H3.1: K36ME2	H3.1: K36ME3	H3.3: K27UN	H3.3: K27AC
H3.3: K27M*	H3.3: K27ME1	H3.3: K27ME2	H3.3: K27ME3	H3.3: K36UN	H3.3: K36AC	H3.3: K36ME1	H3.3: K36ME2	H3.3: K36ME3
H4: K5UN	H4: K5AC	H4: K8UN	H4: K8AC	H4: K12UN	H4: K12AC	H4: K16UN	H4: K16AC	H4: K20UN
H4: K20AC	H4: K20ME1	H4: K20ME2	H4: K20ME3					

* Modification Available upon Request

ac=Acetylated, me=Methylated, ub=Ubiquitylated, number refers to the degree of modification. H3K9me3 indicated the trimethylation of lysine 9 of H3. Unmodified peptides are also included.

Appendix Figure 6: Epiproteomic Histone Modification Panel B
Schematic of the experimental conditions and the histone modifications surveyed from the Northwestern Proteomic Core Epiproteomic Histone Modification Panel B. (A) (Left) Nuclei was isolated from HeLa cells mock-treated or treated with IFNα ± TSA for 15 min, 1 hr, 4 hr, 10 hr. (Right) Extracted histones were evaluated with LC-MS for different histone modification states depicted in the diagram. (B) List of the histone modifications surveyed from Epiproteomic Histone Modification Panel B. Both histone modification images are courtesy of the Northwestern Proteomics Core web site.

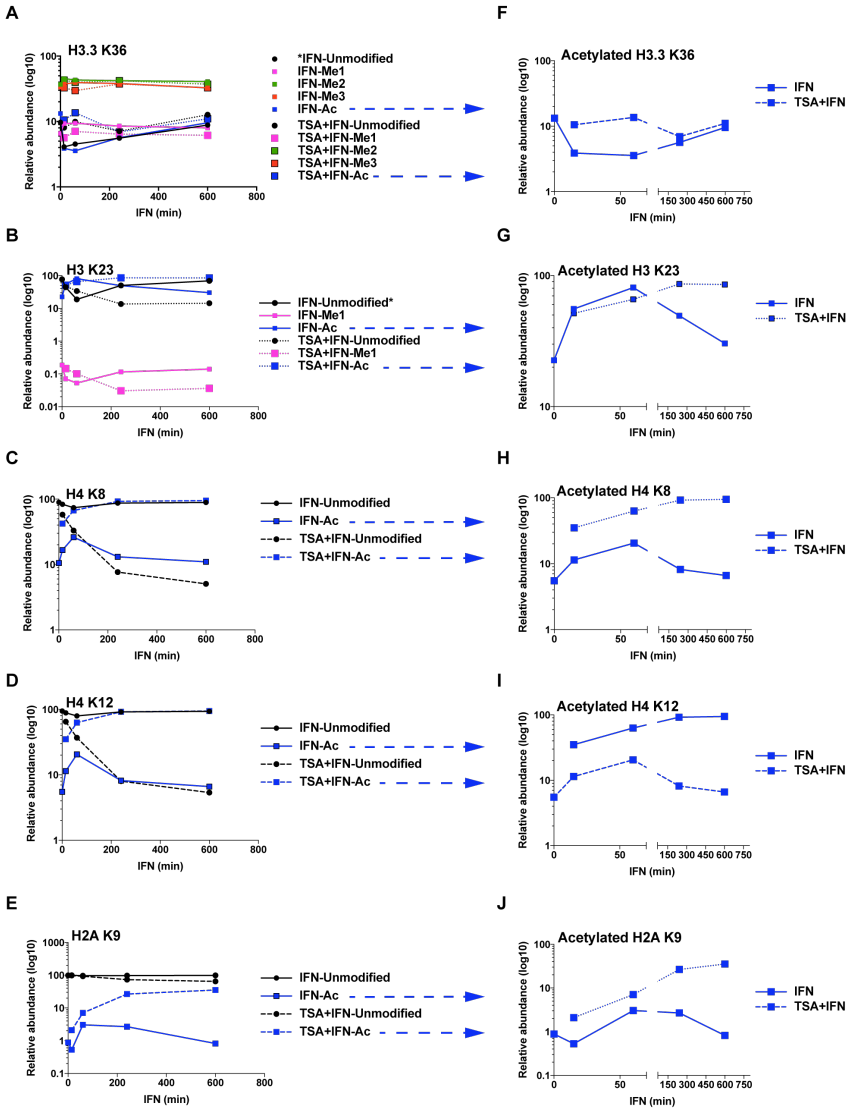

Appendix Figure 7: Histone residues with altered abundance of acetylation and methylation in response to IFN stimulation

(A-E) Relative percent abundance (log10 scale) of unmodified and modified forms of histone residues, H3.3K36, H3K23, H4K8, H4K12, and H2AK9 with IFN or TSA+IFN treatment for 15 min, 1 hr, 4 hr, or 10 hr. Modified forms include: mono-methylated, Me1; di-methylated, Me2; tri-methylated, Me3; acetylated, Ac. (F-J) Only the acetylated histone residue data from (A-E). X-axis break zooms into early treatment of 0-70 min IFN or TSA+IFN.

Appendix Table 1. Relative abundance of unmodified and modified histone residues screened from the Epiproteomic Histone Modification Panel B

Histone	Residue	PTM	Treatment	Relative abundance (%)	Standard Deviation (%)
H4	K5	Unmodified	Mock	90.2381124651994	0.277235141758981
			15 min IFNα	87.7617275500847	0.273955191853968
			1 hr IFNα	81.6368069799026	0.602529040612429
			4 hr IFNα	89.1995552908563	0.0874065030102687
			10 hr IFNα	90.4695108503219	0.109947950445163
			15 min IFNα/TSA	16.2335372202754	0.0907858389890163
			1 hr IFNα/TSA	67.1511164891246	0.205893924851534
			4 hr IFNα/TSA	44.4151983055838	0.21235612046871
			10 hr IFNα/TSA	10.2539783371356	0.240973196436641
		Acetylation	Mock	9.76188753480064	0.277235141758979
			15 min IFNα	12.2382724499152	0.273955191853963
			1 hr IFNα	18.3631930200974	0.602529040612422
			4 hr IFNα	10.8004447091438	0.0874065030102723
			10 hr IFNα	9.5304891496781	0.109947950445159
			15 min IFNα/TSA	83.7664627797246	0.0907858389890123
			1 hr IFNα/TSA	32.8488835108754	0.205893924851528
			4 hr IFNα/TSA	55.5848016944162	0.212356120468708
			10 hr IFNα/TSA	89.7460216628644	0.240973196436646
	K8	Unmodified	Mock	89.4516932318638	0.304774671565649
			15 min IFNα	83.3523369966578	0.342130819209121
			1 hr IFNα	73.8711509672434	1.00179662903828
			4 hr IFNα	86.8775422877695	0.12597268218643
			10 hr IFNα	89.0148191670621	0.0586938688258815
			15 min IFNα/TSA	11.3221263151374	0.0211329897863637
			1 hr IFNα/TSA	57.803117639573	0.443367856353538
			4 hr IFNα/TSA	33.075194424399	0.125707804794918
			10 hr IFNα/TSA	7.66155636198875	0.171078968561694
		Acetylation	Mock	10.5483067681363	0.304774671565651
			15 min IFNα	16.6476630033422	0.342130819209114
			1 hr IFNα	26.1288490327567	1.00179662903827
			4 hr IFNα	13.1224577122305	0.125972682186433
			10 hr IFNα	10.9851808329379	0.0586938688258746
			15 min IFNα/TSA	88.6778736848626	0.0211329897863598
			1 hr IFNα/TSA	42.196882360427	0.443367856353531
			4 hr IFNα/TSA	66.924805575601	0.125707804794918
			10 hr IFNα/TSA	92.3384436380113	0.171078968561687
	K12	Unmodified	Mock	94.4861892823743	0.106353630551925
			15 min IFNα	88.6035073064897	0.297338320740319
			1 hr IFNα	79.4474167080709	1.23811232557722
			4 hr IFNα	91.8108387979717	0.079806856898972
			10 hr IFNα	93.3874661228226	0.0286729864988226
			15 min IFNα/TSA	12.1074386745101	0.0386473970130341
			1 hr IFNα/TSA	65.0525244700791	0.397987442855693
			4 hr IFNα/TSA	36.9285386766873	0.102899280725838
			10 hr IFNα/TSA	8.0180099005774	0.181696574604185
		Acetylation	Mock	5.51381071762574	0.106353630551918
			15 min IFNα	11.3964926935103	0.297338320740317
			1 hr IFNα	20.5525832919291	1.23811232557723
			4 hr IFNα	8.1891612020283	0.0798068568989806
			10 hr IFNα	6.61253387717738	0.0286729864988273
			15 min IFNα/TSA	87.8925613254899	0.0386473970130358
			1 hr IFNα/TSA	34.9474755299209	0.397987442855691

			4 hr IFNα/TSA	63.0714613233127	0.102899280725839
			10 hr IFNα/TSA	91.9819900994226	0.181696574604184

Histone	Residue	PTM	Treatment	Relative abundance (%)	Standard Deviation (%)
H4	K16	Unmodified	Mock	67.6863149576102	0.624074411938981
			15 min IFNα	62.4607877188564	0.706730465428002
			1 hr IFNα	57.8908285859436	0.203950169790317
			4 hr IFNα	65.841708009372	0.410929009486308
			10 hr IFNα	66.3210499159363	0.456159131941415
			15 min IFNα/TSA	9.9572852833649	0.0522205235741988
			1 hr IFNα/TSA	45.4509914035228	0.415186516939522
			4 hr IFNα/TSA	26.470949901006	0.0640768103652416
			10 hr IFNα/TSA	7.05685721525547	0.151008379965818
		Acetylation	Mock	32.3136850423898	0.624074411938983
			15 min IFNα	37.5392122811435	0.706730465428
			1 hr IFNα	42.1091714140563	0.203950169790317
			4 hr IFNα	34.158291990628	0.410929009486312
			10 hr IFNα	33.6789500840637	0.456159131941405
			15 min IFNα/TSA	90.0427147166351	0.0522205235741987
			1 hr IFNα/TSA	54.5490085964773	0.415186516939514
			4 hr IFNα/TSA	73.529050098994	0.0640768103652352
			10 hr IFNα/TSA	92.9431427847445	0.151008379965823

Histone	Residue	PTM	Treatment	Relative abundance (%)	Standard Deviation (%)
H3	K4	Unmodified	Mock	96.9561552657567	0.0807063890627182
			15 min IFNα	84.7548907157679	0.140814538556256
			1 hr IFNα	73.6038002461663	0.567353764536551
			4 hr IFNα	87.3852104494065	0.389594078621273
			10 hr IFNα	92.0906589155903	0.393221879128772
			15 min IFNα/TSA	88.3819322291607	0.267158139034049
			1 hr IFNα/TSA	94.67332190794	0.0303258511447402
			4 hr IFNα/TSA	94.3880573484397	0.173780653898872
			10 hr IFNα/TSA	86.9885872431424	0.952919375131543
		Mono-Methylation	Mock	2.28679356475469	0.0654119933859953
			15 min IFNα	7.37256061986008	0.0910679416277233
			1 hr IFNα	15.6195038742872	0.276528708329596
			4 hr IFNα	6.21679965052088	0.129431556173756
			10 hr IFNα	4.04947397167933	0.335758630023727
			15 min IFNα/TSA	9.24282307171336	0.322991051122182
			1 hr IFNα/TSA	3.02024354632015	0.0361159231319197
			4 hr IFNα/TSA	3.03337619498904	0.142897569684749
			10 hr IFNα/TSA	5.74541081578507	0.530838464033936

Histone	Residue	PTM	Treatment	Relative abundance (%)	Standard Deviation (%)
H3	K4	Di-Methylation	Mock	0.350044523585735	0.00767746944068028
			15 min IFNα	4.02687889393359	0.0172710845674351
			1 hr IFNα	7.43811190696865	0.290416919599978
			4 hr IFNα	4.1302701237331	0.223048039414055
			10 hr IFNα	2.10363175201032	0.0617194868962093
			15 min IFNα/TSA	1.25814537585696	0.0515049148600436
			1 hr IFNα/TSA	1.31172082847362	0.0200497447093987
			4 hr IFNα/TSA	1.32646188234358	0.0304154571481577
			10 hr IFNα/TSA	3.69795304495018	0.27318220530424
		Tri-Methylation	Mock	0.330738571690269	0.00374572625307915
			15 min IFNα	3.46498620922901	0.0650846173444914
			1 hr IFNα	2.91473423018744	0.0127070739925217
			4 hr IFNα	2.07466978874715	0.0726010203986581
			10 hr IFNα	1.63036321301588	0.0273841461720337
			15 min IFNα/TSA	0.867245443452432	0.0348628752557983
			1 hr IFNα/TSA	0.771325432245203	0.0114548313907283
			4 hr IFNα/TSA	0.966818418642791	0.0147562949285176
			10 hr IFNα/TSA	2.68904954231878	0.156200973106065
		Acetylation	Mock	0.0762680742126032	0.025693433011584
			15 min IFNα	0.38068356120948	0.0226884338503699
			1 hr IFNα	0.423849742390385	0.0106557405720674
			4 hr IFNα	0.193049987592342	0.0182416945301741
			10 hr IFNα	0.125872147704153	0.0106481099104198
			15 min IFNα/TSA	0.249853879816547	0.0362072558210072
			1 hr IFNα/TSA	0.223388285021069	0.00984919140005322
			4 hr IFNα/TSA	0.285286155584882	0.00590065427529829
			10 hr IFNα/TSA	0.878999353803575	0.00514779374016637

Histone	Residue	PTM	Treatment	Relative abundance (%)	Standard Deviation (%)
H3	K9	Unmodified	Mock	37.6274292751336	0.326051270807601
			15 min IFNα	30.5909219715636	0.207304857965043
			1 hr IFNα	30.950771327732	0.751525858340705
			4 hr IFNα	29.8386233017052	0.66779629206988
			10 hr IFNα	30.1884822329619	0.990960796476829
			15 min IFNα/TSA	26.474893135175	0.138251520949188
			1 hr IFNα/TSA	35.6842053023243	1.14066052408731
			4 hr IFNα/TSA	32.4056940781169	1.09021172549178
			10 hr IFNα/TSA	19.1014929939341	0.912343260352272
		Mono-Methylation	Mock	33.2114255753505	0.914888632935785
			15 min IFNα	30.3626434034634	0.231672330422914
			1 hr IFNα	26.2932516997085	0.620767651510622
			4 hr IFNα	26.2817834321173	0.630633532689355
			10 hr IFNα	30.2160433570461	1.23550787301124
			15 min IFNα/TSA	26.4781048073293	1.22033687722484
			1 hr IFNα/TSA	30.8744763184496	0.179468625442344
			4 hr IFNα/TSA	27.5024167438793	0.173595359293845
			10 hr IFNα/TSA	23.8624839065865	0.580951921824267

Histone	Residue	PTM	Treatment	Relative abundance (%)	Standard Deviation (%)
H3	K9	Di-Methylation	Mock	25.7358340018041	0.716419389183699
			15 min IFNα	34.9528563851669	0.387497210938788
			1 hr IFNα	38.1587950859063	0.234454145197743
			4 hr IFNα	39.1702589339043	0.618335332894046
			10 hr IFNα	35.105329864677	0.165985502219302
			15 min IFNα/TSA	26.2299158033265	1.36911273092784
			1 hr IFNα/TSA	25.3871784323026	1.2266819704222
			4 hr IFNα/TSA	29.2651322254611	1.08703270013631
			10 hr IFNα/TSA	35.9602816652091	1.55193715670141
		Tri-Methylation	Mock	1.90241673870643	0.0569909579008377
			15 min IFNα	2.26699486286525	0.0379072222575831
			1 hr IFNα	2.63046848642527	0.0766042135582711
			4 hr IFNα	2.68856720451346	0.0439708874177223
			10 hr IFNα	2.70197060238178	0.0711828807746747
			15 min IFNα/TSA	1.54041838865889	0.0463712492074063
			1 hr IFNα/TSA	1.45233745357139	0.0646432102577876
			4 hr IFNα/TSA	1.64286968312084	0.0691873683107823
			10 hr IFNα/TSA	1.9633842138409	0.0562601750398631
		Acetylation	Mock	1.52289440900535	0.0148687160987944
			15 min IFNα	1.82658337694076	0.00686922874522144
			1 hr IFNα	1.96671340022794	0.127974873904039
			4 hr IFNα	2.02076712775969	0.0267445966888432
			10 hr IFNα	1.78817394293321	0.0668677358033109
			15 min IFNα/TSA	19.2766678655103	0.744068044272433
			1 hr IFNα/TSA	6.60180249335215	0.19119678828958
			4 hr IFNα/TSA	9.18388726942188	0.124271505710425
			10 hr IFNα/TSA	19.1123572204294	0.229428788109917

Histone	Residue	PTM	Treatment	Relative abundance (%)	Standard Deviation (%)
H3	K14	Unmodified	Mock	58.653612447464	0.224706522758788
			15 min IFNα	37.1429539105222	0.140949651023532
			1 hr IFNα	41.9527045434091	0.375765501543239
			4 hr IFNα	42.8742571001631	0.298161897004616
			10 hr IFNα	58.8578884894105	0.981898876294482
			15 min IFNα/TSA	9.94632793032229	0.30833466727414
			1 hr IFNα/TSA	29.413224762369	0.598326225775932
			4 hr IFNα/TSA	17.6263956798504	0.133078069061274
			10 hr IFNα/TSA	8.33855967159796	0.238472928555054
		Acetylation	Mock	41.346387552536	0.224706522758788
			15 min IFNα	62.8570460894779	0.140949651023532
			1 hr IFNα	58.0472954565909	0.375765501543242
			4 hr IFNα	57.1257428998369	0.298161897004609
			10 hr IFNα	41.1421115105895	0.981898876294481
			15 min IFNα/TSA	90.0536720696777	0.30833466727414
			1 hr IFNα/TSA	70.586775237631	0.598326225775936
			4 hr IFNα/TSA	82.3736043201496	0.133078069061273
			10 hr IFNα/TSA	91.6614403284021	0.238472928555065

Histone	Residue	PTM	Treatment	Relative abundance (%)	Standard Deviation (%)
H3	K18	Unmodified	Mock	94.3052155682087	0.045969131934651
			15 min IFNα	93.1977787738221	0.0717248403520508
			1 hr IFNα	92.3000990909626	0.084021670707138
			4 hr IFNα	92.7298044689566	0.0155972379472162
			10 hr IFNα	94.0622157254064	0.0312701093402015
			15 min IFNα/TSA	63.0244638756435	0.352883384270909
			1 hr IFNα/TSA	85.8899054779816	0.106003542420703
			4 hr IFNα/TSA	77.6554759161901	0.145972529858653
			10 hr IFNα/TSA	57.7242414365401	0.49849086184426
		Mono-Methylation	Mock	0.321642857931025	0.0419566387384806
			15 min IFNα	0.132275295859911	0.0133530157359695
			1 hr IFNα	0.110721872690351	0.00678723416035116
			4 hr IFNα	0.226293200418993	0.00946796021426217
			10 hr IFNα	0.273564931496983	0.0403879359312311
			15 min IFNα/TSA	0.0863403608621691	0.00139163690796737
			1 hr IFNα/TSA	0.25013662052623	0.0269966276207043
			4 hr IFNα/TSA	0.179692990054716	0.00810117787491509
			10 hr IFNα/TSA	0.0545376467030145	0.0113992804519728
		Acetylation	Mock	5.37314157386025	0.0296248039917848
			15 min IFNα	6.66994593031796	0.0585949154400221
			1 hr IFNα	7.58917903634701	0.087638870189914
			4 hr IFNα	7.04390233062437	0.0237418840771922
			10 hr IFNα	5.66421934309658	0.050492585354997
			15 min IFNα/TSA	36.8891957634943	0.352338392893053
			1 hr IFNα/TSA	13.8599579014922	0.113039864090272
			4 hr IFNα/TSA	22.1648310937552	0.149879976279472
			10 hr IFNα/TSA	42.2212209167569	0.50312152699857

Histone	Residue	PTM	Treatment	Relative abundance (%)	Standard Deviation (%)
H3	K23	Unmodified	Mock	77.2209794078375	0.207922798509366
			15 min IFNα	44.3338645231733	0.318394416853623
			1 hr IFNα	18.8824281542088	0.339640683093908
			4 hr IFNα	50.4782676481081	0.485741161924073
			10 hr IFNα	69.5184087599318	0.285330522589862
			15 min IFNα/TSA	18.8923551013553	0.29706250139629
			1 hr IFNα/TSA	48.3455600325008	0.147272154794523
			4 hr IFNα/TSA	34.0672131695418	0.0780201732550963
			10 hr IFNα/TSA	13.62993613652	0.0591596002492639
		Mono-Methylation	Mock	0.187577242490981	0.0207501523985794
			15 min IFNα	0.0702630779522588	0.00614137181600009
			1 hr IFNα	0.0526802033786449	0.0222018883711371
			4 hr IFNα	0.114939445695192	0.0025623888639914
			10 hr IFNα	0.13991190920336	0.00474798318010733
			15 min IFNα/TSA	0.0475321249039315	0.00197362987685379
			1 hr IFNα/TSA	0.146236608653968	0.00629396747998958
			4 hr IFNα/TSA	0.10134687144815	0.00643788665265097
			10 hr IFNα/TSA	0.030649839288196	0.00575584306322949

Histone	Residue	PTM	Treatment	Relative abundance (%)	Standard Deviation (%)
H3	K23	Acetylation	Mock	22.5914433496715	0.193693318431178
			15 min IFNα	55.5958723988745	0.321822241822265
			1 hr IFNα	81.0648916424126	0.323710340221301
			4 hr IFNα	49.4067929061967	0.48789264140269
			10 hr IFNα	30.3416793308648	0.28712988100322
			15 min IFNα/TSA	81.0601127737407	0.298201917317727
			1 hr IFNα/TSA	51.5082033588453	0.153452899702391
			4 hr IFNα/TSA	65.8314399590101	0.0805618224718995
			10 hr IFNα/TSA	86.3394140241918	0.0550799438157924

Histone	Residue	PTM	Treatment	Relative abundance (%)	Standard Deviation (%)
H3	K56	Unmodified	Mock	99.6380334551149	0.044844155693678
			15 min IFNα	99.6028599386431	0.0296573813697817
			1 hr IFNα	99.1669276776751	0.191371357139759
			4 hr IFNα	99.754371731689	0.0532853256417338
			10 hr IFNα	99.8055299883445	0.0238070707542193
			15 min IFNα/TSA	99.8413525775057	0.0426034767588287
			1 hr IFNα/TSA	99.8120477413032	0.00965509717696015
			4 hr IFNα/TSA	99.7745398657489	0.0330169450277052
			10 hr IFNα/TSA	99.7237393598613	0.0377922034299291
		Mono-Methylation	Mock	0.350915368424924	0.0431979476448186
			15 min IFNα	0.371789833275522	0.0274542598221973
			1 hr IFNα	0.691880004067801	0.254614892450029
			4 hr IFNα	0.232293779258297	0.0495634162423007
			10 hr IFNα	0.181302529806327	0.0284329701718256
			15 min IFNα/TSA	0.135162874121631	0.0312290806281472
			1 hr IFNα/TSA	0.168227925541284	0.00796207568260486
			4 hr IFNα/TSA	0.206592501986637	0.0333311625013491
			10 hr IFNα/TSA	0.241500960074714	0.0240295313560099
		Acetylation	Mock	0.0110511764602237	0.00304916006779837
			15 min IFNα	0.025350228081358	0.0161245746579421
			1 hr IFNα	0.141192318257044	0.0853866960357402
			4 hr IFNα	0.0133344890527398	0.0048681322546192
			10 hr IFNα	0.0131674818491518	0.00498066758550592
			15 min IFNα/TSA	0.023484548372655	0.0137944054150992
			1 hr IFNα/TSA	0.0197243331554685	0.010224218678728
			4 hr IFNα/TSA	0.0188676322644996	0.0034741985906747
			10 hr IFNα/TSA	0.0347596800640344	0.0215365598729281

Histone	Residue	PTM	Treatment	Relative abundance (%)	Standard Deviation (%)
H3	K79	Unmodified	Mock	74.3528314134437	0.592342734593695
			15 min IFNα	49.8181977096638	0.370986275686544
			1 hr IFNα	53.3131873539357	0.272028863295191
			4 hr IFNα	58.1448384498586	0.37345845692994
			10 hr IFNα	66.5830507623307	0.433062319120627
			15 min IFNα/TSA	69.2578461221566	0.19069319012051
			1 hr IFNα/TSA	74.2050690562878	0.554311718076459
			4 hr IFNα/TSA	70.0557633927558	0.152121032457416
			10 hr IFNα/TSA	64.4149833656226	0.602489074231487

Histone	Residue	PTM	Treatment	Relative abundance (%)	Standard Deviation (%)
H3	K79	Mono-Methylation	Mock	17.6783273578692	0.406282348093403
			15 min IFNα	31.4289150817915	0.388306576889158
			1 hr IFNα	28.5304383289875	0.102509671624907
			4 hr IFNα	25.2104342823553	0.398658735233763
			10 hr IFNα	20.4425195306749	0.15426092298733
			15 min IFNα/TSA	20.9618159283559	0.25384271881914
			1 hr IFNα/TSA	17.9051325300348	0.183222872188775
			4 hr IFNα/TSA	19.9507363863684	0.143964034527032
			10 hr IFNα/TSA	21.1445484245477	0.422098385042019
		Di-Methylation	Mock	6.9915765418276	0.157977316981243
			15 min IFNα	17.9988980817172	0.0289884329211865
			1 hr IFNα	16.4626040844256	0.203955548827147
			4 hr IFNα	15.6595444567693	0.0568385446370983
			10 hr IFNα	11.2239966770619	0.207989837605043
			15 min IFNα/TSA	8.51892559849473	0.0382175361509453
			1 hr IFNα/TSA	6.86193514532231	0.188104748371725
			4 hr IFNα/TSA	8.80165794330874	0.045864818874045
			10 hr IFNα/TSA	12.8691503745857	0.378459049976285
		Tri-Methylation	Mock	0.940277290525564	0.0368055359734059
			15 min IFNα	0.672869490732068	0.0231429250574245
			1 hr IFNα	1.50001895427747	0.0628479563676659
			4 hr IFNα	0.928726465054633	0.0599767373737714
			10 hr IFNα	1.6727739617086	0.0843095593657452
			15 min IFNα/TSA	1.19742965298136	0.0589732723766506
			1 hr IFNα/TSA	0.97472699003528	0.217600400023076
			4 hr IFNα/TSA	1.14087241673215	0.0960271976623692
			10 hr IFNα/TSA	1.45215016447236	0.076102599051979
		Acetylation	Mock	0.036987396333947	0.00807284528077119
			15 min IFNα	0.0811196360953917	0.0115037243980514
			1 hr IFNα	0.193751278373823	0.0878018776811188
			4 hr IFNα	0.0564563459620745	0.0258601851729571
			10 hr IFNα	0.0776590682239419	0.0253512618918626
			15 min IFNα/TSA	0.0639826980115069	0.023178354751564
			1 hr IFNα/TSA	0.0531362783197467	0.0221272934979563
			4 hr IFNα/TSA	0.0509698608349967	0.0093819516602381
			10 hr IFNα/TSA	0.119167670771718	0.0301658892087318

Histone	Residue	PTM	Treatment	Relative abundance (%)	Standard Deviation (%)
H4	R49	Unmodified	Mock	91.0337756142069	0.299551555635369
			15 min IFNα	98.2431504359868	0.0702201863599423
			1 hr IFNα	98.1533099246384	0.305336955959479
			4 hr IFNα	97.7571483662234	0.0277293646514588
			10 hr IFNα	92.6142424742235	0.14823584524241
			15 min IFNα/TSA	94.4123625582737	0.054128915378686
			1 hr IFNα/TSA	92.6451684592591	0.274048348897585
			4 hr IFNα/TSA	92.0117646476789	0.119562602902256
			10 hr IFNα/TSA	96.0557677893332	0.086810312725561
		Di-Methylation	Mock	1.25731348363548	0.090488132267877
			15 min IFNα	0.304283038421193	0.0199294890532213
			1 hr IFNα	0.578993606706474	0.0930773059919275
			4 hr IFNα	0.458622486100588	0.0351653227853107
			10 hr IFNα	0.954814217104124	0.142900089129536
			15 min IFNα/TSA	0.90033804438504	0.0163906041546909

			1 hr IFNα/TSA	0.933333578970887	0.111103915181092
			4 hr IFNα/TSA	0.813534276645634	0.0153989070475238
			10 hr IFNα/TSA	0.740478659317009	0.0534473897447827

Histone	Residue	PTM	Treatment	Relative abundance (%)	Standard Deviation (%)
H3.1	K27	Unmodified	Mock	41.7113098058691	0.655287899471431
			15 min IFNα	31.4866621388022	0.0449090467801069
			1 hr IFNα	33.2821573046357	0.404427404812396
			4 hr IFNα	33.737137463976	0.644042108679118
			10 hr IFNα	37.9218546037047	0.500080937848803
			15 min IFNα/TSA	25.539199781944	1.30230740550612
			1 hr IFNα/TSA	41.3515014113721	0.483185060897808
			4 hr IFNα/TSA	39.5720461640934	0.624706344303272
			10 hr IFNα/TSA	25.7426779181789	0.439305439851278
		Mono-Methylation	Mock	35.5647094370456	0.431664279277658
			15 min IFNα	40.0322077437625	0.113452828438492
			1 hr IFNα	40.3743444160196	0.999090783004726
			4 hr IFNα	39.0340649791887	0.106924244066862
			10 hr IFNα	35.7086344877641	1.01214954224355
			15 min IFNα/TSA	40.8352189447607	1.2441943272873
			1 hr IFNα/TSA	33.3384352567483	0.902521078216445
			4 hr IFNα/TSA	31.6228197420041	0.857584962725706
			10 hr IFNα/TSA	34.4456770109816	0.808150554718071
		Di-Methylation	Mock	16.3123769034617	0.161489201744518
			15 min IFNα	20.7615777351527	0.146092556826869
			1 hr IFNα	19.606064777891	0.468933370665087
			4 hr IFNα	19.983007203972	0.355179678552449
			10 hr IFNα	19.4134130932305	0.291146127867425
			15 min IFNα/TSA	16.8085464334631	0.337757262750822
			1 hr IFNα/TSA	16.5570173627881	0.427669406990824
			4 hr IFNα/TSA	16.7763815044765	0.107281106569868
			10 hr IFNα/TSA	19.149421875261	0.245481679294773
		Tri-Methylation	Mock	5.55971541414962	0.196864258977392
			15 min IFNα	6.48449271604959	0.0601444050525013
			1 hr IFNα	5.62605548075383	0.146085072600355
			4 hr IFNα	6.23265029156537	0.194923890018673
			10 hr IFNα	6.01441147626055	0.182848865551759
			15 min IFNα/TSA	9.21763209146488	0.10474427074225
			1 hr IFNα/TSA	5.14090318021329	0.350288843072633
			4 hr IFNα/TSA	5.56620467440529	0.0613536670782611
			10 hr IFNα/TSA	9.59769711957718	0.145696950512021
		Acetylation	Mock	0.851888439473916	0.0257781639250799
			15 min IFNα	1.23505966623307	0.0134979079429043
			1 hr IFNα	1.11137802069983	0.00778007991120387
			4 hr IFNα	1.01314006129782	0.0400125340443529
			10 hr IFNα	0.941686339040064	0.0433892643726784
			15 min IFNα/TSA	7.59940274836736	0.108789418509159
			1 hr IFNα/TSA	3.61214278887821	0.268255869732357
			4 hr IFNα/TSA	6.46254791502069	0.203452113659243
			10 hr IFNα/TSA	11.0645260760013	0.150484420466338

Histone	Residue	PTM	Treatment	Relative abundance (%)	Standard Deviation (%)
H3.1	K36	Unmodified	Mock	23.3169536527518	0.577415257216407
			15 min IFNα	9.63277086152353	0.1153141465332
			1 hr IFNα	8.70511609697138	0.262213772305423
			4 hr IFNα	14.2029644068686	0.74481534098185
			10 hr IFNα	20.9495847871507	0.768393708466611
			15 min IFNα/TSA	18.2413081690388	0.47819380021898
			1 hr IFNα/TSA	19.4482747409279	0.453651746202392
			4 hr IFNα/TSA	23.8194653218852	1.08757904424515
			10 hr IFNα/TSA	17.7852793915239	0.424992155944291
		Mono-Methylation	Mock	10.7457051835492	0.170484025465743
			15 min IFNα	18.1179676449646	0.173684930810538
			1 hr IFNα	17.2862210882217	0.361622319288716
			4 hr IFNα	14.7396171816789	0.228595365200686
			10 hr IFNα	13.3296816638298	0.185142488650679
			15 min IFNα/TSA	11.9557808111785	0.240216611753358
			1 hr IFNα/TSA	9.74937172779724	0.111690541660223
			4 hr IFNα/TSA	11.3957920109369	0.517890790433758
			10 hr IFNα/TSA	12.8839599271826	0.202758224903562
		Di-Methylation	Mock	52.4056900478633	0.452870532564972
			15 min IFNα	58.5599744863763	0.221972902741691
			1 hr IFNα	59.9396203547028	0.282147465678941
			4 hr IFNα	57.4368272217222	0.282750074799511
			10 hr IFNα	52.1960365798744	1.02063805462549
			15 min IFNα/TSA	56.6034078712369	0.543073707134824
			1 hr IFNα/TSA	57.8177788710015	0.640973199779345
			4 hr IFNα/TSA	52.886895339803	1.66386031374774
			10 hr IFNα/TSA	55.8185887046448	0.173785241037697
		Tri-Methylation	Mock	13.5316511158357	0.379816272599567
			15 min IFNα	13.6892870071356	0.0591335579699192
			1 hr IFNα	14.0690424601041	0.0620432815738118
			4 hr IFNα	13.6205911897302	0.295526612734446
			10 hr IFNα	13.5246969691451	0.0899579876027778
			15 min IFNα/TSA	13.1995031485458	0.553571510223355
			1 hr IFNα/TSA	12.9845746602733	0.301993577985149
			4 hr IFNα/TSA	11.8978473273748	0.104224521362222
			10 hr IFNα/TSA	13.5121719766486	0.419266378675509

Histone	Residue	PTM	Treatment	Relative abundance (%)	Standard Deviation (%)
H3.3	K27	Unmodified	Mock	60.3961411820179	0.942957167779333
			15 min IFNα	47.2268823611383	0.733115349225035
			1 hr IFNα	48.2876896812245	0.917049405089095
			4 hr IFNα	51.2568198117276	0.966896966137312
			10 hr IFNα	58.315553727915	1.45104794677522
			15 min IFNα/TSA	33.4406504571096	1.4467902718627
			1 hr IFNα/TSA	51.1576212670541	1.62300585994006
			4 hr IFNα/TSA	45.550667870273	1.15779886459966
			10 hr IFNα/TSA	30.1191323703477	0.984199928957505
		Mono-Methylation	Mock	26.8689515658028	0.932869092245583
			15 min IFNα	33.6766564971228	0.787706331907294
			1 hr IFNα	31.9374368700753	1.29992962945187
			4 hr IFNα	30.5593416323755	0.782324822369108
			10 hr IFNα	26.2822347318835	1.37549604218785
			15 min IFNα/TSA	28.8634562544952	1.39088705514896

			1 hr IFNα/TSA	24.7263874886676	1.24677524956183
			4 hr IFNα/TSA	22.2952769797705	0.812779578026083
			10 hr IFNα/TSA	20.9489409810023	1.09467950209018
Histone	**Residue**	**PTM**	**Treatment**	**Relative abundance (%)**	**Standard Deviation (%)**
H3.3	**K27**	**Di-Methylation**	Mock	7.04515353967856	0.296349843413445
			15 min IFNα	10.7288747450391	0.0807566208908944
			1 hr IFNα	11.0899205620907	0.288548932409896
			4 hr IFNα	9.77422786661308	0.447682012309733
			10 hr IFNα	8.32491002381959	0.1150802905352
			15 min IFNα/TSA	6.81152134466745	0.164054505801235
			1 hr IFNα/TSA	7.85278377179543	0.140628333007683
			4 hr IFNα/TSA	6.89287529481021	0.648648339446541
			10 hr IFNα/TSA	7.39825199555014	0.323548927170646
		Tri-Methylation	Mock	2.75046394750904	0.270685448223856
			15 min IFNα	4.26980177391084	0.0794715930796007
			1 hr IFNα	4.37335227508508	0.204127548343184
			4 hr IFNα	4.04740545254561	0.154377265357357
			10 hr IFNα	3.32775829235238	0.129730822995898
			15 min IFNα/TSA	9.1420198332034	0.239096727361054
			1 hr IFNα/TSA	4.37045590549957	0.466289593488153
			4 hr IFNα/TSA	5.63281006350753	0.166266458340407
			10 hr IFNα/TSA	10.9558289883338	0.353170407380788
		Acetylation	Mock	2.93928976499174	0.171176187905142
			15 min IFNα	4.09778462278894	0.0678432581884352
			1 hr IFNα	4.31160061152447	0.176667717377949
			4 hr IFNα	4.3622052367382	0.234967143556639
			10 hr IFNα	3.74954322402944	0.0807309615846381
			15 min IFNα/TSA	21.7423521105243	0.30692160331328
			1 hr IFNα/TSA	11.8927515669833	1.06442369384702
			4 hr IFNα/TSA	19.6283697916388	0.776100382173073
			10 hr IFNα/TSA	30.577845664766	0.0432355451232186

Histone	**Residue**	**PTM**	**Treatment**	**Relative abundance (%)**	**Standard Deviation (%)**
H3.3	**K36**	**Unmodified**	Mock	0.0971438188408626	0.0971438188408626
			15 min IFNα	0.0810911891864334	0.0810911891864334
			1 hr IFNα	0.053697270889985	0.053697270889985
			4 hr IFNα	0.109618656387816	0.109618656387816
			10 hr IFNα	0.255525843152645	0.255525843152645
			15 min IFNα/TSA	0.365386895551271	0.365386895551271
			1 hr IFNα/TSA	0.16491906125615	0.16491906125615
			4 hr IFNα/TSA	0.211836950850824	0.211836950850824
			10 hr IFNα/TSA	0.0971438188408626	0.0971438188408626
		Mono-Methylation	Mock	6.57321846208548	0.241366562165064
			15 min IFNα	9.32656399062516	0.114489406198911
			1 hr IFNα	9.43112174409177	0.235306209173008
			4 hr IFNα	8.51319634397906	0.393448166004208
			10 hr IFNα	8.0324290084607	0.0753378013576758
			15 min IFNα/TSA	6.33983806497485	0.292023441941379
			1 hr IFNα/TSA	5.65454907492694	0.267058481501685
			4 hr IFNα/TSA	7.0724512009994	0.0415128664040428
			10 hr IFNα/TSA	6.42843685022932	0.256565830104394
			Mock	36.8912973779599	0.658914797035803

		Di-Methylation	15 min IFNα	45.2524148881487	0.326622780705938
			1 hr IFNα	43.0951658525085	1.48891169930918
			4 hr IFNα	42.157780245549	1.01675303726597
			10 hr IFNα	40.8825977738184	0.575080149467114
			15 min IFNα/TSA	39.2508787073305	0.294703266799194
			1 hr IFNα/TSA	42.9119060772995	1.74551997191578
			4 hr IFNα/TSA	39.6593832587326	0.633946292432313
			10 hr IFNα/TSA	42.0618533390924	1.05594068274059

Histone	Residue	PTM	Treatment	Relative abundance (%)	Standard Deviation (%)
H3.3	**K36**	**Tri-Methylation**	Mock	33.5552148470549	0.493314266652216
			15 min IFNα	37.4267488909971	0.411181825216269
			1 hr IFNα	39.368530994928	1.37014716290733
			4 hr IFNα	38.0871108453423	0.849329106524399
			10 hr IFNα	32.7142373409972	0.419452502129978
			15 min IFNα/TSA	39.1100365358605	0.17300914609745
			1 hr IFNα/TSA	32.8192986758578	0.973870309188447
			4 hr IFNα/TSA	29.692842612993	1.03920479631985
			10 hr IFNα/TSA	37.4756707378937	0.704850906840006
		Acetylation	Mock	13.266552413155	0.0765029533234356
			15 min IFNα	3.88915796130742	0.0658512104941126
			1 hr IFNα	3.5747220557056	0.193451309576608
			4 hr IFNα	5.6628236168682	0.118323102788137
			10 hr IFNα	9.55582039928942	0.144289632464708
			15 min IFNα/TSA	8.23630243473757	0.183048915714829
			1 hr IFNα/TSA	10.5503789526279	0.532442233169392
			4 hr IFNα/TSA	13.6380064053784	0.605731754782217
			10 hr IFNα/TSA	6.92584652302866	0.300349496421639

Histone	Residue	PTM	Treatment	Relative abundance (%)	Standard Deviation (%)
H2A	**K5**	**Unmodified**	Mock	93.4652188173063	0.0748838545291095
			15 min IFNα	94.3439648662904	0.0791070022046213
			1 hr IFNα	94.0347197744928	1.28598799710983
			4 hr IFNα	91.153076348154	3.01755198565513
			10 hr IFNα	92.3285398037921	0.262799401618149
			15 min IFNα/TSA	48.4832278150491	6.30507680567572
			1 hr IFNα/TSA	81.5887947895657	0.485119424778574
			4 hr IFNα/TSA	67.6130851808874	0.247468543106633
			10 hr IFNα/TSA	39.8732105816898	0.618948796469699
		Acetylation	Mock	6.53478118269366	0.0748838545291093
			15 min IFNα	5.65603513370963	0.0791070022046194
			1 hr IFNα	5.9652802255072	1.28598799710983
			4 hr IFNα	8.84692365184603	3.01755198565513
			10 hr IFNα	7.67146019620792	0.262799401618136
			15 min IFNα/TSA	51.5167721849509	6.30507680567572
			1 hr IFNα/TSA	18.4112052104343	0.485119424778582
			4 hr IFNα/TSA	32.3869148191126	0.247468543106632
			10 hr IFNα/TSA	60.1267894183102	0.618948796469699

Histone	Residue	PTM	Treatment	Relative abundance (%)	Standard Deviation (%)
H2A	K9	Unmodified	Mock	99.1183124711383	0.0124710353426765
			15 min IFNα	99.4698012919895	0.0103717588405515
			1 hr IFNα	96.9477611045267	0.320314468151305
			4 hr IFNα	97.3198880310663	2.99123408262198
			10 hr IFNα	99.1794674099383	0.0146801935862312
			15 min IFNα/TSA	92.6542880088736	0.760907928177123
			1 hr IFNα/TSA	97.902703442011	0.12542366890374
			4 hr IFNα/TSA	92.9447025065899	0.231015574952771
			10 hr IFNα/TSA	73.4253611325324	0.905629597847963
		Acetylation	Mock	0.881687528861693	0.0124710353426694
			15 min IFNα	0.530198708010547	0.0103717588405581
			1 hr IFNα	3.05223889547335	0.320314468151317
			4 hr IFNα	2.6801119689337	2.99123408262198
			10 hr IFNα	0.820532590061741	0.0146801935862318
			15 min IFNα/TSA	7.34571199112642	0.760907928177127
			1 hr IFNα/TSA	2.09729655798899	0.125423668903738
			4 hr IFNα/TSA	7.05529749341007	0.231015574952769
			10 hr IFNα/TSA	26.5746388674676	0.905629597847962

Histone	Residue	PTM	Treatment	Relative abundance (%)	Standard Deviation (%)
H2A1	K13	Unmodified	Mock	99.9661248538492	0.0165269979332963
			15 min IFNα	99.9732075080416	0.00744655216526442
			1 hr IFNα	99.8990646311606	0.0112550602953327
			4 hr IFNα	99.9191242205378	0.0109089368337411
			10 hr IFNα	99.9549261479721	0.00407484286635918
			15 min IFNα/TSA	99.9947965525362	0.00300377276384332
			1 hr IFNα/TSA	99.9756826481288	0.0050138701578535
			4 hr IFNα/TSA	99.9851860945559	0.00362956310289948
			10 hr IFNα/TSA	99.9774306893333	0.00386374757459499
		Acetylation	Mock	0.0338751461508111	0.0165269979332957
			15 min IFNα	0.0267924919583678	0.00744655216526517
			1 hr IFNα	0.100935368839433	0.0112550602953235
			4 hr IFNα	0.0808757794621753	0.0109089368337388
			10 hr IFNα	0.0450738520278604	0.00407484286635832
			15 min IFNα/TSA	0.00520344746376229	0.00300377276384212
			1 hr IFNα/TSA	0.024317351871244	0.00501387015785019
			4 hr IFNα/TSA	0.0148139054440917	0.00362956310289714
			10 hr IFNα/TSA	0.0225693106667339	0.00386374757459871

Histone	Residue	PTM	Treatment	Relative abundance (%)	Standard Deviation (%)
H2A1	K15	Unmodified	Mock	39.4023197957706	1.40420856813479
			15 min IFNα	54.3430472275736	0.565598838129198
			1 hr IFNα	51.214951549831	0.832166601427025
			4 hr IFNα	51.6023168992514	0.373728116695792
			10 hr IFNα	48.2065944861669	1.29590748548139
			15 min IFNα/TSA	44.6853229649272	1.09991606792401
			1 hr IFNα/TSA	50.2760247584391	1.30653103987672
			4 hr IFNα/TSA	50.1826232427766	0.316812738449983
			10 hr IFNα/TSA	50.7083493549432	1.43310355881819
		Acetylation	Mock	60.5976802042294	1.40420856813479
			15 min IFNα	45.6569527724264	0.565598838129197
			1 hr IFNα	48.785048450169	0.832166601427018
			4 hr IFNα	48.3976831007486	0.373728116695797
			10 hr IFNα	51.7934055138331	1.29590748548138
			15 min IFNα/TSA	55.3146770350728	1.09991606792401
			1 hr IFNα/TSA	49.7239752415609	1.30653103987672
			4 hr IFNα/TSA	49.8173767572234	0.316812738449982
			10 hr IFNα/TSA	49.2916506450568	1.43310355881819

Histone	Residue	PTM	Treatment	Relative abundance (%)	Standard Deviation (%)
H2A3	K13	Unmodified	Mock	99.9575878663044	0.0213946902495725
			15 min IFNα	99.9208878721191	0.0426346990079061
			1 hr IFNα	99.6309574963457	0.395061855282418
			4 hr IFNα	99.2311664061786	0.0752385975181197
			10 hr IFNα	99.734912519543	0.130070742851988
			15 min IFNα/TSA	99.9600613903847	0.00426903725772674
			1 hr IFNα/TSA	99.9728792635965	0.0317864818654894
			4 hr IFNα/TSA	99.9821031918061	0.0131401515902179
			10 hr IFNα/TSA	99.9308443336386	0.0475672180147932
		Acetylation	Mock	0.0424121336955858	0.0213946902495724
			15 min IFNα	0.0791121278808632	0.0426346990079092
			1 hr IFNα	0.369042503654268	0.39506185528242
			4 hr IFNα	0.768833593821349	0.0752385975181212
			10 hr IFNα	0.265087480456993	0.130070742851987
			15 min IFNα/TSA	0.0399386096153378	0.00426903725772411
			1 hr IFNα/TSA	0.0271207364035279	0.0317864818654961
			4 hr IFNα/TSA	0.0178968081939002	0.0131401515902134
			10 hr IFNα/TSA	0.0691556663613997	0.0475672180147933

APPENDIX C. MATERIALS AND METHODS

METHODS

Cell culture and treatment with interferon or chemical inhibitor

Human cells lines, HeLa S3, 293T/17, 2fTGH, U2A, U3A and U6A cells were grown in Dulbecco's modified Eagle's medium (DMEM) containing 10% cosmic calf serum (CCS) and 1% pen-strep (PS) at 37ºC with 5% CO_2. Lentiviral-transduced HeLa or 2fTGH cells harboring shRNA were cultured in DMEM containing 10% CCS, 1% PS and 5-10 μg/ml puromycin (Sigma, St. Louis, MO) at 37ºC with 5% CO_2. Cells were mock-treated or treated with 1000 units/ml of IFNα (Hoffman-Roche) for the specified amount of time. Chemical inhibitors, PFI-3 (0.9 mM, Sigma), TSA (1.3 mM; EMD Millipore, Burlington, MA), MB-3 (0.5 mM, Sigma), JQ1 (10 μM; Apexbio, Houston, TX), and BIC1 (0.5 mM, Sigma) were added 1 hr pre-IFN treatment and not removed during IFN treatment.

mRNA Expression

RNA was isolated from cells with Trizol, extracted with phenol/chloroform and isopropanol-precipitated. RNA was treated with DNase I, primed with random primers and reverse transcribed to cDNA with Superscript III (Invitrogen, Carlsbad, CA). Relative mRNA abundance was determined by SYBR green qPCR (Invitrogen) using specific primers. Analysis was based on the delta Ct method using GAPDH to normalize for relative abundance.

Lentivirus-mediated RNA interference

293T/17 cells were transfected with pGIPZ lentiviral short hairpin RNA vectors, pΔ8.91 and pUC-MDG using either lipofectamine 2000 or polyethylenimine in DMEM media for 15 hr followed by a change to DMEM media supplemented with 10% CCS and 1% PS for 24 hr. Lentivirus-containing supernatant was centrifuged and filtered to remove cell debris. HeLa or 2fTGH cells were transduced 2-3 times with fresh lentivirus and polybrene for 24 hr each time.

siRNA-mediated RNA interference

HeLa or 2fTGH cells were transfected with 40 nM siRNA using lipofectamine 2000 for 48 hr. Cells were mock- or IFN-treated and harvested by Trizol for RNA analysis or processed for ChIP sample preparation.

Antiviral plaque assay

Lentivirus-shRNA-transduced HeLa or 2fTGH cells were mock-treated or treated with 1000 units/ml of IFNα for the specified amount of time, then infected with vesicular stomatitis virus (Indiana strain) for 24-72 hr at 37ºC with 5% CO_2. Cells were fixed with 3.7% formaldehyde and stained with crystal violet.

Immunoblot

Cells were lysed on ice in whole cell extract buffer (50 mM Tris pH 8.0, 280 mM NaCl, 0.5% Igepal, 0.2 mM EDTA, 2 mM EGTA, 10% glycerol) supplemented with fresh

DTT, protease inhibitor and sodium vanadate for 15-30 min, then sonicated for 5 minutes (15 sec on, 45 sec off) at 4°C using a cuphorn sonicator (Misonix). The sonicated sample was centrifuged at 14,000 x g for 15 minutes to remove the cellular debris. Total protein was denatured at 100°C in SDS loading buffer, separated by SDS-PAGE, transferred to nitrocellulose membrane, blocked in milk/TBST solution, probed with specific antibody (H2A.Z ab4174 Abcam, Cambridge, MA; GAPDH sc-47724 Santa Cruz, Dallas, TX; STAT1 Santa Cruz sc-345, STAT2 sc-476) and the corresponding HRP conjugated secondary antibody (Invitrogen). Chemiluminescent detection (PerkinElmer, Waltham, MA) was performed using Vision Works software. Relative density was quantified using ImageJ software.

ChIP sample preparation

Chromatin immunoprecipitation (ChIP) samples were prepared according to Lee et al., 2006. Adherent cells were crosslinked for 10 minutes with 11% formaldehyde solution (50 mM HEPES-KOH pH 7.5, 100 mM NaCl, 1 mM EDTA pH 8.0, 0.5 mM EGTA pH 8.0, 11% formaldehyde) and quenched for 5-10 minutes with glycine at room temperature. Crosslinked cells were lysed at 4ºC with lysis 1 buffer (50 mM HEPES-KOH pH 7.5, 140 mM NaCl, 1 mM EDTA, 10% glycerol, 0.5% NP-40, 0.25% Triton X-100, 1X protease inhibitors), pelleted to isolate the nuclei, washed with lysis 2 buffer (10 mM Tris-HCl pH 8.0, 200 mM NaCl, 1 mM EDTA, 0.5 mM EGTA, 1x protease inhibitors) and pelleted. Nuclei was resuspended in lysis buffer 3 (10 mM Tris-HCl pH 8.0, 100 mM NaCl, 1 mM EDTA, 0.5 mM EGTA, 0.1% Na-Deoxycholate, 0.5% N-lauroylsarcosine, 1X

protease inhibitiors) and sonicated at 4ºC with intervals of 15 seconds on and 45 seconds off until DNA fragments were ≤1000 bp. Triton-X was added to the sonicated lysate to a final concentration of 1% and centrifuged to pellet the cell debris. The cleared lysate was removed and 1% input sample was saved. The lysate was incubated with Dynabeads bound to antibody (STAT1 Santa Cruz sc-345, STAT2 Santa Cruz sc-476, IRF9 Santa Cruz sc-496, RNA Pol II CTD Abcam ab817, H2A.Z Abcam ab4174, H2A Abcam ab18255, H2B Abcam ab1790, H3 Abcam ab1791, H4 Abcam ab7311) overnight at 4ºC followed by 5 times wash with cold RIPA buffer (50 mM HEPES pH 7.5, 500 mL LiCl, 1 mM EDTA, 1% NP-40, 0.7% Na-Deoxycholate) and once with cold Tris-EDTA (TE) pH 8.0 + NaCl. Immunoprecipitated complexes were eluted off the beads with 30 minutes of 65ºC water bath incubation and periodic vortexing. The eluate was further incubated in a 65ºC heated incubator for 12-15 hr. TE buffer was added to the reverse-crosslinked sample and incubated with RNase A for 2 hr at 37ºC, Proteinase K for 2 hr at 55ºC and isolated with phenol:chloroform:isoamyl. The sample was eluted with ethanol (EtOH), glycogen and NaCl at -20ºC overnight, washed with 80% EtOH and resuspended in Tris-HCl pH 8.0. ChIP DNA was used either for qPCR assays using specific primers or prepared into a sequencing library for Applied Biosystems (ABI, Foster City, CA) SOLiD 5500xl sequencing.

ChIP library preparation for SOLiD 5500xl sequencing

The purified ChIP DNA was prepared for sequencing following ABI SOLiD 5500xl library preparation protocol. Purified DNA was end-repaired (NEBNext; NEB, Ipswich,

MA). The DNA was size-selected with Ampure beads followed by addition of a single dA-tail to the ends. ABI SOLiD 5500xl DNA adaptor barcodes were ligated onto the DNA with Quick Ligase (NEB) for 30 minutes at room temperature and size-selected with Ampure beads. Size-selected DNA was pseudo nick-translated to fill in the 5' overhang and remove the 3' end (NEBNext). Ampure beads was used to purify the final adaptor-ligated ChIP DNA. The adaptor-ligated ChIP DNA library was amplified for 11-13 cycles using the SOLiD P1 and P2 primers and DNA size was verified by Bioanalyzer.

ChIP assays, deep sequencing and data analysis

ChIP and input DNA abundance was analyzed using SYBR green qPCR for ChIP assays. ChIP DNA was normalized using the percent input method. For high-throughput sequencing, ChIP DNA was prepared following the SOLiD 5500xl library preparation protocol. Reads were aligned to the human hg19 build with Bioscope v1.3.1. The reference genome was converted to colorspace. MACS software was used to identify unique peaks. Genomic regions that were statistically enriched in the ChIP-Seq data (p-value $\leq 1 \times 10^{-5}$) relative to the control input DNA were identified by the MACS software (Zhang et al., 2008), and represent regions bound by IFN-induced STAT1, STAT2 or IRF9. Additional data analysis was performed with the HOMER software.

Direct selection MNase nucleosome preparation, deep sequencing and data analysis

Mononucleosome DNA (mnDNA) from (~147-167 bp) was isolated, processed and sequenced as described in Freaney et al., 2014 and Yigit et al., 2013. Briefly, a sequencing library was prepared with isolated mononucleosome DNA (mnDNA) and ligated with SOLiD 5500xl adaptor DNA barcodes. The sequencing library was hybridized to 10 biotin-labeled bacteria artificial chromosomes (BACs; BACPAC Resources, Oakland, CA) to enrich for 20 target interferon-stimulated gene genomic loci. The target DNA was captured and eluted from streptavidin-conjugated beads. The eluted library was amplified for 13-15 cycles using SOLiD P1 and P2 primers and paired-end sequenced on the SOLiD 5500xl platform.

To obtain mnDNA, crude nuclei was isolated from HeLa cells. Approximately 5 x 10^7 adherent HeLa cells were pelleted, washed, and lysed with MC lysis buffer (10 mM Tris-HCl pH 7.5, 10 mM NaCl, 3 mM $MgCl_2$, 0.5% Igepal). The nuclear pellet was resuspended in micrococcal nuclease (MNase) reaction buffer (10 mM Tris-HCl pH 7.5, 10 mM NaCl, 3 mM $MgCl_2$, 1 mM $CaCl_2$, 4% Igepal, fresh 1 mM PMSF). MNase (800 units/5 x 10^7 cells) was added to the nuclear pellet and digested the chromatin for the appropriate amount of time to generate mononucleosome DNA at 25°C. The digestion reaction was terminated with addition of a stop reaction solution (10 mM EGTA, 1X PMSF, 1X PI, 1% SDS, 200 mM NaCl or 10 mM EDTA). The digested chromatin sample was treated with RNase A for 30 min at 37°C followed by a phenol/chloroform extraction to obtain the DNA. The DNA (~1.5 µg) was loaded onto a 3.5% NuSieve 3:1 agarose gel in

0.5% TBE solution to resolve the nucleosomal DNA bands. The mononucleosomal-sized DNA (mnDNA) band (~147 bp) was excised from the gel and isolated by the crush and soak method. Briefly, the gel was incubated with 3 times volume to gel of crush and soak buffer (300 mM NaOAc, 1 mM EDTA pH 8.0, 0.1% SDS) with gentle shaking at room temperature overnight. The crush and soak buffer containing the mnDNA was filtered (Amicon Ultrafree-Cl) and the filtrate was concentrated. The concentrated mnDNA was purified and used to prepare the sequencing library.

The purified mnDNA was prepared for sequencing following ABI SOLiD 5500xl library preparation protocol. Purified mnDNA was end-repaired. The DNA was size-selected (~147 bp) with Ampure beads followed by addition of a single dA-tail to the ends. ABI SOLiD 5500xl DNA adaptor barcodes were ligated onto the DNA with Quick Ligase for 30 minutes at room temperature and size-selected with Ampure beads. Size-selected DNA was pseudo nick translated to fill in the 5' overhang and remove the 3' end. Ampure beads was used to purify the adaptor-ligated mnDNA.

To enrich for mnDNA from 20 target ISG genomic regions, bacterial artificial chromosomes (BACs) encoding these regions were used to hybridize and enrich the target ISGs. The 10 biotin-dUTP-labeled BACs allows capture of ~1.76 Mb of the genome corresponding to 20 ISG loci and their surrounding genomic regions. The lyophilized biotin-dUTP-labeled BACs was resuspended with human *cot-1* DNA to reduce nonspecific repetitive DNA sequences with a mineral oil overlay, followed by denaturation at 95°C for 5 min, incubated at 65°C for 15 min, and then incubated with 5 µl of 2× hybridization buffer (1.5 M NaCl, 40 mM sodium phosphate buffer pH 7.2, 10 mM EDTA

pH 8, 10× Denhardt's, 0.2% SDS) at 65°C for 6 hr. Then 2 µg of the adaptor-ligated mnDNA in 5 µl of dH_2O was denatured at 95°C for 5 min and incubated at 65°C for 15 min with a mineral oil overlay. The mnDNA was transferred to a tube containing the *cot-1* suppressed BACs and allowed to hybridize with the BACs at 65°C for 72 hr. The hybridization mixture of BAC and mnDNA was added to pre-washed streptavidin magnetic beads in 150 µl Streptavidin bead binding buffer. Binding of the streptavidin magnetic beads with the biotin-dUTP labeled BAC hybridized with mnDNA was carried out on a rotator at room temperature for 30 min with periodic mixing. The magnetic beads were washed once with 1 ml 1× sodium-saline citrate (SSC) buffer with 0.1% SDS at 25°C for 15 min, and then three times with 1 ml 0.1× SSC buffer with 0.1% SDS. The hybridized BAC-mnDNA was eluted off the streptavidin beads with 100 µl of 0.1 M NaOH at 25°C for 10 min. The BAC-mnDNA eluate was neutralized by addition of 100 µl 1M Tris-HCl pH 7.5 and desalted through a Sephadex G-50 column. The eluted mnDNA was PCR-amplified for 13-15 cycles using the SOLiD P1 and P2 primers.

Sequencing reads were aligned with the Bowtie software v0.12.7 using the human reference genome build hg19/GR37. Aligned reads corresponding to the BAC-selected genomic coordinates were used to generate nucleosome occupancy maps using a center-weighted algorithm and selecting reads that were 137-157 bp, representing single nucleosome-protected regions (Freaney et al., 2014; Yigit et al., 2013). The occupancy scores from the center-weighted algorithm was normalized to 10 million reads to generate nucleosome occupancy maps. To identify nucleosome occupancy changes between the

steady state and different time points of IFN-induced states, additional analysis was performed using the DANPOS software (Chen et al., 2013).

DNase I nuclease sensitivity assay

Cells were mock-treated or treated with 1000 units/ml of IFNα (Hoffman-Roche), 50 mg/ul IFNγ (PBL Interferon Source) or heat-shocked at 42°C for the specified amount of time. HeLa cells were pelleted, washed, and lysed with MC lysis buffer (10 mM Tris-HCl pH 7.5, 10 mM NaCl, 3 mM $MgCl_2$, 0.5% Igepal). The nuclear pellet was resuspended in DNase I reaction buffer (4% Igepal (or NP-40), 10 mM Tris-HCl pH 7.6, 2.5 mM $MgCl_2$, 0.5 mM $CaCl_2$, and freshly added 1mM PMSF). DNase I (50U per 2.5 x 10^7 cells) digestion was performed at 25C. The digestion reaction was terminated with addition of a stop reaction solution (10 mM EGTA, 1X PMSF, 1X PI, 1% SDS, 200 mM NaCl or 10 mM EDTA). The digested chromatin sample was treated with RNase A for 30 min at 37°C followed by a phenol/chloroform extraction to obtain the DNA.

MATERIALS

REAGENT or RESOURCE	SOURCE	IDENTIFIER
Antibodies		
STAT1	Santa Cruz	sc-345
STAT2	Santa Cruz	sc-476
IRF9	Santa Cruz	sc-496
H2A.Z	Abcam	ab4174
RNA Pol II CTD	Abcam	ab817
H2A	Abcam	ab18255
H2B	Abcam	ab1790
H3	Abcam	ab1791
H4	Abcam	ab7311
Phospho-STAT1 (Tyr 701)	Cell Signaling Technology	7649
Phospho-STAT2 (Tyr 689)	EMD Millipore	07-224
H2A.Z Acetyl K4, K7, K11	Abcam	Ab18262
GAPDH	Santa Cruz	sc-47724
Bacterial and Virus Strains		
Vesicular stomatitis virus	N/A	Indiana strain
Lentivirus (pUC-MDG, pΔ8.91, harbors pGIPz shRNA)	This thesis project	See table below
Chemicals, Peptides, and Recombinant Proteins		
Dynabeads Protein G	Invitrogen	10004D
IFNα	Hoffmann-La Roche Inc	RO 22-8181/001
PFI-3	Sigma Aldrich	SML0939
MB-3	Sigma Aldrich	M2449
JQ1	Fisher Scientific	50-101-4886
BIC1	Sigma Aldrich	203830
TSA	EMD Millipore	647925
iProof HF DNA Polymerase	Biorad	172-5302
Critical Commercial Assays		
SOLiD library preparation: Fragment Library Core Kit	Applied Biosystems	4464412
SOLiD library preparation: Enzyme Module	Applied Biosystems	4464413
SOLiD library preparation: Barcode adapters	Applied Biosystems	4464406
SOLiD library preparation: Standard adapter kit	Applied Biosystems	4464411
NEBNext: END Repair Module	NEB	E6050L

NEBNext: dA-Tailing Module	NEB	E6053L
Deposited Data		
STAT1, STAT2, IRF9 ChIP-Seq data (HeLa cells)	This thesis project	GEO: GSE110067
H2A.Z Encode data (HeLa cells)	(Consortium, 2012)	UCSC: wgEncodeEH002395; GEO: GSM1003483 https://genome.ucsc.edu/encode/
Human reference genome NCBI build 37, GRCh37	Genome Reference Consortium	http://www.ncbi.nlm.nih.gov/projects/genome/assembly/grc/human/
Experimental Models: Cell Lines		
Human: HeLa	N/A	N/A
Human: 2fTGH	George Stark	N/A
Human 2fTGH-derived (-/- IRF9): U2A	George Stark	U2A
Human 2fTGH-derived (-/- STAT1): U3A	George Stark	U3A
Human 2fTGH-derived (-/- STAT2): U6A	George Stark	U6A
Human: 293T	ATCC	CRL-11268
Oligonucleotides		
Primers for RT and ChIP qPCR	Eurofins, Invitrogen	See tables below
Recombinant DNA		
pUC-MDG (VSV-G pseudotyped viral envelope)	Xiaomin Bao	N/A
p∆8.91 (Lentiviral Gag, Pol)	Xiaomin Bao	N/A
pGIPZ shRNA	GE Dharmacon	See tables below
Software and Algorithms		
Bowtie	(Langmead et al., 2009)	https://sourceforge.net/projects/bowtie-bio/files/bowtie/0.12.7/

MACS	(Zhang et al., 2008)	http://liulab.dfci.harvard.edu/MACS/
DANPOS	(Chen et al., 2013)	https://sites.google.com/site/danposdoc/
HOMER	(Heinz et al., 2010)	http://homer.ucsd.edu/homer/
R	R Development Core Team	https://www.r-project.org/
Galaxy	(Afgan et al., 2016)	Usegalaxy.org

mRNA/cDNA RT-PCR Primers

Gene	Forward Primer	Reverse Primer
H2A.Z	CTCACCGTGGGTCCGATTAG	CGCCTTTGTCTTGGCCTTTC
OAS3	TTCATCCAGGACCACCTGA	GCCAAATGAGCCCCCTTTAC
IFIT1/ISG56	CAGAACGGCTGCCTAATTT	GGCCTTTCAGGTGTTTCAC
IFIT2/ISG54	GGAAGATTTCTGAAGAGTGCAG	CTCCCTCCATCAAGTTCCAG
IFITM1/9-27	CCTTCCAAGGTCCACCGT	ACGTCGCCAACCATCTTC
LOC100419583	GCTTGCTCAGGTCTCTGTCC	CTGCCCGGTAGTTATTCAGC
ISG15	GACCTGACGGTGAAGATGCT	CGATCTTCTGGGTGATCTGC
GAPDH	ACAGTCAGCCGCATCTTCTT	ACGACCAAATCCGTTGACTC

Genomic DNA/ChIP RT-PCR Primers

Genomic region	Forward Primer	Reverse Primer
OAS3 promoter	CAAGTTTGGGGAAGACAGGA	TCGGATTTCTGGTTTCGTTT
OAS3 gene body	AAAGCCAGCCAGTGAACAGT	ATCCAAGCCACTCTCCTCAA
IFIT1/ISG56 promoter	GCAGGAATTCCGCTAGCTTT	GCTAAACAGCAGCCAATGGT
IFIT1/ISG56 gene body	CCTCCTTGGGTTCGTCTACA	GGCTGATATCTGGGTGCCTA
IFITM1/9-27 promoter	CAGCAGGAAATAGAAACTTAAGAGAAA	GGGGAAGGAAGTGTTGAGTG
IFITM1/9-27 gene body	CTGATTCTGGGCATCCTCAT	AGGCTATGGGCGGCTACTA

LOC100419583 promoter	TTGCTGATCTCATCACTGCAT	ACTTTCCCGTCCTGGTTTCT
ISG15 promoter	CGTGTGTGCCTCAGGCTTAT	ACGGCACAAGCTCCTGTACT
IFIT3/ISG60 promoter	ATTTTCCTCCTCCCAACGAT	GAGAGTAGGGCACGCATCAG
βActin promoter	CTGGGTTCTGTACGCTCCTG	GACCCACCCAGCACATTTAG

Plasmids or siRNA

shRNA: Target	**Sequence**	**Clone ID**
shRNA: H2AFZ	CGTATTCATCGACACCTAA	V2LHS_132986
shRNA: H2AFZ	GCCGTATTCATCGACACCT	V2LHS_132984
shRNA: H2AFZ	CCGTATTCATCGACACCTA	V2LHS_132985
shRNA: Non-silencing	N/A	RHS 4346
shRNA: INO80	ATTTCTTCCAGTACAGAAG	V2LHS_238013
shRNA: RVB1	TTAGCAAGCAAGTTGGCCG	V2LHS_14740
shRNA: RVB2	TGCTGGTCGATCAATCTGG	V3LHS_641743
shRNA: CBP	TAAGTGATAATATTCATCC	V2LHS_24251
siRNA: SRCAP	Dharmacon On-TARGETplus SMARTpool	L-004830-00-0005

Bacterial artificial chromosomes (BAC)

BAC	**BAC start-end**	**Hybridization ISG target(s)**
RP11-1065J8	Chr1: 158892666-159066838	*IFI16, AIM2*
RP11-1107P24	Chr10: 91017523-91231100	*IFIT1, IFIT2, IFIT3, IFIT5*
RP11-932J23	Chr12: 113297537-113465374	*OAS1, OAS2, OAS3*
RP11-120C17	Chr21: 42708733-42858453	*MX1, MX2*
CTD-2344F1	Chr11: 212684-355505	*IFITM1, IFITM2, IFITM3, IFITM5*
CTD-3113J13	Chr1: 838835-1031922	*ISG15*
RP11-553K16	Chr1: 27887559-28085894	*IFI6*
RP11-641G12	Chr2: 191780297-191951049	*STAT1*
RP11-348M3	Chr12: 56684981-56848839	*STAT2*
RP11-668H1	Chr14: 94486463-94670429	*IFI27*

APPENDIX D. BIOINFORMATIC WORKFLOWS AND SCRIPTS

Bowtie alignment script for BEM-seq nucleosome reads, Related to Figure 2.5-2.10, Table 2.5

Bowtie alignment (version 0.12.7) was performed on the Northwestern University Quest Cluster

```
export PATH=$PATH:/home/bowtie_0.12.7
#!/bin/bash

#the folder of the index
folder_index="/home/nancy/data"
#the index
index="hg19_c"

#the folder of the raw sequence data
folder_originalReads="/home/nancy/data"
#the folder to save the alignment results, under the current directory
folder_alignment="/home/nancy/data/bowtieAlignment"

#F3 reads
F3_reads="Mock_mnDNA_F3.csfasta"
#F3 reads quality
F3_QV="Mock_mnDNA_F3.QV.qual"
#F5 reads
F5_reads="Mock_mnDNA_F5-DNA.csfasta"
#F5 reads quality
F5_QV="Mock_mnDNA_F5-DNA.QV.qual"

echo "F3:50bp, F5:35bp; mismatch 3"
bowtie -C -S ${folder_index}/${index} -B 1 -p 6 -v 3 -m 1 --col-keepend --fr -f -1 ${folder_originalReads}/${F3_reads} -2 ${folder_originalReads}/${F5_reads} --Q1 ${folder_originalReads}/${F3_QV} --Q2 ${folder_originalReads}/${F5_QV} --max multiple --un notMatch > map_mismatch3.sam

#sam output file is directly used in DANPOS software for nucleosome quantification and visualization
```

Convert bowtie alignment file from .sam to .bam for use in further analysis

Used samtools (version 0.1.19) on the Northwestern University Quest Cluster

```
#convert .sam file to .bam file
samtools view -bS ChIP03_unique.sam > ChIP03_unique.bam
```

BEM-seq nucleosome reads quantification and visualization, Related to Figure 2.6-2.10

Bowtie .sam output file was used with DANPOS software (version 2.1.3) and executed on the Northwestern University Quest Cluster

```
#!/bin/bash

#PBS -j oe
#PBS -N danpos
#PBS -m abe
#PBS -1 nodes=1:ppn8
#PBS -1 walltime=10:00:00
#PBS -q normal

module load python/ActivePython-2.7

#pwd

#echo $PATH
#echo $PYTHONPATH

#python
#cd /home/ywa969/Python-2.7.5/bin
#pwd
#python
python /home/ywa969/danpos-2.1.3/danpos.py /projects/p20491/Nancy/Danpos/2
hr_all.bam:/projects/p20491/Nancy/Danpos/Mock_a
ll.bam,/projects/p20491/Nancy/Danpos/6h_all.bam:/projects/p20491/Nancy/Danpos/Mock_all.ba
m,/projects/p20491/Nancy/Danpos
/10h_all.bam:/projects/p20491/Nancy/Danpos/Mock_all.bam -k 1 -p 1 -o
/projects/p20491/Nancy/Danpos/
```

#Final wig output files were loaded onto usegalaxy.org, converted to bigWig files and directly linked to visualize on UCSC genome browser. EPS image files were outputted from UCSC genome browser to use with Adobe Illustrator for creating figures.

ChIP-seq data analysis using HOMER software (version 4.7.2)

The following workflows and command lines require loading a compatible output file from the aligned sequencing reads or peak files such as .sam/.bam or .bed.
Bed files of the ChIP-seq peaks generated from Matt Schipma/NU core were used for analysis with the HOMER software.

WORKFLOW AND COMMAND LINES:

Generate DNA annotation table with HOMER software, Related to Figure 2.3:
annotatePeaks.pl mypeaks.bed hg19 > anno_mypeaks.txt

Use file with R software:
```
# Calculate frequency of DNA type then create pie chart so Illustrator can alter colors of pie chart
#in R: change working directory to where annoPeak....txt file exists

anno = read.table("annoPeaks_2fold-annoPie_gO_go_022617.txt", sep="\t", header=T, quote="")

pietable = table(unlist(lapply(strsplit(as.character(anno$Annotation), "\\("),"[[",1)))

newtable = table(c("3' UTR","5' UTR","exon","Intergenic","intron", "non-coding","promoter-TSS","TTS"))

newtable[names(pietable)] = pietable

names(newtable) = paste(names(newtable), "(", round(newtable/sum(newtable)*100), "%, ", newtable, ")", sep="")

pie(newtable, main="mypeaks 2-fold annotation", col=rainbow(8))

dev.copy(png, "anno_mypeaks.png", width=800, height=600);dev.off();
```

***De novo* motif analysis with HOMER software, Related to Figure 2.3:**
findMotifs.pl <inputfile.txt> <promoter set> <output directory> [options]
cmd = findMotifs.pl Input_peak.txt Output_Motifs_folder

Use the output file (file.motif) containing power-weighted matrix values to to generate DNA sequence logo with R software:
```
> source("http://bioconductor.org/biocLite.R")
> biocLite("seqLogo","Biostrings")
> library(seqLogo)
> library(Biostrings)

#read in input data (power-weighted matrix (PWM), but not in right format)
> pwm <-read.table("known1.motif", sep="\t", quote="", fill=T, header=T)
> str(pwm)
'data.frame':      12 obs. of  6 variables:
 $ X.GTCCCCWGGGGA                        : num  0.184 0.067 0.021 0.012 0.021 0.038 0.537 0.146
0.179 0.019 ...
 $ EBF1.EBF..Near.E2A.ChIP.Seq.GSE21512..Homer: num  0.17 0.17 0.618 0.93 0.862 0.917 0.055
0.006 0.001 0.001 ...
 $ X6.752028                             : num  0.443 0.263 0.075 0.001 0.001 0.001 0.003 0.77 0.794 0.979 ...
```

```
 $ X.51.205599                          : num  0.203 0.5 0.286 0.057 0.116 0.044 0.405 0.078 0.026 0.001 ...
 $ X0                                   : logi  NA NA NA NA NA NA ...
 $ T.8522.0.6.78...B.7739.8.6.10...P.1e.22    : logi  NA NA NA NA NA NA ...

#change column names corresponding to DNA bases and the weight (i.e. frequency)
> colnames(pwm) [1] <- "A"
> colnames(pwm) [2] <- "C"
> colnames(pwm) [3] <- "G"
> colnames(pwm) [4] <- "T"
> pwm
      A     C     G     T X0 T.8522.0.6.78...B.7739.8.6.10...P.1e.22
1  0.184 0.170 0.443 0.203 NA                                    NA
2  0.067 0.170 0.263 0.500 NA                                    NA
3  0.021 0.618 0.075 0.286 NA                                    NA
4  0.012 0.930 0.001 0.057 NA                                    NA
5  0.021 0.862 0.001 0.116 NA                                    NA
6  0.038 0.917 0.001 0.044 NA                                    NA
7  0.537 0.055 0.003 0.405 NA                                    NA
8  0.146 0.006 0.770 0.078 NA                                    NA
9  0.179 0.001 0.794 0.026 NA                                    NA
10 0.019 0.001 0.979 0.001 NA                                     NA
11 0.210 0.045 0.724 0.021 NA                                     NA
12 0.500 0.204 0.242 0.054 NA

#header is not columns really so removed column 5 and 6, only need 4
> pwm.name <- pwm[,c(1,2,3,4)]
> pwm.name
      A     C     G     T
1  0.184 0.170 0.443 0.203
2  0.067 0.170 0.263 0.500
3  0.021 0.618 0.075 0.286
4  0.012 0.930 0.001 0.057
5  0.021 0.862 0.001 0.116
6  0.038 0.917 0.001 0.044
7  0.537 0.055 0.003 0.405
8  0.146 0.006 0.770 0.078
9  0.179 0.001 0.794 0.026
10 0.019 0.001 0.979 0.001
11 0.210 0.045 0.724 0.021
12 0.500 0.204 0.242 0.054

#transpose so the columns becomes rows. This puts it into the right format/PWM
> pwm.name.row <- t(pwm.name)
> pwm.name.row
  [,1]  [,2]  [,3]  [,4]  [,5]  [,6]  [,7]  [,8]  [,9] [,10] [,11] [,12]
A 0.184 0.067 0.021 0.012 0.021 0.038 0.537 0.146 0.179 0.019 0.210 0.500
C 0.170 0.170 0.618 0.930 0.862 0.917 0.055 0.006 0.001 0.001 0.045 0.204
G 0.443 0.263 0.075 0.001 0.001 0.001 0.003 0.770 0.794 0.979 0.724 0.242
T 0.203 0.500 0.286 0.057 0.116 0.044 0.405 0.078 0.026 0.001 0.021 0.054

# Plots out motif and bits/weight
> seqLogo(pwm.name.row)
```

Compute Heatmap values with HOMER software, Related to Figure 3.2:

#Generates heatmap
annotatePeaks.pl <peak file> <genome> -size <#> -hist <#> -ghist -d <tag directory 1> [tag directory2] ... > <output matrix file>
cmd = annotatePeaks.pl STAT2-2 hrIFN-peak.txt hg19 -size 5000 -hist 25 -ghist -d /ChIP-seq_data/STAT2/Mock-STAT2_HomerTagDirectory/ /ChIP-seq_data/STAT2/IFN-STAT2_HomerTagDirectory/ /ChIP-seq_data/H2AZ/HomerTagDirectory/ /ChIP-seq_data/H3K4me3/HomerTagDirectory/ /ChIP-seq_data/H3K27me/HomerTagDirectory/ > heatmap.txt

#output file can be used with R or other programs.
#output file was loaded in Gene Cluster 3.0 and clustered (k-means) by genes into one cluster with center correlation for the similarity metric.
#Gene Cluster 3.0 output file was loaded into Java Tree View to output heatmap image